Simulated Mass, Heat and Freshwater Budgets of the Arctic Mediterranean - Present and Future

Master Thesis in Oceanography

Ingo Bethke
Bergen 2004

Geophysical Institute
University of Bergen

Abstract

The majority of recent climate forecast studies suggest a dramatic thinning of the Arctic multi year ice and eventually the disappearing of all summer ice within just a few decades. Moreover, in the maritime Arctic a large number of regional impacts are reflected in changes of the ocean circulation, energy balance, and hydrological cycle. The Bergen Climate Model is one of the approximately 20 AOGCMs which simulate possible near-future climates while trying to distinguish between human caused changes and natural variability. To address the question of how the ocean contributes to the predicted or probably already observed Arctic climate change is subject of this work. With the help of budget and flux products of mass, heat and freshwater, an attempt is made to propose quantitatively consistent answers to these problems.

Thanks

Hjertelig takk til Tore Furevik for veiledning og mye støtte.

Tusen takk til Helge Drange for hjelp med studium, jobb og turen til Kina.

Vielen Dank an meine Familie für die aktive moralische und finanzielle Unterstützung während meines Studiums.

Various analyses and figures of this work are a product of a very fruitful collaboration with Olivier Laurantin who analyzed the BCM atmospheric and sea-ice data during his stay in Bergen in spring 2004. Merci beaucoup!

Special thanks to Misha Bowles for teaching English and inviting me to delicious dinners.

Thanks to Asgeir Sorteberg, Jan Even Nilsen, Nils Gunnar Kvamstø and Mats Bentsen for help and support in my studies.

Thanks to Yngvar Gjessing for helping me with my transition to the University of Bergen.

Many thanks to Frank, Thomas and Ole for serving coffee every morning. Thanks to Roar for always providing me with the latest football and weather news.

Contents

Chapter 1

Introduction

1.1 Motivation

Major research efforts have contributed to sharpen our awareness of the vulnerability of the Arctic ecosystem, and the outstanding sensitivity of the Arctic ecosystem onto climate change. But until now, virtually all attempts to provide a simple picture or concept to explain the main features of the physical behavior of the Arctic climate failed on the complexity of it's system. Therefore, the global coupled climate model appears to be the most powerful tool to advance our understanding. It exploits all observational information and combines the efforts of many researches and many disciplines. However, the lack of consensus among the competing models gives rise to the need for clarification and especially quantification. The latter is essential for the scientific community to be able to enforce drastic political actions in order to minimize the human impact on the environment, which in general is associated with harm (Intergovernmental Panel on Climate Change - IPCC 2001). In this context, we investigate the representation of the Arctic Ocean from several experiments of a global coupled climate model. Thereby, most attention is paid to integrated mass, heat and freshwater budgets as well as the large scale ocean circulation. Their importance for the ongoing discussion about the diminishing polar ice cap, a changing global circulation, and a general warming is fundamental. How extreme the future changes might possibly be is illustrated in figure 1.1.

1.2 The Arctic Region

Geography. The study area shown in figure 1.2-*left* is confined to the marine Arctic from the International Hydrographic Organization defined regional limits (Jakobsson 2002). These have been projected onto the ocean model grid as described in Laurantin (2004), and shown in figure 1.2-*right*. Towards the Pacific Ocean the Arctic Seas are limited by the Bering Strait. Towards the Atlantic Ocean the Davis Strait, Denmark Strait, Iceland Sea and Norwegian Sea define their border. Here, we refer to the

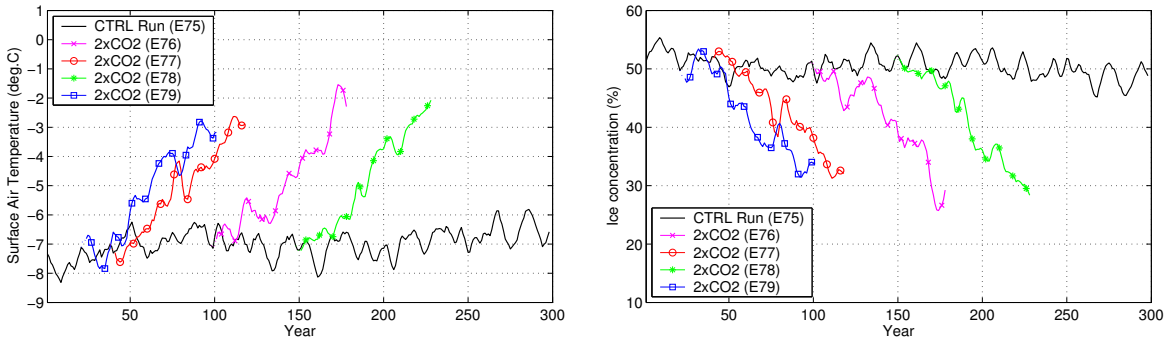

Figure 1.1: Temporal development of surface temperature *(left)* and ice concentration *(right)* for the BCM control and double CO_2 experiments, averaged over the total study area.

Canadian Basin joined with the Eurasian Basin as the Central Arctic Ocean. The Arctic Shelf Seas comprise of the Northwestern Passages, Beaufort Sea, Chukchi Sea on the Canadian side, and the East Siberian Sea, Laptev Sea , Kara Sea, Barents Sea on the Asian side. The White Sea and the Lincoln Sea are included for completeness but considered as irrelevant for this study. The Central Arctic Ocean together with the Arctic Shelf Seas is finally termed the Arctic Ocean. In relation to the position of the Polar Front and the ice edge, in some circumstances it is considered more appropriate to exclude the Barents Sea. The region covered by the Greenland Sea, Iceland Sea, Norwegian Sea and Denmark Strait is termed the GIN Seas or Nordic Seas, which usually include the Barents Sea, alternatively.

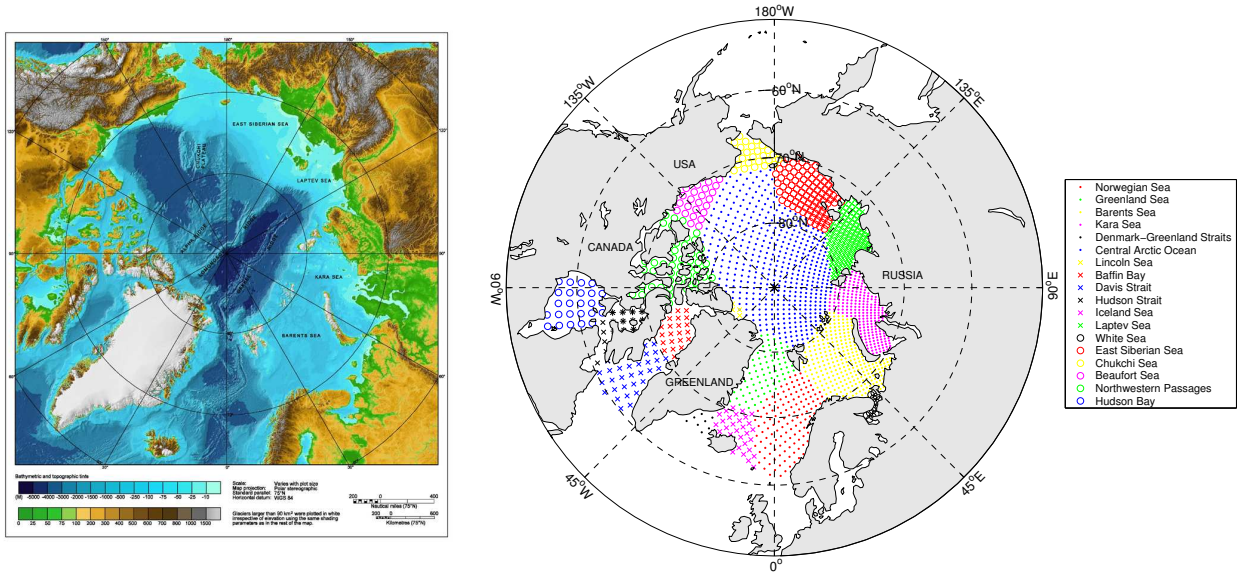

Figure 1.2: IBCAO Map of Arctic Ocean bathymetry *(left)*. Projection of the IHO defined regional limits on the model grid *(right)* (Laurantin 2004)

Bathymetry. The Arctic Seas can be separated into two major basins, the Arctic Ocean proper containing the major Arctic basins and the Greenland/Norwegian basins. The Arctic basins, are divided into the Canadian and Eurasian Basins. They are separated by the Lomonosov Ridge which has a maximum depth of 1400 m. The Canadian Basin has a mean depth of approximately 3800 m. It is split into the Canada and Makarow Basins which are divided by the Alpha Ridge. The Eurasian Basin has a mean depth of 4200 m. It is divided by the Arctic Mid-Ocean Ridge into the Amundson and Nansen Basins.

Pathways. The exchanges with the World Oceans are confined to a few straits and passages. This limits the Arctic Ocean ventilation significantly, hence the Arctic Ocean is frequently referred to as the Arctic Mediterranean. The total exchange with the North Pacific is through the narrow (approximately 85 km wide) and very shallow (45 m deep) Bering Strait. The 450 km wide and 2500 m deep Fram Strait was long considered as the primary route of exchange of water with the North Atlantic (Aagaard and Greisman 1975; Hopkins 1991). However, recent investigation suggests that the flow through the Barents Sea is of equal or even higher importance (Maslowski, Marble, Walczowski, Schauer, and Semtner 2004). Even though the flow is restricted by the shallow shelf bathymetry, important water mass modification takes place which eventually contributes to the upper and intermediate water ventilation in the Central Arctic. The Nordic Seas are separated from the North Atlantic by the Greenland-Scotland ridge with a sill depth of approx. 600 m in the Denmark Strait, 500 m east of Iceland and 850 m in the Faroe-Bank Channel (Hansen and Østerhus 2000). Another exchange route is the Canadian Archipelago with outflows through the Smith, Jones and Lancaster Sounds that continue through the Labrador Sea into the western part of the North Atlantic.

1.3 The Arctic Climate

Atmospheric Circulation. The atmospheric circulation over the Arctic comprises of several components. Firstly, a zonally symmetric vertical overturning circulation associated with the large scale sinking of air and the resulting anti-cyclonic surface circulation. Secondly, a stationary planetary wave pattern accounts for the deviations from the zonal mean flows, and transient waves that explain most of the synoptic variability.

Arctic Oscillation. The complex interaction of these components leads to two preferred atmospheric states. These states are statistically identified by the Northern-Hemisphere Annual Mode (NAM), or popularly referred to as the Arctic Oscillation (AO) (Thompson and Wallace 2000) . Their regional manifestation in the Atlantic sector is the North Atlantic Oscillation (NAO) which is explored and monitored by Hurrell et al. (2000). Consensus exists that jet stream dynamics in the sub-tropics and

the lower-stratospheric vortex in the higher latitudes play key roles but the physical mechanisms are still under debate.

Ambaum and Hoskins (2002) proposed a theoretical framework, promoting that tropospheric jet stream variability over the Atlantic sector induces changes in the stratospheric polar vortex over the central Arctic. They suggest that with a positive NAO index associated intensification of the tropospheric jet over the North Atlantic sector impedes upward propagation of large-scale horizontal meanders which generally tend to decelerate the stratospheric jet by wave braking. In other words, the lack of wave breaking in the stratosphere results in a stronger than normal stratospheric jet. A lifting of the tropopause with an associated surface level pressure drop over the central Arctic is then followed from simple vorticity arguments. Yet, the feedback from the Arctic surface pressure drop on the NAO is still unclear.

In contrast, Haynes et al. (2000) and Thompson and Wallace (2000) favor the stratospheric downward control principle which basically promotes the opposite, i.e. that tropospheric variability over the Atlantic sector originates in the Arctic stratosphere. Therefore, the response to GHG emission of the variability modes is hardly understood even though GCM simulations project statistically significant trends to positive index values (Shindell et al. 1999), i.e. a more cyclonic surface wind field (Serreze et al. 2000).

Winter Circulation. The low pressures over the northeast North-Atlantic Ocean, labeled the Icelandic Low, and over the northern Pacific Ocean, labeled the Aleutian Low, together with the high pressure over the continents determine the lower tropospheric circulation during the winter months. The Siberian High directs air from Siberia and Eastern Europe on its western side into the high Arctic while the high pressure ridge over North America forces air southwards at the western side of Greenland. In this way a net transport establishes out of Eurasia into the Arctic, across the Arctic and south over North America. The Icelandic Low produces westerly winds over the eastern North Atlantic and south-westerly winds over the Norwegian Sea providing a second conduit for the mid-latitude air masses into the Arctic. Finally, the Aleutian Low tends to steer air that has crossed the Pacific from Asia up into Alaska, the Yukon, and the Bering Sea. During winter, i. e. the active season, these three routes into the Arctic - southerlies in the Norwegian Sea with 40%, over Eastern Europe/Siberia with 15%, and over the Bering Sea with 25%, account for about 80% of the annual south-to-north air transport (Iversen 1996).

Summer Circulation The summer pressure fields differ significantly from those of winter. The troposheric low-pressure cells weaken and the continental high-pressure cells vanish such that the northward transport from the middle latitudes decreases. The summer, or inactive season, accounts for only 20% of the annual south-to-north air transport, whereby the southerlies in the Bering Sea contribute with 5%, in eastern Europe/Siberia with 5% and in the Norwegian Sea with 10% (Iversen 1996).

The Northern-hemisphere Annual Mode, here referred to as Arctic Oscillation (AO), accounts for 20% of the natural atmospheric variability of the northern Hemisphere and

is associated with the strength of the polar vortex (Wallace and Thompson 2002). It carries much the same information as the NAO and their correlation exceeds 85% during the winter months. However, it is recognized that the AO by construction captures more hemispheric variability than the NAO. Since recent changes associated with the AO occurred far away from the NAO's center of action, i.e. in the Beaufort, Chukchi, East Sibirian and Laptev Sea (Johnson and Polyakov 2001), the AO formulation is preferred in this study. Moreover, influence of the North Pacific Decadal Oscillation on the Bering Sea and Mackenzie Basin (Stabeno and Overland 2001) and of the Southern Oscillation on the Baffin Bay Ice Climate (Newell 1996) have been reported. These are at least partly taken into account by the conventional AO index defined as the leading mode of surface pressure north of 20°N.

With a high winter AO index (or NAO index), the Icelandic Low intensifies and extends farther into the the Arctic across the Barents Sea and into the Kara and Leptev Seas (Johnson et al. 1999). This causes an increased wind transport east across the North Atlantic, across southern Europe and up into the Norwegian Sea. At the same time, strong winds are to be found over the Labrador Sea (Mysak 2001).

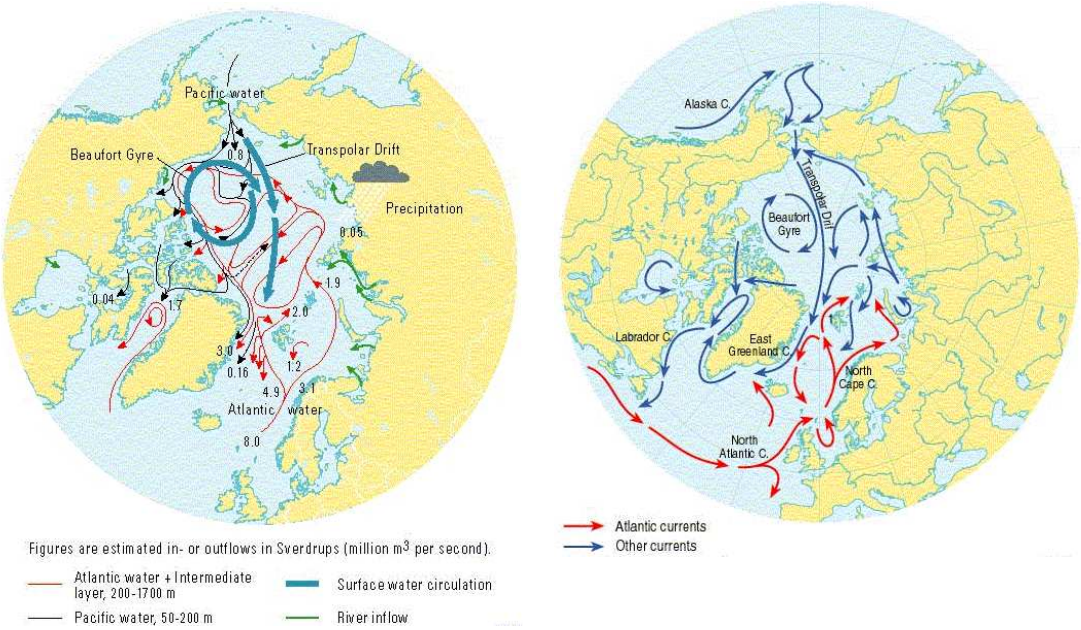

Figure 1.3: Circulation in the Arctic Ocean. (Macdonald and Bewers 1996)

Ocean Circulation and Hydrography. The Arctic Ocean hydrography is characterized by a cold, fresh surface, referred to as the Polar Surface Water, a warm salty intermediate layer, which has its origin in Atlantic Water, and waters that are near uniform in temperature and salinity, referred to as the Arctic Bottom Water.

Cold Halocline. The Temperature and salinity of the Polar Surface Water ranges from $-1.5°$ to $-1.9°C$ and 28 psu to 33.5 psu respectively. The Polar Surface Water may further be separated. The upper part is occupied shallow Polar Mixed Layer which extends down to 30-50 m only, and is close to the freezing point all year round. The lower part called the Cold Halocline extends to about 200 m depth and is characterized

by a strong gradient in salinity and the absence of any temperature gradient at the top. Waters occupying the Cold Halocline Layer cannot be formed by simple mixing of water masses i.e. no mixing lines crossing the Halocline Water have been detected in arctic Θ/S diagrams. Therefore, surface heat and freshwater fluxes related to sea ice processes are essential for the renewal of the Halocline Water (Aagaard et al. 1981). The problem with the details of its renewal, a convective and an advective solution have been proposed, and recent findings indicating an eastward retreat of the halocline are subject to active research (Steele and Boyd 1998). A consensus exists that the presence of the Cold Halocline and its changes have significant implications on the Arctic sea ice cover, since its strong salinity gradient prevents upwelling of intermediate, warm Atlantic Layer water (Steele and Boyd 1998; Wallace and Thompson 2002).

Atlantic Layer. The Atlantic Layer is found at intermediate depths at approx. 200-800m and is relatively warm and salty with temperature and salinity ranges of $0-3°C$ and 34.85-35.00 psu. Its water originates from the North Atlantic Drift which partially enters the Nordic Seas over the Iceland-Scotland ridges and then continues into the Arctic Ocean through the Fram Strait while mixing and cooling on its way.

Water Masses and Circulation. Figure 1.3 shows a simplified picture of the circulation in the Arctic. The Atlantic Layer Water circulates counter-clockwise, merges with the Modified Atlantic Water which enters from the Barents sea branch and after a cyclonic loop part of it exits somewhat modified through the Fram Strait again. The Arctic Ocean Deep Water occupies the the Eurasian Basin as the Eurasian Basin Deep Water and the Canadian Basin as the Canadian Basin Deep Water below 900m depth. With temperatures between $-0.7°C$ and $-0.8°C$ it is significantly colder than the Atlantic Water but still considerable salty with a salinity range of 34.9-35.00 psu. The Arctic Deep Water has it's origin in the Greenland Sea Deep Water and Norwegian Sea Deep Water entering through the Fram Strait.

Sea-Ice Distribution and Transports. The large-scale ice-drift in the Arctic can be decomposed into the Transpolar Drift and the Beaufort Gyre. Trajectory data from the International Buoy Program, with observations from 1979 to 1998, suggests two prominent drift modes. They are due to surface wind stress anomalies which are related to the positive and negative phase of the AO. During weak AO^- conditions the ice in the Transpolar Drift moves directly from the Laptev Sea to the Fram Strait, whereas during strong AO^+ conditions it takes a more cyclonic path across the Lomonosov Ridge and into the Canada Basin. In addition, the Beaufort Gyre retreats further into the Beaufort Sea while exporting less ice to the East Siberian Sea (Macdonald et al. 2002). This is illustrates schematically in Figure 1.4.

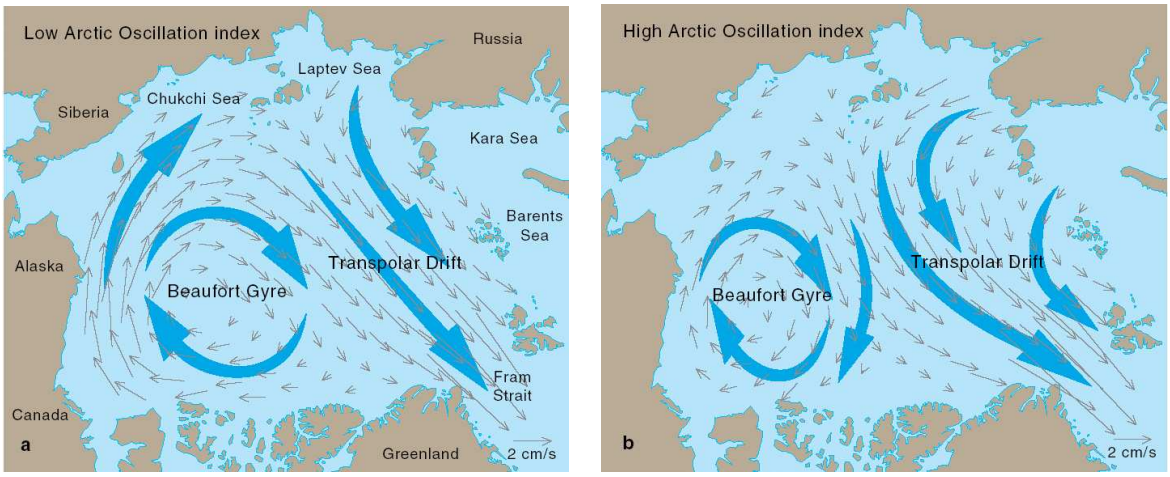

Figure 1.4: Observered ice drift pattern during the negative AO^+ and positive AO^- phase. (Macdonald 2002)

1.4 Thesis Objectives

This work has four main objectives

1. **To present a complete, comprehensive picture of transports, energy balance, and hydrological cycle of the Arctic Seas.** Simultaneous observational monitoring of the property exchanges of all major pathways is a major challenge and has not been achieved yet. In comparison to collecting observational data climate simulations are relative inexpensive. Furthermore, one does not need to wait for half a decade before starting to analyze variability on longer time scales.

2. **To provide products of simulated mass, heat and freshwater exchanges of the Arctic Seas for the present and future climate.** The purpose of this is to construct a database for later reference. Observational or simulation studies, for instance future experiments with the Bergen Climate Model or other climate models, can then use the results for easy comparison. In addition, the database can be used for other upcoming projects regarding Arctic climate variability. They might find useful information which we currently are not aware of.

3. **To explain natural variability of the Arctic climate system by identifying and quantifying internal mechanisms.** 300 years control simulation are available for exploring flux and exchange variability of the Arctic Seas on interannual and longer time scales. Here, we focus on identifying the relationships between different path ways, and the impacts of atmospheric forcing on these exchanges.

4. **To compare recent observed trends in the maritime Arctic with future projections.** The extrapolation of the present trends into the future is a common practice. But recent studies showed that trends derived from a few years of data only are in most cases not representative for long term climate trends. Likely, various fractions of the signals reflect internal variability which has little relation to antrophogenic forcing.

Related to the main objectives, a set of more concrete specified problems are addressed. These are divided into the three categories: mass, heat and freshwater. In turn, these build the basis of the chapters.

1.5 Outline of the Thesis

In chapter 2, we outline theory and computational details behind the budget products. Particularly two different concepts are explored, i.e. how to assess heat and freshwater transports. Furthermore, a small set of statistical analyzing techniques is introduced.

Chapter 3 provides a description of the Bergen Climate Model, a state-of-the-art global coupled model, various experiments are described and a short evaluation for the Arctic region is performed.

Chapter 4 describes the ocean circulation, currents and mass exchanges of the Arctic Seas as well as their relation to the atmospheric circulation.

At the beginning of Chapter 5 the global context for the energy balance is defined through investigating the meridional heat transports in ocean and atmosphere. Then this picture is refined by focusing on the heat budgets of the Arctic Seas. Moreover, we address the propagation of warm water signals from the North Atlantic into the Barents Sea via the Nordic Seas as well as their implications on winter sea-ice conditions and potential feedbacks with the atmosphere.

Chapter 6 presents simulated freshwater budgets with emphasis on the role of river discharges into the Arctic shelf seas. Projections are explored of how changes in the hydrological cycle might effect the freshwater balance globally and the Arctic Seas in particular.

Finally, chapter 7 summarizes and combines the main aspects of the preceding chapters and offers some general conclusions.

In appendix A tabulated mass, heat and freshwater exchanges of the Arctic Seas are listed.

In appendix B an Internet interface for visualization of the BCM output fields is introduced.

The temporal context of the thesis is very much defined by the extensive use of the concepts of present climate mean state, natural variability from inter-annual to multi-decadal time scale, and future projections for the next couple of decades.

Chapter 2

Methodology

In this chapter we will outline how the presented products are generated and review theory where necessary. The first part addresses the computation of the advective and diffusive components of the direct transports estimates. In the following, the residual method for the computation of meridional atmosphere and ocean heat and freshwater transports is presented. Supplementary, a set of statistical tools is introduced. These comprise the identification and quantification of climate changes with linear regression, the use of correlation studies to detect coherent climate signals, and the application of Empirical Orthogonal Functions (EOF) analyses.

2.1 Direct Transport Estimates

Advective Transports. The products presented are vertically integrated storages, fluxes and divergences. The analytical, exact definitions are reformulated into discrete equations. An attempt to optimize the approximations has been made by fully exploiting all available grid information and computing with highest numerical precision. To calculated the budgets for any property F that represents a quantity per m^3 volume we proceed illustrated as in table 2.1.

The properties considered are

$$F_{mass} = \rho \tag{2.1}$$

$$F_{heat} = \rho\, c_{p_{sw}} (T - T_{ref}) \tag{2.2}$$

$$F_{freshwater(liquid)} = -\rho \frac{S - S_{ref}}{S_{ref}} \tag{2.3}$$

$$F_{freshwater(ice)} = l_{ice}\, h_{ice}\, f_{ice} \tag{2.4}$$

A reference temperature of $T_{ref} = -0.1°C$ and a reference salinity of $S_{ref} = 34.8$ have been applied. The volumetric latent heat for ice $c_{ice} = 3.2 \cdot 10^8\, JK^{-1}m^{-3}$ and the specific heat for sea water $c_{p_{sw}} = 3987\, JK^{-1}kg^{-1}$ are taken from the model. The conversion from salt to freshwater fluxes in equation 2.3 is further discussed in Howard and Cresswell (2000).

Grid Interpolations. Note that special care is paid to the conservation of mass. For the cell boundaries no layer thickness information is stored, but it can be reconstructed with the help of the bathymetry at the u and v points. This is done by equation 2.7 and 2.9. The rule the model applies is that the depth of the layer top or bottom at an u or v point is the minimum between the bathymetry at that point and the arithmetic mean of the corresponding depths at the four adjacent cell mid-points. Thereby, with depth we mean the absolute distance from the surface i.e. positive is downward. Test computations with a more simplified, inaccurate interpolation scheme exhibited mass residuals of several per cent. In comparison the products presented have residuals which are one or two orders smaller in magnitude.

Table 2.1: Budget and flux computations - analytical exact equations vs. discrete approximations.

Storage

$$
\begin{aligned}
< \mathbf{S}(x,y,t) >_{t_1,t_2} &= \frac{1}{t_2-t_1}\int_{t_1}^{t_2}\int_{z_{bottom}}^{z_{surface}} F(x,y,z,t)\,dz\,dt \\
\hookrightarrow \quad \mathbf{S}^p_{i,j,n} &= \frac{1}{(t_2-t_1)\Delta t}\sum_{l=t_1}^{t_2}\sum_{k=1}^{N_l} F^p_{i,j,k,l}\,\Delta z^p_{i,j,k,l}\Delta t \qquad (2.5)
\end{aligned}
$$

Flux in x-grid direction

$$
\begin{aligned}
< \mathbf{U}(x,y,t) >_{t_1,t_2} &= \frac{1}{t_2-t_1}\int_{t_1}^{t_2}\int_{z_{bottom}}^{z_{surface}} u(x,y,z,t)\,F(x,y,z,t)\,dz\,dt \\
\hookrightarrow \quad \mathbf{U}^u_{i,j,n} &= \frac{1}{(t_2-t_1)\Delta t}\sum_{l=t_1}^{t_2}\sum_{k=1}^{N_l}\frac{1}{2}\left(F^p_{i+1,j,k,l}+F^p_{i,j,k,l}\right)u^u_{i,j,k,l}\,\Delta z^u_{i,j,k,l}\,\Delta t \qquad (2.6) \\
where \quad \Delta z^u_{i,j,k,l} &= \min\Big(H^u_{i,j},\sum_{\tilde{k}=1}^{k}\frac{z^p_{i+1,j,\tilde{k},l}+z^p_{i,j,\tilde{k},l}}{2}\Big)-\min\Big(H^u_{i,j},\sum_{\tilde{k}=1}^{k-1}\frac{z^p_{i+1,j,\tilde{k},l}+z^p_{i,j,\tilde{k},l}}{2}\Big) \qquad (2.7)
\end{aligned}
$$

Flux in y-grid direction

$$
\begin{aligned}
< \mathbf{V}(x,y,t) >_{t_1,t_2} &= \frac{1}{t_2-t_1}\int_{t_1}^{t_2}\int_{z_{bottom}}^{z_{surface}} v(x,y,z,t)\,F(x,y,z,t)\,dz\,dt \\
\hookrightarrow \quad \mathbf{V}^v_{i,j,n} &= \frac{1}{(t_2-t_1)\Delta t}\sum_{l=t_1}^{t_2}\sum_{k=1}^{N_l}\frac{1}{2}\left(F^p_{i,j+1,k,l}+F^p_{i,j,k,l}\right)v^v_{i,j,k,l}\,\Delta z^v_{i,j,k,l}\,\Delta t \qquad (2.8) \\
where \quad \Delta z^v_{i,j,k,l} &= \min\Big(H^v_{i,j},\sum_{\tilde{k}=1}^{k}\frac{z^p_{i,j+1,\tilde{k},l}+z^p_{i,j,\tilde{k},l}}{2}\Big)-\min\Big(H^v_{i,j},\sum_{\tilde{k}=1}^{k-1}\frac{z^p_{i,j+1,\tilde{k},l}+z^p_{i,j,\tilde{k},l}}{2}\Big) \qquad (2.9)
\end{aligned}
$$

Divergence

$$
\begin{aligned}
< \mathbf{D}(x,y,t) >_{t_1,t_2} &= \frac{1}{t_2-t_1}\int_{t_1}^{t_2}\int_{z_{bottom}}^{z_{surface}}\Big(\lim_{\omega\to 0}\iint_{\omega} F(x,y,z,t)\,\vec{u}(x,y,z,t) \\
&\quad \circ\vec{\partial}\omega(x,y)\Big)\,dz\,dt \\
\hookrightarrow \quad \mathbf{D}^p_{i,j,n} &= \frac{\mathbf{U}^u_{i+1,j,n}s^u_{i+1,j}-\mathbf{U}^u_{i,j,n}s^u_{i,j}+\mathbf{V}^v_{i,j+1,n}s^v_{i,j+1}-\mathbf{V}^v_{i,j,n}s^v_{i,j}}{A^p_{i,j}} \qquad (2.10)
\end{aligned}
$$

Diffusive Transports. Turbulent heat and freshwater fluxes are generated by eddies or other oscillations around the mean state of the flow field that are not resolved by the model, or that have time scales shorter than the storage time. Mathematically, they show up when time averaging the equations of motion (e.g. the Navier-Stokes Equation) in form of covariance terms of the velocity field with the advective variables including momentum itself. For instance, the turbulent meridional momentum flux of zonal momentum is $\overline{u'v'}$ and can further be transformed to $-\rho\overline{u'v'}$ which is called Reynold Stress. In analogy, $-\rho\overline{u'T'}$ is proportional to the turbulent zonal heat flux and called Reynold Flux (Pond and Pickard 1978). Since in the model these are neither in space nor in time explicitly resolved, they need to be parametrized.

As eddies always act to reduce the gradients, a common procedure is to write the parametrized fluxes as the gradient of the properties times an eddy-coefficient, e.g. $A_x\frac{\partial T}{\partial x}$. The eddy coefficients can be a function of stability, mean current sheer, etc. Note that the parametrization has the same form as the molecular diffusion, hence the name turbulent diffusion, though it is typically several orders of magnitudes larger. In the MICOM model, grid spacing dependent eddy coefficients are chosen for the parametrization of the heat diffusion, i.e. the coefficients are proportional to the grid-cell dimensions. They have the form

$$\frac{A_x}{\Delta x} = u_{diff} = constant \tag{2.11}$$

and

$$\frac{A_y}{\Delta y} = v_{diff} = constant. \tag{2.12}$$

The quotients are labeled diffusion velocities u_{diff} and v_{diff} since the units of diffusivity over length are the same as those of a velocity. These are set to a constant, default model value of $1\,cm/s$ (Bleck et al. 1992). In that way, the turbulent heat fluxes may be written in the discrete form

$$F_x^{eddy} = -u_{diff}(\Delta_x T) \qquad and \qquad F_y^{eddy} = -v_{diff}(\Delta_y T) \tag{2.13}$$

respectively. Δ_x and Δ_y are difference operators with $\Delta_x T|_{i,j} = T|_{i,j} - T|_{i-1,j}$ and $\Delta_y T|_{i,j} = T|_{i,j} - T|_{i,j-1}$. Since the diffusion velocities are neither depth nor time dependent, the integration of the fluxes can be simplified to the integration of the temperature gradient alone, i.e.

$$\frac{1}{t_2 - t_1}\int_{t_1}^{t_2}\int_{-h}^{0} F_x^{eddy}(\Delta_x T)dzdt = F_x^{eddy}\big(\frac{1}{t_2 - t_1}\int_{t_1}^{t_2}\int_{-h}^{0}(\Delta_x T)dzdt\big). \tag{2.14}$$

In other words, it is possible to compute climatologies of the turbulent diffusion directly from the climatological temperature field.

However, freshwater is diffused implicitly since temperature and density (layer thickness) are the prognostic variables in the model. The layer thickness is proportional to the vertical density gradient which in turn is related to salinity and temperature through the equation of state. So, both layer thickness and temperature diffusion

contribute non-linearly to the salt diffusion. For this reason, a reconstruction of the freshwater fluxes is not attempted.

2.2 Residual Transport Estimates

The residual method is used to compute energy transport and transport divergence in the atmosphere and ocean. It provides a vertical integrated picture and in simplified form also a zonally and time integrated one. It's basic idea is based on the Gaussian theorem outlined in equation 2.15, that the integral of the total divergence over any region is equal to the flux through it's boundaries.

$$\iiint_{\Omega} \nabla \cdot \vec{F}\, dV \;=\; \iint_{\partial\Omega} \vec{F} \cdot d\vec{A} \tag{2.15}$$

Ω presents a three dimensional region which underlies certain constrains, e.g. is mathematically compact, and $\partial\Omega$ is it's boundary with $d\vec{A}$ the differential surface element times the surface normal vector that points outside the region. Observe that this relations also holds for the two dimensional case. Applied to the atmosphere we say that for every horizontal surface element the difference of the vertical heat fluxes between the top and bottom of the atmosphere plus the vertically integrated energy storage tendency is balanced by the vertical integrated net energy flux through the boundaries of the surface element. The most common exercise is to integrate all energy divergences north of a latitudinal circle which provides the northward energy flux (with a negative sign) through that circle. Equation 2.16 outlines the mathematical formulation.

$$\begin{aligned} &\frac{2\pi}{360} \int_{\lambda=90^\circ S}^{\lambda=\lambda'} \int_{\phi=0^\circ E}^{\phi=360^\circ E} [F_{toa} - F_{surf}](r_{earth} \cos(\frac{2\pi}{360}\lambda) d\phi)(r_{earth} d\lambda) \\ &\quad = \frac{2\pi}{360} \int_{z=z_{surf}}^{z=z^{toa}} \int_{\phi=0^\circ E}^{\phi=360^\circ E} T_{meridional}|_{\lambda=\lambda'} (r_{earth} \cos(\frac{2\pi}{360}\lambda') d\phi) dz \end{aligned} \tag{2.16}$$

Trenberth and Caron (2001) successfully applied this method to estimate meridional atmosphere and ocean heat transports using surface fluxes from the NCEP/NCAR (Kalney et al. 1996) and ECMWF re-analyzed datasets and top of the atmosphere (TOA) radiation data from the Earth Radiation Budget Experiment (ERBE).

However, the method requires a closed balance with only one unknown in the atmosphere and the ocean. Unfortunately, the atmospheric part of the BCM doesn't perfectly conserve atmospheric water, i.e. latent heat, which leads to an artificial sink of about 0.5 TW globally with an unknown spatial distribution. Based on the assumption that this error is systematic rather than stochastic we can expect that during the integration from pole to pole it just sums up with negligible error compensation. That means if one starts in the south, smallest errors are expected close to the South Pole and largest close to the North Pole, and vice versa if one starts at the North Pole. Therefore, we argue that a linear weighted combination of both solution can provide a

compromise for both hemispheres with low systematic errors in the high latitudes and satisfy the constraint that the meridional flux goes to zero at the poles. Consequently, the budget generated is closed by construction. The linear combination applied in this work is outlined in equation 2.17

$$f(\lambda) = a\, f_{S-N}(\lambda) + b f_{N-S}(\lambda), \quad a = \frac{90^\circ - \lambda}{180^\circ}, \quad b = \frac{90^\circ + \lambda}{180^\circ} \tag{2.17}$$

where f_{N-S} and f_{S-N} denote the 'north' and 'south' solutions respectively. Note that the sum $a(\lambda) + b(\lambda) = 1$ which implies that if both solutions are the same then the linear combination is also the same. The 'north' and 'south' solutions indicate the systematic error or imbalance of the system like illustrated in figure 2.1.

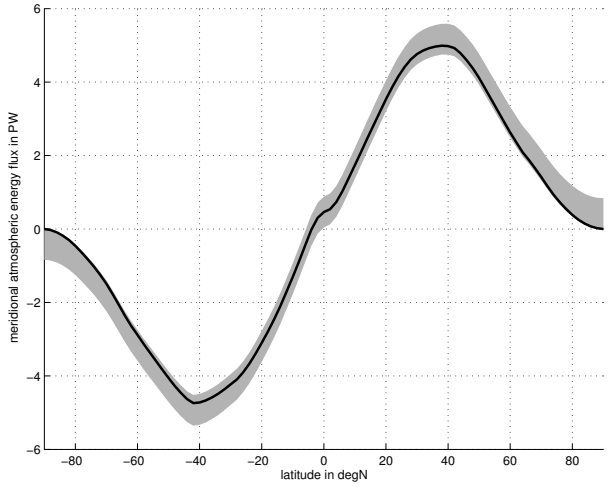

Figure 2.1: Mean meridional atmospheric energy transport derived from the 300yr BCM control integration. The upper limit of the shaded area is the solution with the integration starting from the South Pole and the lower starting from the North Pole. The solid line presents a linear combination of both solutions.

2.3 Statistical Analysis Tools

Quantifying Climate Changes with Linear Regression. The problem is to quantify the impact of CO_2 doubling on climate variables, e.g. surface temperature or surface pressure. A method proposed in Holland and Bitz (2003) is to take the average of the years 60 to 80 as representative for double CO_2 conditions and then to subtract the mean of the full 80 year control run. It can be shown that this approach is not robust with respect to internal decadal variability of the climate system which leads to disagreement between different General Circulation Models (GCMs) and also ensemble runs of single GCMs. Here, a more robust method is chosen. The time series of control and double CO_2 experiment are assimilated with a linear fit and consequently the difference after exactly 70 years is read. In this case all available years are used to process the double CO2 run, i.e. the decadal variability is partially filtered out.

Detecting Coherent Climate Signals with Correlations Studies. The most basic, but very successful method to identify statistical links in geophysical data is the correlation study of time series. Primarily, the result provides an error estimate of a proposed linear relation derived by regression, with a high correlation value for the perfect linear case. Or more precisely, the correlation coefficient-squared is equal to the fraction of variance explained by a linear least-squares fit between two variables. (Hartmann 2004)

To detect non-linear relations methods like composite studies are more appropriate. Since the correlation value highly depends on the size and characteristics of the data set additional confidence or significance information should be supplied. In the following, a very simple but presumably the most frequently used significance test is presented.

Concept of Independent Data Points. Preparatory, the concept of the dataset-size is introduced. The size of a time series is defined as the number of independent data points N^* (sometimes referred to as degrees of freedom). If the frequency spectrum consists of white noise, as it can be assumed in the case of a random time series, then the number of independent data points N^* equals the actual number of data points N. The frequency spectra of physical time series are most likely red noise, i.e. these exhibit some auto-correlation which drops to $1/e$ after a time lag τ. The period τ can be used as a threshold to define the minimum temporal distance between two data points in order to be considered as independent. It follows that $N^* = \frac{T}{\tau}$ and the number of independent data points of two time series is not smaller than

$$N^* \geq \frac{T}{\max(\tau_a, \tau_b)} \tag{2.18}$$

where T is the total length of the time series, and τ_a and τ_b are the time lags where the auto-correlation drops to $1/e$ for each of the two time series (Leith 1973). To be on the safe side, we chose N^* equal to $\frac{T}{\max(\tau_a,\tau_b)}$.

Significance Test - Rejection of the Null Hypothesis. By rejecting the hypothesis that the correlation is zero the proposition of existence of a link between two time series is supported. Since the hypothesis is that the true correlation of the two variables is zero, the corresponding distribution for correlation realizations should be centered in the interval $[-1, 1]$. Hence, one can assume that the distribution density function is symmetric and therefore directly apply the Student's t distribution. The corresponding transformation/statistic is

$$t = \frac{r\sqrt{N^* - 2}}{\sqrt{1 - r^2}}. \tag{2.19}$$

From the student t-distribution follows that for 95% percent of all correlation realizations t the inequality $-t_{0.025} > t > t_{0.025}$ holds. Thus, the probability that our realization of t is outside this interval is 5%. If this is indeed the case then the null hypothesis is reject with a confidence of 95%. Table 2.2 list bounds for t for various confidence levels and degrees of freedom.

It is emphasized here, that the statistical significance is merely a prerequisite but does not prove the existence of a proposed causal relation. Generally, climate datasets

Table 2.2: t-statistic critical values for one-tailed test with ν degrees of freedom (Hartmann 2004).

ν	0.2	0.1	0.05	0.025	0.01	0.005	0.001	0.0005	0.0001
1	1.3764	3.0777	6.3137	12.706	31.821	63.656	318.29	636.6	3185.3
2	1.0607	1.8856	2.9200	4.3027	6.9645	9.9250	22.328	31.600	70.706
3	0.9785	1.6377	2.3534	3.1824	4.5407	5.8408	10.214	12.924	22.203
4	0.9410	1.5332	2.1318	2.7765	3.7469	4.6041	7.1729	8.6101	13.039
5	0.9195	1.4759	2.0150	2.5706	3.3649	4.0321	5.8935	6.8685	9.6764
6	0.9057	1.4398	1.9432	2.4469	3.1427	3.7074	5.2075	5.9587	8.0233
7	0.8960	1.4149	1.8946	2.3646	2.9979	3.4995	4.7853	5.4081	7.0641
8	0.8889	1.3968	1.8595	2.3060	2.8965	3.3554	4.5008	5.0414	6.4424
9	0.8834	1.3830	1.8331	2.2622	2.8214	3.2498	4.2969	4.7809	6.0094
10	0.8791	1.3722	1.8125	2.2281	2.7638	3.1693	4.1437	4.5868	5.6939
11	0.8755	1.3634	1.7959	2.2010	2.7181	3.1058	4.0248	4.4369	5.4529
12	0.8726	1.3562	1.7823	2.1788	2.6810	3.0545	3.9296	4.3178	5.2631
13	0.8702	1.3502	1.7709	2.1604	2.6503	3.0123	3.8520	4.2209	5.1106
14	0.8681	1.3450	1.7613	2.1448	2.6245	2.9768	3.7874	4.1403	4.9849
15	0.8662	1.3406	1.7531	2.1315	2.6025	2.9467	3.7329	4.0728	4.8801
16	0.8647	1.3368	1.7459	2.1199	2.5835	2.9208	3.6861	4.0149	4.7905
17	0.8633	1.3334	1.7396	2.1098	2.5669	2.8982	3.6458	3.9651	4.7148
18	0.8620	1.3304	1.7341	2.1009	2.5524	2.8784	3.6105	3.9217	4.6485
19	0.8610	1.3277	1.7291	2.0930	2.5395	2.8609	3.5793	3.8833	4.5903
20	0.8600	1.3253	1.7247	2.0860	2.5280	2.8453	3.5518	3.8496	4.5390
21	0.8591	1.3232	1.7207	2.0796	2.5176	2.8314	3.5271	3.8193	4.4925
22	0.8583	1.3212	1.7171	2.0739	2.5083	2.8188	3.5050	3.7922	4.4517
23	0.8575	1.3195	1.7139	2.0687	2.4999	2.8073	3.4850	3.7676	4.4156
24	0.8569	1.3178	1.7109	2.0639	2.4922	2.7970	3.4668	3.7454	4.3819
25	0.8562	1.3163	1.7081	2.0595	2.4851	2.7874	3.4502	3.7251	4.3516
26	0.8557	1.3150	1.7056	2.0555	2.4786	2.7787	3.4350	3.7067	4.3237
27	0.8551	1.3137	1.7033	2.0518	2.4727	2.7707	3.4210	3.6895	4.2992
28	0.8546	1.3125	1.7011	2.0484	2.4671	2.7633	3.4082	3.6739	4.2759
29	0.8542	1.3114	1.6991	2.0452	2.4620	2.7564	3.3963	3.6595	4.2538
30	0.8538	1.3104	1.6973	2.0423	2.4573	2.7500	3.3852	3.6460	4.2340
40	0.8507	1.3031	1.6839	2.0211	2.4233	2.7045	3.3069	3.5510	4.0943
50	0.8489	1.2987	1.6759	2.0086	2.4033	2.6778	3.2614	3.4960	4.0140
75	0.8464	1.2929	1.6654	1.9921	2.3771	2.6430	3.2024	3.4249	3.9116
100	0.8452	1.2901	1.6602	1.9840	2.3642	2.6259	3.1738	3.3905	3.8615
∞	0.8416	1.2816	1.6449	1.9600	2.3264	2.5758	3.0902	3.2905	3.7189

may comprise several Terra-bytes of data with thousands of statistical highly significant links. Ideally, a physical basis for a proposed link should exist prior to the statistical analysis. The sequence of analyze steps is then to state the significance level, to state the null hypotheses, to state the statistics used, and finally to evaluate the statistic and to state the conclusion. Thus, it is questionable to compute the statistic without expecting a causal link and then state what significance it has passed.

Finding Leading Modes with PC/EOF Analysis. *Application.* Generally, Empirical Orthogonal Function (EOF) analysis is used to effectively reduce datasets while preserving as much information as possible. This linear method has a wide range of applications in all fields (see Hartmann (2004) for examples). For instance, in climatology it suggests a solution to the problem reducing the information of the entire atmospheric circulation to a small set of time series and spatial patterns.

Mathematical Background. We briefly outline the mathematical formulation of the problem which leads to algorithms used to compute EOF/PCs. The starting point is a two dimensional dataset, for instance with a spatial dimension m and a time dimension n. The data can then be organized in matrix form $M_{m\times n}$. Next, a projection is considered defined by the projection vector $u_{1\times m}$ which has a fixed length.

The leading principal component is now identified as the linear projection of the

dataset M

$$PC1 \equiv uM \tag{2.20}$$

such that the sum over all variance estimates of the time series is maximum

$$\sum_m var(uM) \equiv (uM)(uM)^t = maximum. \tag{2.21}$$

The projection vector u is the corresponding spatial pattern $EOF1$ of the leading principal component $PC1$. The extreme value problem is solved by setting all partial derivatives

$$\frac{\partial}{\partial u_i}(uM)(uM)^t = 0, \quad i = 1, \ldots, m \tag{2.22}$$

to zero. This provides a set of m linear equation. Replacing the projection vector u with a projection matrix $U_{n\times m}$ the problem can be generalized to a classical eigenvalue problem. A Single Value Decomposition algorithm can be applied to solve the set of linear equation for u. The advance of using a SVD algorithm is that in most cases it provides sensible solutions even if the problem is under or over-determined i.e. $n < m$ or $n > m$. (Hartmann 2004)

Empirical Orthogonal Function Recipe. First, in every spatial point the seasonal cycle is removed by subtracting the January mean from all January months, the February mean from all February months etc. In case seasonal or annual analyzes are desired additional averaging is performed. Then the data is weighted with the square root of the cell area, which is equivalent with weighting the variance with the cell area. Since the idea of the method is to maximize the variance this is considered the most appropriate option. Now, the principle component analysis is performed by a robust single value algorithm. After the PCs have been normalized, regression on the de-seasoned original data is performed. Because of the similarity with the strictly defined EOFs the resulting spatial patterns are labeled as EOFs.

EOF/PC Interpretation and Misinterpretation. A very visual and intuitive demonstration for misinterpretation of EOFs is present by Dommenget and Latif (2001). As a rule, EOF patterns should be treated with care and supported by other statistical tools.

Chapter 3

Bergen Climate Model

3.1 Model Description

The following model description outlines only the most relevant features for this study. A more complete and detailed description is found in Furevik et al. (2003).

General. The global synchronously coupled atmosphere-ocean model referred to in this study consists of the atmospheric model ARPEGE/IFS and a global version of the ocean model MICOM. It is mainly designed and configured to address the dynamics and development of the recent and near-future climate, i.e. to perform integrations over approximately 100 to 500 years. Special effort has been put into the representations of the high latitudes as the resolution increases towards the poles.

Vertical Coordinates. There are 31 vertical layers in the atmosphere, ranging from the surface up to 10 hPa pressure level. Compared with most climate models, this is a relatively high resolution of the troposphere and the lower stratosphere. Moreover, in lower levels terrain following hybrid coordinates are used. There are 24 isopycnical layers in the ocean, ranging from $\sigma_\theta = 23.54\,kg/m^3$ to $\sigma_\theta = 28.10\,kg/m^3$ potential density layers referenced to surface pressure.

Horizontal Coordinates. The horizontal grid cell distribution of ocean and atmosphere configuration are shown in figure 3.1. The horizontal grid of the spectral atmospheric model T_L63 is linear with 64 nearly equidistant latitudes and a spectral truncation of the wave number 63. The curvlinear ocean grid is almost regular with horizontal grid spacing of approximately $2.4^\circ \times 2.4^\circ$. The meridional resolution is increasing to 1.2° near the Equator and the reolution is also increasing towards the model poles over Siberia and Antarctica.

Sea-Ice. The sea-ice model is an integrated part of the ocean model and shares the same grid. The thermodynamics follow Drange and Simonsen (1996), based on

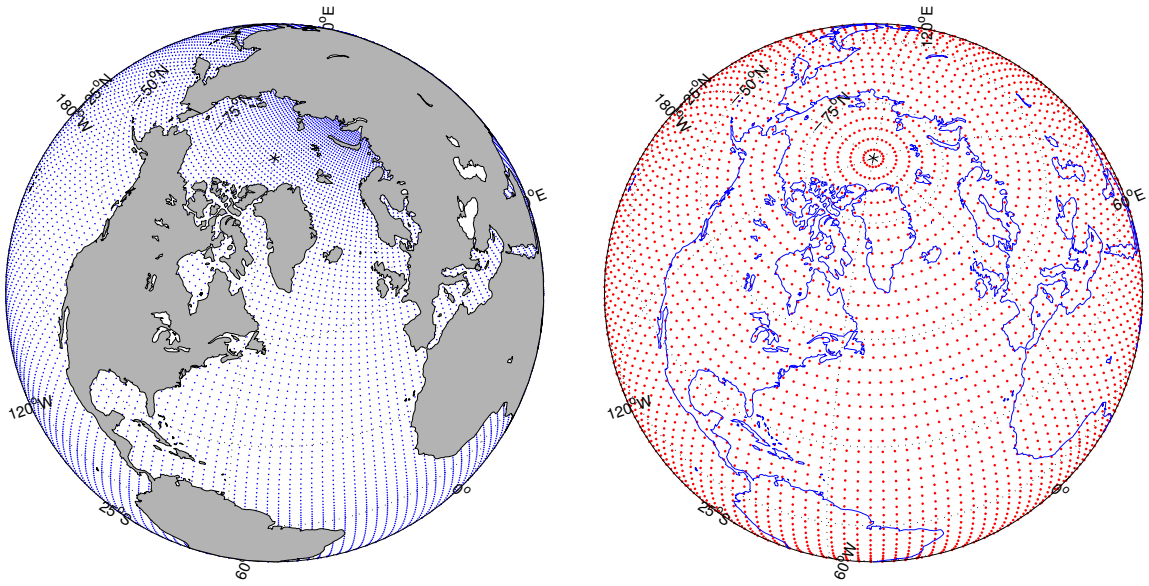

Figure 3.1: Ocean *(left)* and atmospheric grid *(right)* of the BCM model.

Semtner (1976), Parkinson and Washington (1979) and Fichefet and Gaspar (1988). The dynamics are based on the viscous-plastic rheology of Hibler (1979) with the modifications of Harder (1996).

Runoff. For the parametrization of the continental runoff the *Total Runoff Integration Pathways* (TRIP) dataset (Oki 1998) is used to define the catchment areas. An e-folding time lag of one week is used for the transportation from the catchment area to the adjacent ocean grid cell (Furevik et al. 2003).

Special Features. Non-standard features of the atmospheric model are the convective gravity-wave drag parametrization from Bossuet et al. (1998), a new snow scheme from Douville et al. (1995), an increase of the orographic wave drag Lott (1999), and modifications in deep convection and soil vegetation schemes. In the ocean the Gaspar (1988) formulation for the turbulent kinetic energy closure in the mixed layer is used. Instead of salinity and potential density, salinity and temperature are chosen as prognostic variables in the mixed layer.

3.2 Model Experiments

The common strategy or practice in the climate model community is to run one reference experiment representing present day or pre-industrial climate as well as a number of perturbation experiments that can be compared with the reference climate. In our case the reference climate is a 300 years long control experiment and the perturbation

experiments are a set of five anthropogenic emission experiments. Some details of the experimental setup will be introduced in this section.

Control Climate Simulation. Preceding the actual control experiment the ocean model is spun up for 125 years. The hydrography is initialized with a Levitus climatology whereas the sea ice is set to a constant thickness at the integration start. During the spin-up period the ocean model is forced with NCEP/NCAR reanalyzed data (Kalney et al. 1996) at the surface as described in Bentsen and Drange (2000). The surface temperature and salinity are relaxed against the Levitus climatology (Levitus and Boyer 1994). Over a 30 years time period the relaxation time scale is increased from 10 days to 30 days. During the last part of that period the relaxation fluxes are stored and used to calculate quasi-weekly flux adjustment terms for the actual control and the perturbation experiments.

The atmospheric model is initialized with a standard atmosphere based on the ECMWF products. The external forcing is limited to climatological solar forcing whereas no other forcing are prescribed in the ocean.

CO_2 Emission Experiments. The double CO_2 scenario experiments follow conventions defined by the Coupled Model Intercomparison Project (CMIP2) (Covey et al. 2003). A 80 years long control run is performed with a constant CO_2 level that compares to recent values. Then, a second run is performed with a CO_2 level which increases 1% per year for 80 years. After 70 years the CO_2 has finally reached twice the initial value. Several proposition are made of how to measure the impact of the CO_2 doubling on climate variables like averaged surface air temperature.

Output Variables The model data explored in this study comprise variables from the BCM atmospheric part ARPEGE, the ocean part MICOM and the sea-ice module. Partly, these exhibit different pre-averaging periods as a result of the independent post-processing.

The daily averaged fields investigated are

- Sea-ice velocity u and v components
- Sea-ice concentration
- Sea-ice thickness
- Snow depth

The 'weekly' (6 days) averaged fields comprise

- Ocean layer depth
- Ocean velocity u and v components
- Ocean temperature

- Ocean Salinity

The monthly averaged fields comprise

- Surface latent heat flux
- Surface sensible heat flux
- Surface net short-wave radiation
- Surface net long-wave radiation
- Top Of the Atmosphere (TOA) net short-wave radiation
- Top Of the Atmosphere (TOA) net long-wave radiation
- Total precipitation rate
- Surface evaporation rate (includes transpiration and sublimation)

3.3 Model Performance

An extensive evaluation of the model mean state, climatic drifts, atmospheric and ocean circulation, leading variability modes, etc. is presented for a global scale in Furevik et al. (2003). In this section, we focus on features of the simulated atmosphere and ocean which are confined to the Arctic region and therefore relevant for the discussion of our results. These comprise the atmospheric circulation or pressure field over the Arctic, the Arctic Ocean circulation and hydrography, the sea-ice extent, and the sea-ice thickness distribution.

Atmospheric Circulation. This work is aimed to describe the Arctic Ocean. Thus, regional features of the mean state, variability, trends, and seasonal cycle of the atmospheric circulation over the Arctic cannot be addressed in full detail. Instead we will make use of atmospheric circulation indices and relate these to simulated changes in the Arctic Seas. Since we address the complete Arctic for comparison with other studies like Black (2001) and Polyakov and Prushutinsky (1999) we have chosen to look at the Arctic Oscillation index (also referred to as Northern Annular Mode, see Thompson and Wallace (2000)). Furthermore, annual means only are considered. Because the active season dominates the atmospheric variability, the annual and winter indices are virtually identical and therefore not distinguished in this study.

Simulated Arctic Oscillation. In figure 3.2 the spatial pattern of the AO is presented for the BCM control run *(top-left panel)* and the NCEP/NCAR dataset *(top-right panel)*. For their computation the same algorithm has been applied on both datasets. Both, the BCM and NCEP/NCAR AO show the zonally symmetric behavior described in (Thompson and Wallace 2000) and their overall agreement is good. Nevertheless, the high pressure center over the North Atlantic sector extends somewhat further into the European Mediterranean in the observational based NCEP/NCAR dataset. Another

difference is the stronger than observed signature of the Pacific storm track variability in the BCM data which in addition exhibits an unrealistic high correlation with the atmospheric variability over the North Atlantic. Thus the Atlantic-Pacific teleconnection is too strong compared to observations. This has to be taken into account when discussing responses on the Pacific side of the Arctic Ocean.

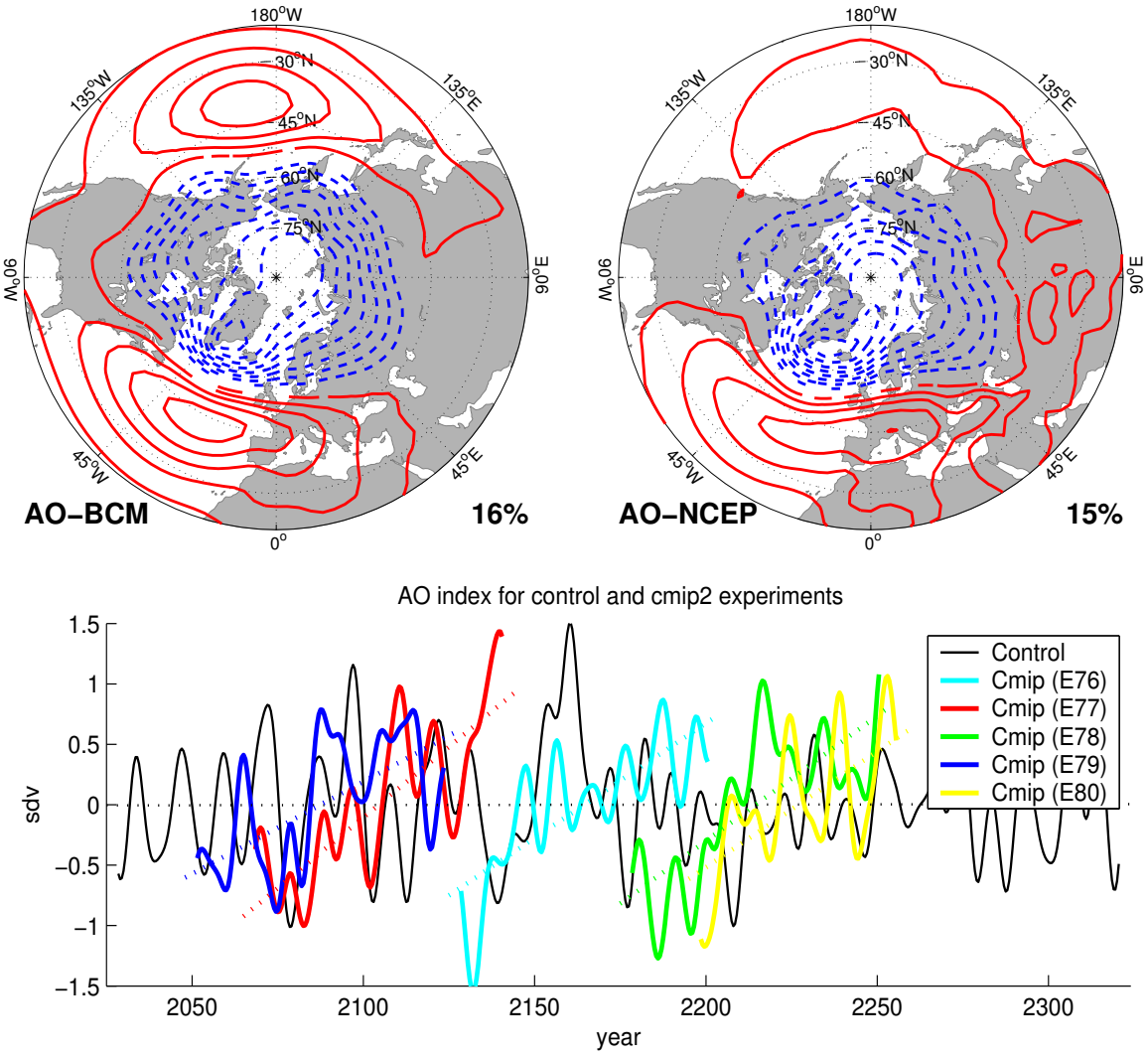

Figure 3.2: Observed and simulated Arctic Oscillation. The top panels show observed and simulated spatial AO patterns, i. e. SLP regressed on the monthly AO index of 50 years NCEP *(right)* reanalysed data and the 300 years BCM *(left)* control experiment. Trends of annualy averaged monthly AO index from the double CO_2 experiments are presented in the lower panel.

In the lower panel of figure 3.2 smoothed time series of the leading mode of monthly mean sea level pressure are shown for the BCM control and greenhouse experiments. Despite the dominating inter-annual variability, distinct positive trends which are all significant at 95% levels are shown for all greenhouse experiments. They are due to a reduction in sea level pressure (SLP) in the high Arctic which dynamically implies a tendency to more cyclonic motion.

Arctic Oscillation Composite Study. There is no evidence that one should expect a linear ocean response to changes in the Atmospheric circulation. Regression maps might therefore be misleading. Nevertheless, the persistence of an atmospheric circulation state over several years, or the occurrence of extreme single events are likely to leave a signature in the ocean. In this study the latter is addressed by the employment of an Arctic Oscillation composite. Here, two subsets are created which comprise all years exceeding twice the standard deviation of the AO index. The result is shown in figure 3.3.

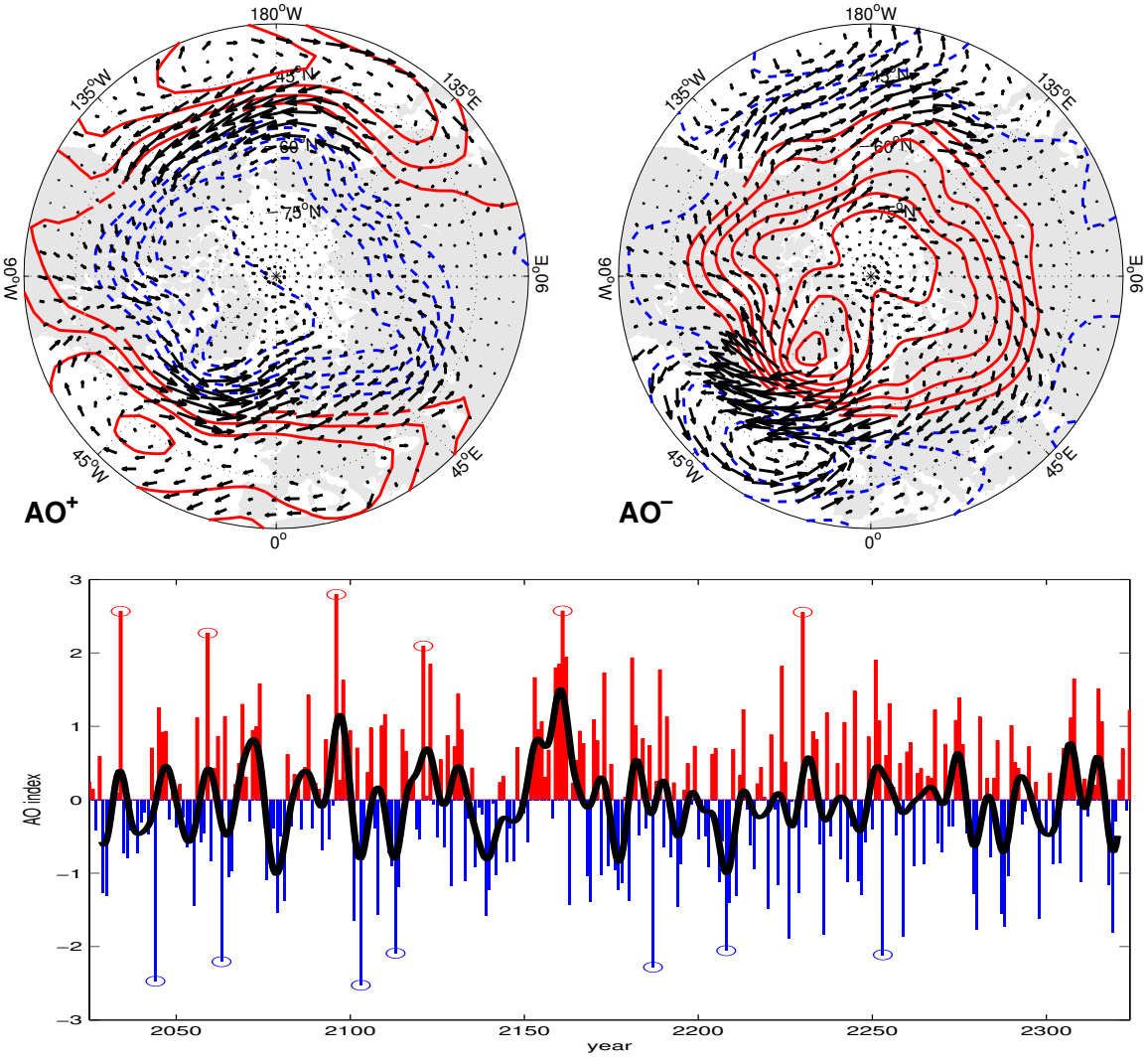

Figure 3.3: AO Composite Study. The lower panel illustrates the annual averaged monthly AO index of the 300 years BCM control experiment. Years marked with circles exceed twice the standard deviation and are used as a sub set for further composite studies. The black line denotes the smoothed index after a low-pass Butterworth with a window of 4 years has been applied. The upper panels show annual surface wind and sea level pressure averaged over the AO^+ and AO^- subsets correspondingly. Winter climatologies are subtracted of the velocity components and the pressure respectively. The contour spacing is 1 hPa.

During the high index phase a strong intensification of the south-westerlies over the North Atlantic is clearly visible. The trajectories continue over the Nordic Seas and parts of Northern Europe as far as to Barents Sea. This agrees well with results of observational studies, that during the positive index phase the storm tracks extent further North and more synoptic low pressure systems reach the Barents Sea region before they break up (Sorteberg et al. 2004). A similar signature is also found on the pacific side. Moreover, horizontal divergence, cyclonic air motion and positive pressure anomalies are present over the Arctic during the negative phase whereas the opposite is shown during positive phase.

Ocean Circulation and Hydrography. As mentioned in section 1.3, the cyclonic intermediate circulation is a key feature of the Arctic Ocean. This has implications for the spreading of Atlantic water and watermass transformations and distribution in general. Steiner et al. (2004) showed that 5 of 6 regional models of the Arctic Ocean Model Intercomparison Project (AOMIP) (Proshutinsky et al. 2001) were capable of reproducing cyclonic circulations that dominate the total stream function.

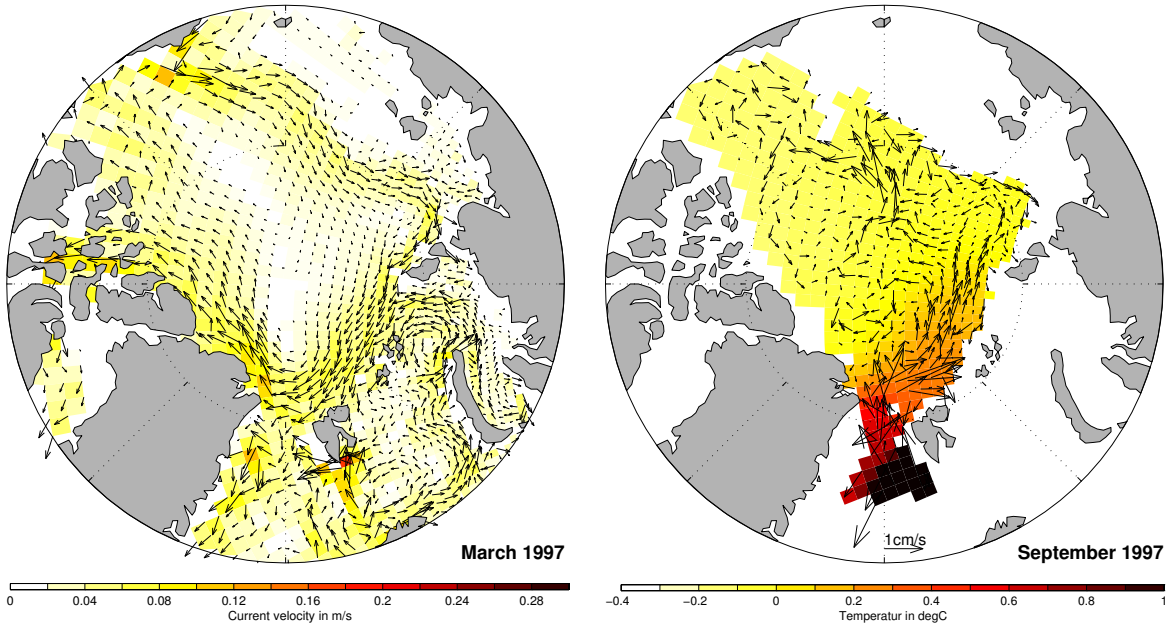

Figure 3.4: Surface layer and $\sigma_\Theta = 27.9$ layer winter circulation are shown for the beginning of the BCM control experiment. The contours indicate the surface circulation strength and the temperature of the $\sigma_\Theta = 27.9$ layer. The $\sigma_\Theta = 27.9$ layer is located below 2000m depth.

At the very beginning of the integration with BCM a cyclonic intermediate circulation is present. This vanishes during the first decades.

In figure 3.4 snap-shoots of the surface and deep circulation at the start of the control experiment presented are. The results clearly show the existence of a deep cyclonic circulation. They are based on computations on the original curvlinear grid with isopycnic layers. Strongest cyclonic motion is found between 2000 m to 3000

m depth, and somewhat deeper in the Canadian Basin than in the Eurasian Basin. However, this is approximately 1000 m deeper than expected, cyclonic Atlantic Layer circulation (Steiner et al. 2004).

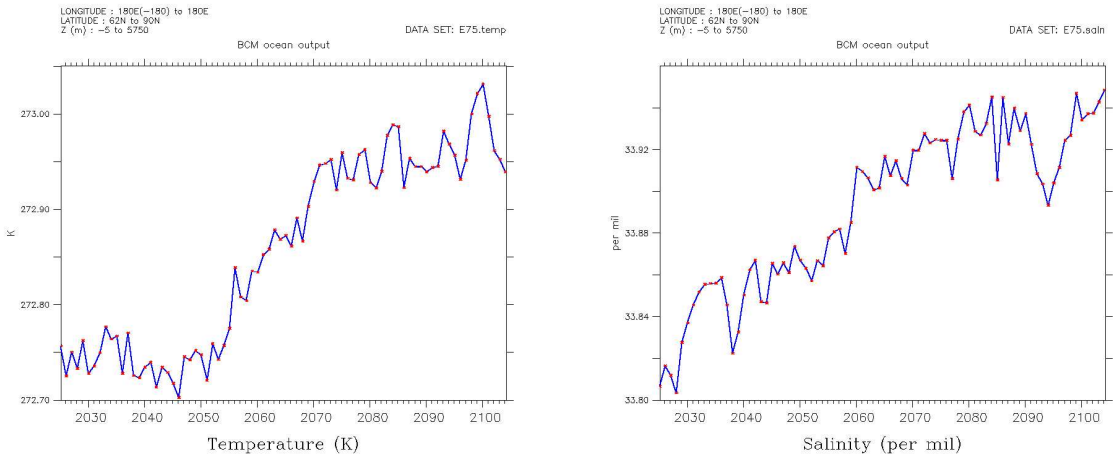

Figure 3.5: Time series of ocean temperature *(left)* and salinity *(right)*, averaged vertically and horizontally north of $62°N$ latitude.

Sea-Ice Distribution and Transport. Observed and simulated Summer and Winter sea-ice extents are shown in figure 3.6. The winter maximum compares rather well with marginal lesser ice in the Greenland, Labrador and Bering Sea, ans has an excellent match in the Barents Sea. However, the Summer/multi-year ice extent is too small, for instance around Svalbard, Franz Josef Land and Sevomaya Zemlya, as well as in the Beaufort, Chukchi, East Siberian Seas, and large parts of the Central Arctic, entirely ice-free areas are found. Possible causes can be the poleward and eastward shift of the Beaufort High (not shown), and a poleward shift of the polar front that denotes the border between Pacific and Atlantic water (John Walsh, personal communication).

The signature of the Beaufort high is clearly visible in the annual ice drift climatology shown in figure 3.7 (see figure 1.4 for comparison). But apart from the displacement of the circulation center, the picture mostly resembles what is observed, e.g. the Trans-Polar Drift, the ice export through the Fram Strait, ice transports between the Kara and Barents Seas, ect.

The simulated Arctic sea-ice behaves rather insensitively to the drift in the hydrography, i.e. a general ocean warming and the retreat of the halocline. But it stays questionable if this is desirable or should be considered as a model deficiency. Simplified conceptual 1d sea-ice models emphasize that the sensitivity of ice growth highly depends on the ice thickness itself. Since the simulated ice is relatively thin we expect a weaker response than might have been the case in reality.

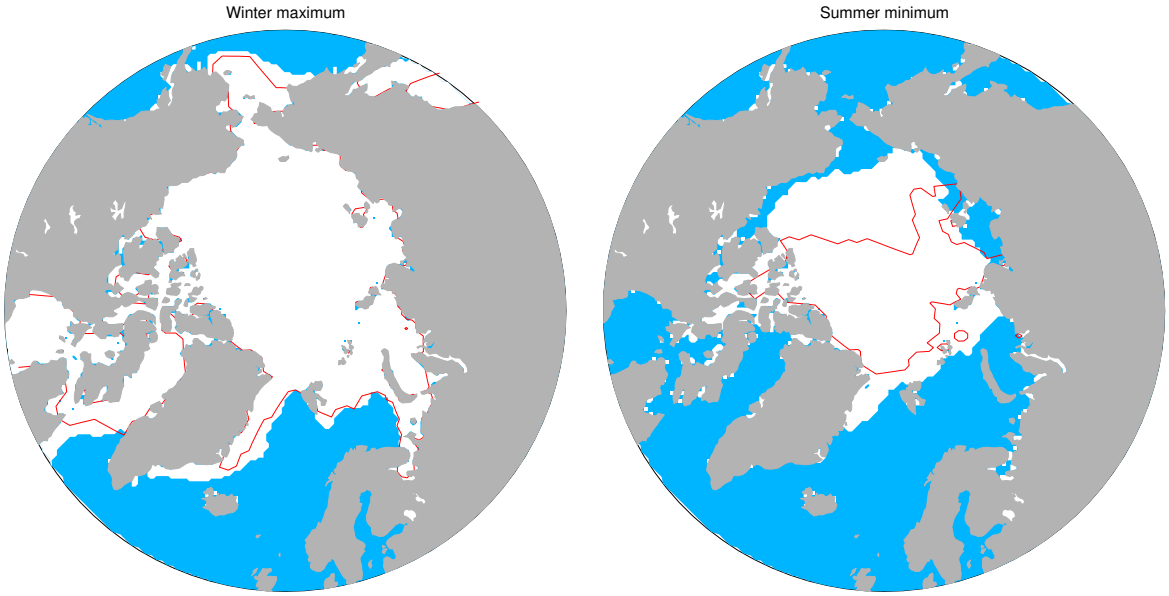

Figure 3.6: The 30% limits of the ice concentration climatologies for march and september derived form the satellite based AICSEX dataset (Johannessen et al 1999) (white shaded) and the BCM control experiment (red line).

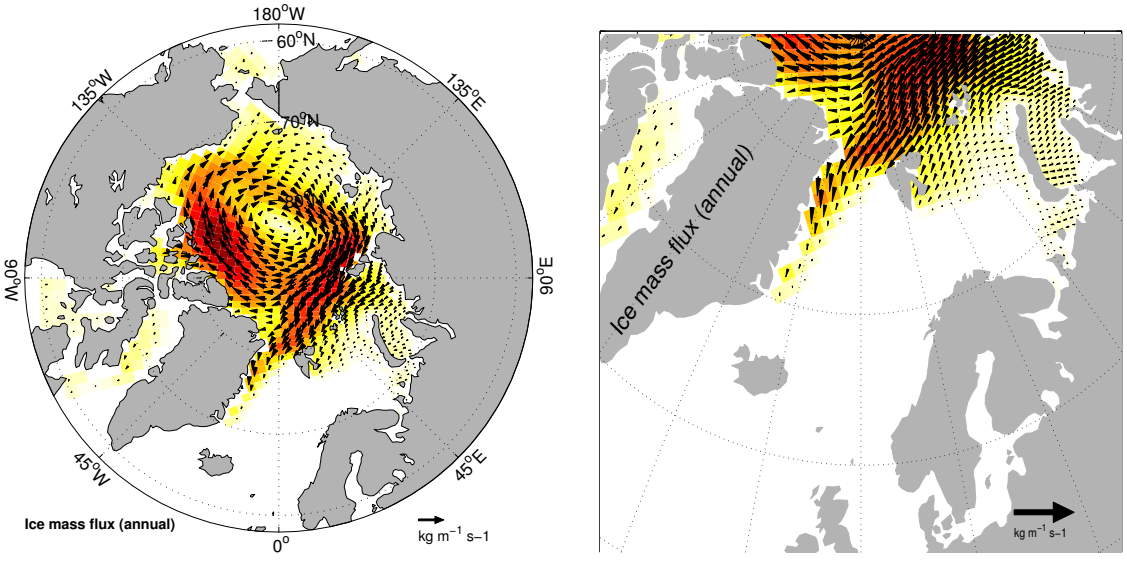

Figure 3.7: Mean ice drift of the BCM control climate.

Chapter 4

Mass Budget

4.1 Introduction

The combined Arctic Mediterranean mass balance constitutes of the water exchange with the Pacific through the Bering Strait and the exchanges with the North Atlantic through the Canadian Archipelago and the Greenland-Norway pathways. For the discussion of the mass transports we neglect the contributions of sea level change, runoff, ice transport, evaporation and precipitation. These terms are much less than the other fluxes. In addition they are not giving any contribution to the simulated mass budgets since the MICOM model treats them as equivalent salt fluxes.

The detailes of all analyses and the main features of the analysis results are described in the next section. Section 4.3 reports about the simulated exchanges and flow patterns of the present climate. The climatological mean state is compared with observational estimates and other simulations. Coherent variations in the exchanges and also effects of variations in the atmospheric winter circulation are investigated. Flux and exchange variability are discussed with respect to the Atmospheric winter circulation as well as cross-related within the ocean system. In section 4.4 a future outlook for the circulation based on the emission scenario experiments is presented.

4.2 Analyses and Results

Mass Exchanges of the Arctic Seas - Present and Future. Monthly averages of section integrated mass transports are computed for in figure 1.2 defined limits. Equivalent volume transports are then by division through a standard sea water density of 1028 kg/m^3. The monthly products for the control and emission scenario simulations are further processed by the use of elementary statistics, e.g. mean, standard deviation, and trend computation. The final products presented in table A.1 in the appendix comprise firstly, averages of net, positive and negative cross-sectional transports as well as the standard deviation for the annual averaged net fluxes for the 300 years control simulation. Secondly, they include projected transport changes with the ensemble

spreading for the net prediction. In order to provide readable budgets for each single region, every transport is listed twice. All tabulated transport values are graphically illustrated in figure 4.1.

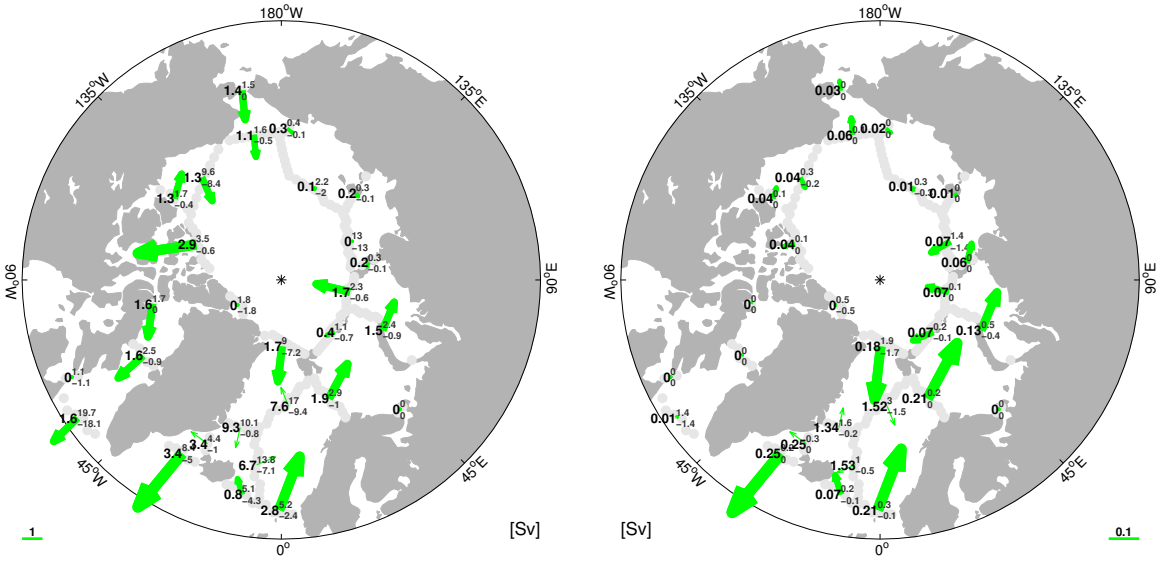

Figure 4.1: Simulated mass exchanges of the Arctic Seas. Average of 300 years control experiment *(left)* and projected echanges *(right)*.

Annual Climatology of Simulated Flow Fields. An annual climatology of vertical averaged mass fluxes is illustrated for the GIN and Barents Sea region as well as for the entire Arctic in figure 4.2. Note that they are virtually proportional with the averaged velocities, where the scale of 100 $kg\,m^{-2}\,s^{-1}$ more or less corresponds to a speed of 10 cm/s. All major flows are well captured, e.g. the Norwegian Coastal Current, the West Spitzbergen Current, the East Greenland Current, the Bering Strait inflow and Canadian Archipelago outflow and so forth. A detailed discussion on these and other features is postponed onto the next chapter. Vertical averaged values have been preferred in order to emphasize the ocean boundaries and to provide an idea of the current speeds. Thus, transports in the ocean interior may have larger contributions to the integrated transports, even though they appear small in the figures.

Dependency of Flux Variability on the Leading Atmospheric Circulation Mode. A complete study of inter-annual variability of simulated Arctic currents comprises vastly more material than we have space to present. Therefore, we limit the study to three particular analyses which are presented here in further discussed in section 4.4. Firstly, an AO composite study has been conducted on the flow fields as described in section 3. In figure 4.3 the vectors represent the component-wise differences between the AO^+ and AO^- subset means. When comparing the positive index phase to the negative one a distinct tendency to more cyclonic motion becomes apparent. Consistently, at the same time the Bering Strait inflow weakens and the Atlantic Water inflow strengthens.

Dependency of Mass Exchange Variability on the Local Atmospheric Circulation.

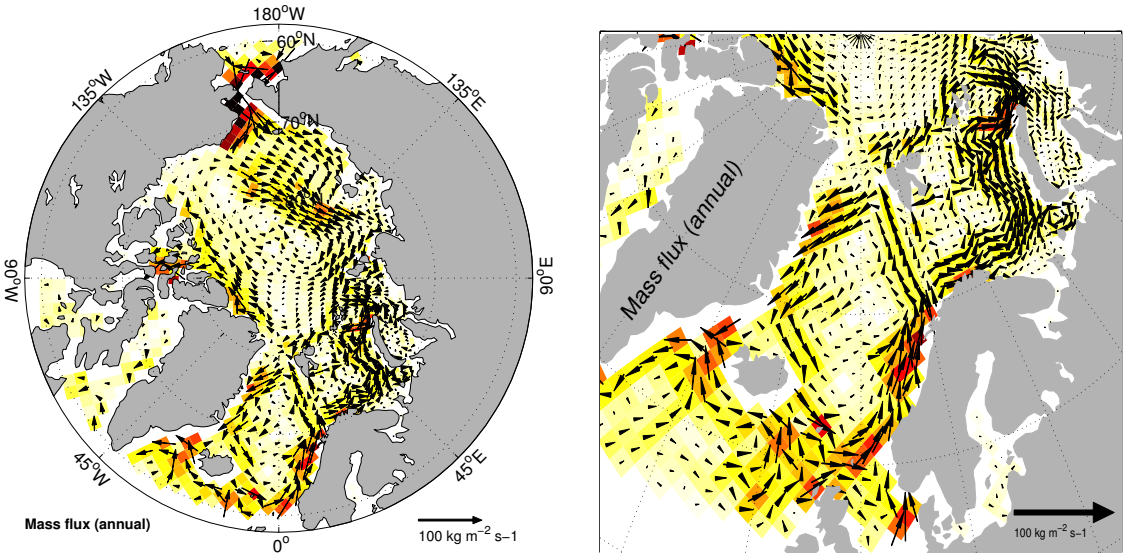

Figure 4.2: Vertical averaged mass fluxes. Shown are annual climatologies of 300 years control experiment.

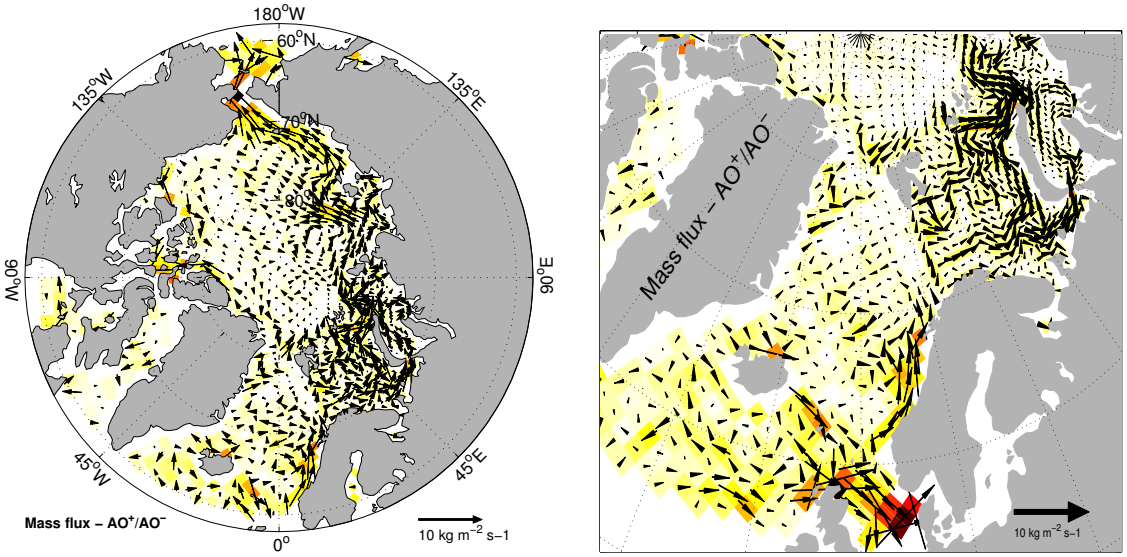

Figure 4.3: AO composite of vertical averaged mass flux. Shown are difference vectors between the AO^+ and AO^- subset mean of the BCM control experiment.

To assess the importance of the local atmospheric circulation for the mass exchanges of the Arctic Seas a correlation study has been conducted between winter averaged mass exchanges and sea level pressures. The results are illustrated in figure 4.4 For most main passages a strong resemblance to the Arctic Oscillation pattern is present. However, in case of the Bering Strait the variability is entirely governed by local wind fields and for the Fram Strait strong links to the atmospheric circulation are absent.

Compensation of Mass Exchanges. A complete control of mass exchange variability by the local atmospheric circulation cannot be the case (at least not at all places

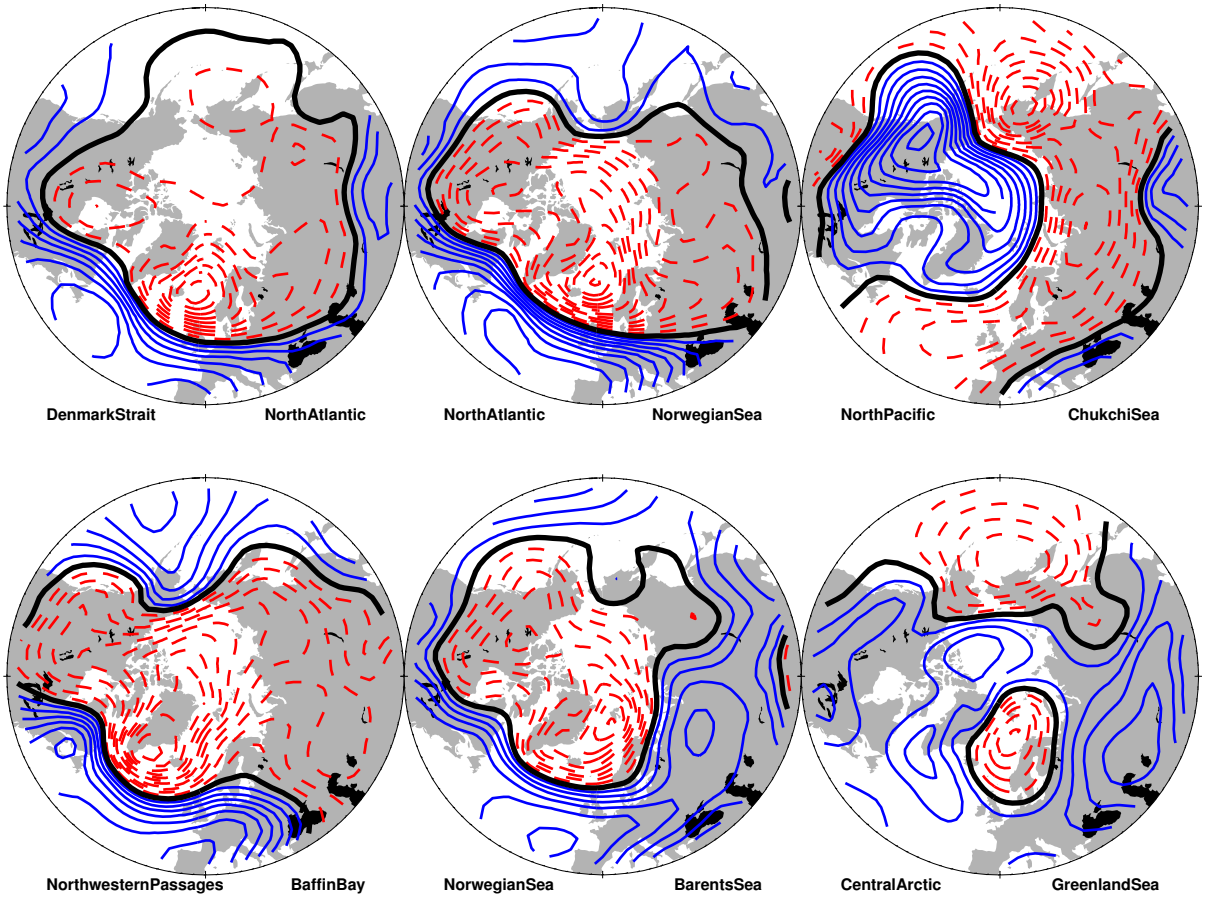

Figure 4.4: winter (djf) averaged volume exchanges of the Arctic Seas correlated with sea level pressure. The thick lines denotes zero correlation, the dashed line negative values and the contour spacing equals 0.05. Positive direction of the transports is defined as out of the region which is written on the left side of the plot.

simultaneously) since the constraint of mass conservation exists. From an energy perspective, it is completely clear that over a longer time period not enough available potential energy exists to build up so much water up that it quantitatively could have an effect. From a dynamic perspective, surface elevation changes as a consequence non-zero horizontal flux convergences induce immense pressure gradients which in turn adjust the fluxes back to a compensating state. The adjustment can be explained in terms of inertia-gravity waves where the analytical solution converges against the steady state, geostrophic balance (Pond and Pickard 1978). To assess how the compensation manifest itself, cross-correlations for winter averaged mass exchanges of the Arctic Seas are presented in table 4.1. The winter season is chosen in order to be able to compare the results with the already introduced Arctic Oscillation and sea level pressure studies.

Atlantic Meridional Overturning Circulation - Present and Future. In figure 4.5 a vertical section of the time averaged, zonal integrated Atlantic Meridional Overturning Circulation (AMOC) is illustrated for the control experiment. Moreover, time series

of it's circulation strength i.e. the volume flux of the total Atlantic overturning are shown for the control and greenhouse experiments. A detailed description of the AMOC features in the BCM is given in Bentsen et al. (2002).

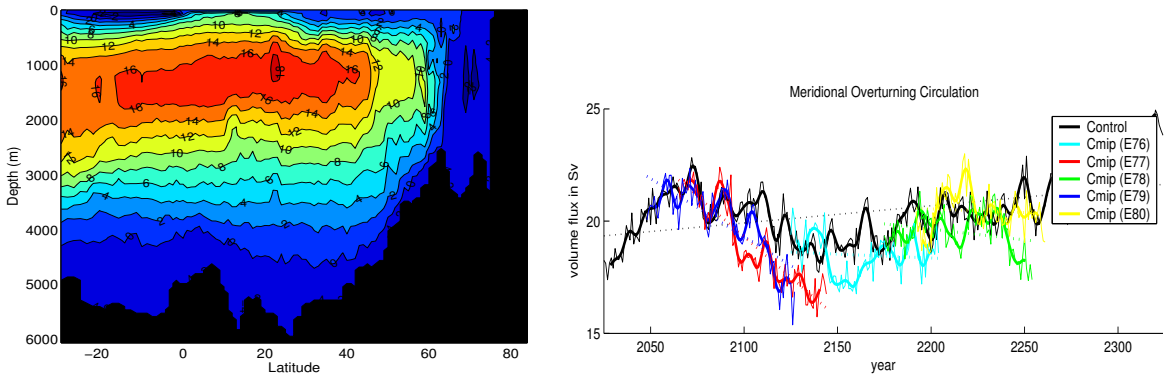

Figure 4.5: Atlantic Meridional Overturning. Basin integrated vertical stream function of the control experiment *(left)* and corresponding time series of the overturning strentgh maximum *(right)*. (reproduced after Bentsen 2002)

Future of the Transports over the Iceland-Scotland Ridges Smoothed time series of summer and winter averaged net volume transport over the Iceland-Scotland Ridges are shown for the BCM control and greenhouse experiments. The summer values are approximately 25% smaller than those of the winter. The most prominent features are the model drift, a substantial inter-annual variability and positive trends during winter and negative trends during summer of the greenhouse experiments relative to the control time series.

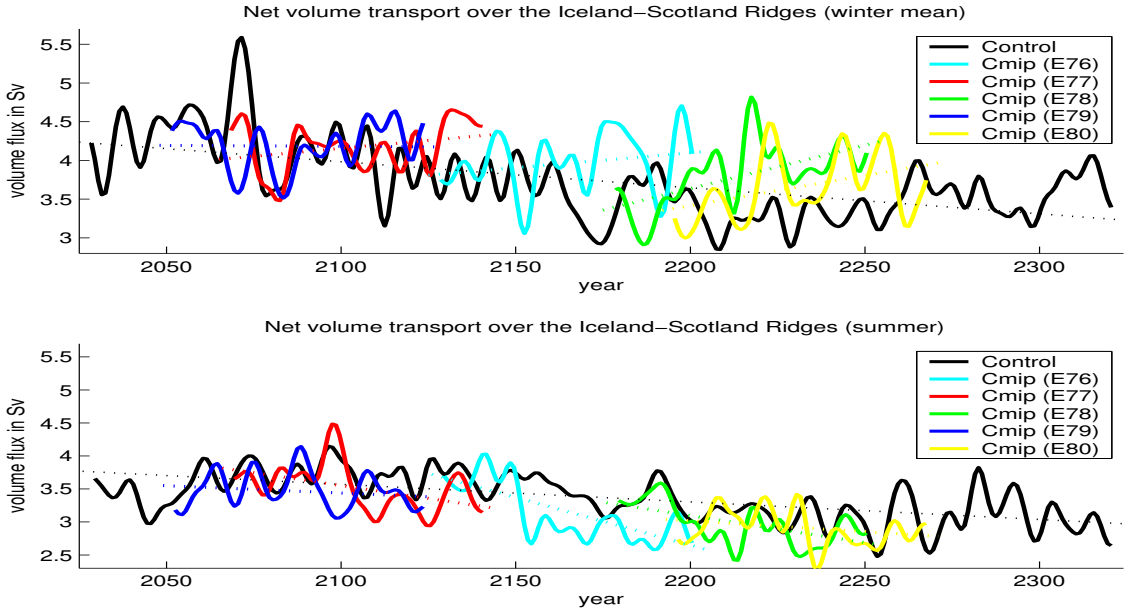

Figure 4.6: Time series of winter (djf) and Summer (jja) volume transports through the Iceland-Shetland section for BCM control and greenhouse experiments.

Table 4.1: Correlations of winter (djf) mass exchanges of the Arctic Seas

			1	2	3	4	5	6	7	8	9	10	11	12	13	14	15	16	17	18	19	20	21	22	23	24	25
north atlantic	-	davis strait	1	0.1	-0.2	-0.3	0	**-1**	1	0.1	-0.3	0.2	0.2	-0.2	0.1	-0.1	0.3	0.3	-0.1	-0.3	0.3	0.1	0.2	0.1	0.1	0.1	-0.1
north atlantic	-	denmark strait	2	0.1	1	-0.4	**-0.7**	-0.1	-0.1	0.1	0	-0.2	0.3	0	0	0.1	0	-0.2	0.2	0.2	0	0	**1**	0	-0.3	0.1	0.3	-0.1
north atlantic	-	iceland sea	3	-0.2	-0.4	**1**	-0.2	0	0.3	-0.3	0	0	0	0	0	0	0	-0.1	0	0	0.2	0	-0.4	0.1	-0.1	0	0.1	0
north atlantic	-	norwegian sea	4	-0.3	**-0.7**	-0.2	**1**	-0.3	0.3	-0.3	-0.1	0.4	-0.4	-0.2	0.2	0.1	0	0.1	-0.4	-0.1	0	-0.2	**-0.7**	-0.3	0.3	-0.2	-0.4	0.3
north pacific	-	chukchi sea	5	0	-0.1	0	-0.3	**1**	0	0	0.3	-0.4	0.3	0	0	**-0.8**	0.1	0.2	0.4	-0.1	0	0.3	-0.1	**0.5**	0	0.1	-0.1	-0.4
baffin bay	-	davis strait	6	**-1**	-0.1	0.3	0.3	0	**1**	**-1**	-0.1	0.3	-0.2	-0.2	0.2	-0.1	0.1	-0.3	-0.3	0.1	0.3	-0.3	-0.1	-0.2	-0.1	-0.1	-0.1	0.1
baffin bay	-	northwestern passages	7	**1**	0.1	-0.3	-0.3	0	**-1**	**1**	0.1	-0.3	0.2	0.2	-0.2	0.1	-0.1	0.3	0.3	-0.1	-0.3	0.3	0.1	0.2	0.1	0.1	0.1	-0.1
barents sea	-	central arctic	8	0.1	0	0	-0.1	0.3	-0.1	**1**	-0.4	0	0.2	-0.2	-0.1	0	0.2	0.3	0.1	0.2	0.3	0	0.4	-0.1	0.3	-0.1	-0.4	0.4
barents sea	-	kara sea	9	-0.3	-0.2	0	0.4	**-0.4**	0.3	-0.3	-0.4	**1**	**-0.9**	-0.2	0.2	-0.2	0.2	**0.6**	**-1**	-0.3	-0.1	-0.3	-0.2	**-0.6**	0.3	0	0.1	**0.7**
barents sea	-	norwegian sea	10	0.2	0.3	0	-0.4	0.3	-0.2	0.2	0	**-0.9**	**1**	0.1	-0.1	-0.2	0.2	**-0.7**	**0.9**	0.2	0	0.2	0.3	**0.5**	-0.2	-0.2	0	**-0.6**
beaufort sea	-	central arctic	11	0.2	0	0	-0.2	0	-0.2	0.2	-0.2	0.1	**1**	**-1**	0.3	-0.2	0	0.2	-0.1	**0.8**	0.5	0	0.4	0	0	0	-0.3	
beaufort sea	-	northwestern passages	12	-0.2	0	0	0.2	0	0.2	-0.2	0.2	-0.1	**1**	**1**	-0.3	0.2	0	-0.2	0.1	**-0.8**	-0.5	0	-0.4	0	0	0	0.3	
central arctic	-	chukchi sea	13	0.1	0.1	0	0.1	**-0.8**	-0.1	0.1	-0.1	0.2	-0.2	0.3	-0.3	**1**	**-0.6**	-0.1	-0.2	0	0.2	0.4	0.1	-0.1	0	0	0.1	
central arctic	-	east siberian sea	14	-0.1	0	0	0	0.1	0.1	-0.1	0	-0.2	0.2	-0.2	0.2	**-0.6**	**1**	-0.2	0.2	0.1	-0.2	**-0.7**	0	0.1	0	-0.1	0	-0.2	
central arctic	-	greenland sea	15	0.3	-0.2	-0.1	0.1	0.2	-0.3	0.3	0.2	**0.6**	**-0.7**	0	0	-0.1	-0.2	**1**	**-0.6**	-0.3	-0.2	0.1	**-0.2**	-0.1	0.3	0.2	0.1	0.3
central arctic	-	kara sea	16	0.3	0.2	0	-0.4	0.4	-0.3	0.3	0.3	**-1**	**0.9**	0.2	-0.2	-0.2	0.2	**-0.6**	**1**	0.2	0	0.2	0.2	**0.5**	-0.2	-0.1	-0.1	**-0.5**
central arctic	-	laptev sea	17	-0.1	0.2	0	-0.1	-0.1	0.1	-0.1	0.1	-0.3	0.2	-0.1	0.1	0	0.1	-0.3	0.2	**1**	-0.1	-0.2	0.2	-0.1	-0.3	0.1	-0.1	-0.5
central arctic	-	northwestern passages	18	-0.3	0	0.2	0	0.3	-0.3	0.2	-0.1	0	**0.8**	**-0.8**	0.2	-0.2	-0.2	0	-0.1	**1**	0.3	0	0.2	-0.1	0	0	0	-0.2
chukchi sea	-	east siberian sea	19	0.3	0	0	-0.2	0.3	-0.3	0.3	-0.3	0.2	0.5	-0.5	0.4	**-0.7**	0.1	0.2	-0.2	0.3	**1**	0	**0.6**	-0.1	0.1	-0.1	-0.1	-0.4
denmark strait	-	iceland sea	20	0.1	**1**	-0.4	**-0.7**	-0.1	-0.1	0.1	0	-0.2	0.3	0	0.1	0	-0.2	0.2	0.2	0	0	**1**	0	-0.3	0.1	0.3	-0.1	
east siberian sea	-	laptev sea	21	0.2	0	0.1	-0.3	**0.5**	-0.2	0.2	0.4	**-0.6**	**0.5**	0.4	-0.4	-0.1	0.1	-0.1	**0.5**	-0.1	0.2	**0.6**	0	**1**	-0.1	0.1	-0.1	**-0.8**
greenland sea	-	iceland sea	22	0.1	-0.3	-0.1	0.3	0	-0.1	0.1	-0.1	0.3	-0.2	0	0	-0.1	0	0.3	-0.2	-0.3	-0.1	-0.1	-0.3	-0.1	**1**	**-0.9**	**0.7**	0.2
greenland sea	-	norwegian sea	23	0.1	0.1	0	-0.2	0.1	-0.1	0.1	0.3	0	-0.2	0	0	0	0.2	-0.1	0.1	0	0.1	0.1	0.1	**-0.9**	**1**	**-0.7**	-0.1	
iceland sea	-	norwegian sea	24	0.1	0.3	0.1	-0.4	-0.1	-0.1	0.1	-0.1	0.1	0	0	0	0	0.1	-0.1	-0.1	0	-0.1	0.3	-0.1	**0.7**	**-0.7**	**1**	0.1	
kara sea	-	laptev sea	25	-0.1	-0.1	0	0.3	-0.4	0.1	-0.1	-0.4	**0.7**	**-0.6**	-0.3	0.3	0.1	-0.2	0.3	**-0.5**	-0.5	-0.2	-0.4	-0.1	**-0.8**	0.2	-0.1	0.1	**1**

4.3 Exchanges and Flow Patterns in the Present Climate

Mean State The simulated mass budgets of the Arctic Seas are virtually closed, that is no residual flux exceeds 1% of the order of magnitude of the in and outgoing fluxes from that region. Smaller variations around 0.1% might be attributable to model uncertainties, precision loss during data post-processing and numerical uncertainties during the actual budget computations. Marginal changes are attributable to the model temperature drift.

In this section flow patterns of vertical integrated transports as well as cross-section integrated mass exchanges of the Arctic Seas are discussed.

Simulated Climatologies. In general, purely observational based estimates of volume, heat and freshwater exchanges of the Arctic Seas are hardly available because of the relatively sparse observational network which is neither homogeneous in space nor time. Mainly for this reason Maslowski et al. (2004) just recently launched a high resolution regional model to simulate flow fields and transport climatologies through the major pathways of the Arctic Seas. This approach follows the successful NCEP/NCAR (Kalney et al. 1996) example which provide a homogeneous, re–analyzed, observational based database. Despite the much coarser resolution of the BCM we can report a good agreement between both, the global BCM and the regional, high resolution model of Maslowski. The spatial current structure of the Barents Sea presented in Maslowski et al. 2004 agrees very well with our results shown in figure 4.2. Fine structures of the Norwegian Atlantic Current, re-circulation of Atlantic Water in the Bear Island Trough, the West Spitzbergen Current and Zemlya Current are well resolved. To distinguish between the simulated North Atlantic Current and the Norwegian Coastal Current and the North Cape Current one needs to compare the volume transports with the corresponding freshwater transports in figure 6.11 as discussed. Grid cells which limit with the coast show an northward freshwater transport whereas the adjacent show a southward transport. Considering the salty nature of the inflowing Atlantic Water and the fresh one of the coastal currents one would expect this signature. It should be noted that the coarseness of the grid is pressed to it's limits. A higher resolution resolution would be more adequate to present these features more accurately.

Hindcasts. Similar to Maslowski, Nilsen et al. (2004) performed hindcasts with the ocean part of the BCM forced with the observed history of the Atmosphere (Furevik et al. 2003; Nilsen et al. 2004). From now on, we will use the Maslowski and Nilsen simulations as our quasi-observational reference data where observations is sparse.

Bering Strait. The average Bering Strait inflow of the BCM (figure 4.1) is generally high with a long-term mean of 1.4 Sv. If compared with a very frequently adopted literature value of 0.8 Sv (Rudels 1987) it implies a 70% stronger inflow of Pacific Water than observed. Likely causes for the strong exchange may be hidden in the relatively deep model bathymetry. It is set to the model minimum of 50 m in the Bering Strait

whereas IBCAO charts (Jakobbson et al. 2003) suggest a 20% shallower mean. The uncoupled, hindcast simulation of Nilsen et al. 2004 shows a reduced inflow of 1 Sv, matching the value of Roach et al. (1995) which is derived from direct measurements. It indicates that a too pronounced atmospheric circulation in the North Pacific sector of the coupled BCM simulation might also have some effect. However, there are other observational estimates with larger influxes, for instance Aagaard and Greisman (1975) and Hopkins (1991) with 1.5 Sv. Apparently, there is need to clarify to which extent the spreading of the observational estimates reflect the true variability of the ventilation of the Arctic Ocean with Pacific waters.

Canadian Archipelago. The 1.6 Sv outflow through the Canadian Archipelago corresponds reasonably well to the 2 Sv observed during the years 1980 and 1981 (Aagaard and Greisman 1975; Prinsenberg 2002). Because the Smith Strait, which is located east of Greenland, is closed in the model, the Barrow Strait exchange has to account for the complete Canadian Archipelago through flow. As a consequence a reduced exchange seems reasonable. However, other observational based estimates, e.g. Fissel et al. (1988) estimate 1.7 Sv, and consequently are very close to the BCM simulation.

Fram Strait. Recent estimates for the years 1997 to 2000 of observed water transport through the Fram Strait suggest an annual mean northward flux between 7 Sv and 10 Sv, a southward flux between 13 Sv and 12 Sv and a net transport between 2 Sv and 4 Sv to the south. The amplitude of the north and southward component of the control experiment is with approximately 7 Sv and 9 Sv somewhat smaller than the observed values whereas the net transport agrees reasonably well with a southward flux of approximately 2 Sv (see figure 4.1). Likely candidates which might cause minor discrepancies are a reduction of the in/out amplitudes due to the weekly pre-averaging of the model data, the relatively coarse model resolution that inhibits explicit resolving of the boundary currents and a questionable representativeness of the three years average of observed data as a climatic mean state.

Variability In the following, two analyses addressing the variability of the exchanges and one analysis addressing the variability of the flow patterns are presented.

To be able to explain the variability of Arctic water mass exchanges and of currents in general, the relative contributions of the thermohaline effects, large scale atmospheric circulation and deviations from the latter need to be accessed.

Atlantic Meridional Overturning Circulation. Bengtsson et al. (2004) reported the presence of a week statistical link between the volume inflow to the Barents Sea and the index of the meridional overturning in the North Atlantic in their ECHAM4/OPYC3 climate simulations. In figure 4.5 the time averaged simulated Atlantic Meridional Overturning Circulation (AMOC) is shown for the BCM control experiment.

The ocean overturning is almost entirely confined to the North Atlantic, south of Island. The natural variability of the AMOC on inter-annual time scales and it's implications on the Arctic budgets is not further investigated in this work.

Sea Level Pressure vs. Ocean Volume Transport. In figure 4.4 winter mass ex-

changes through the the major pathways are correlated with atmospheric sea level pressure, providing a measure of sensitivity of the exchanges to the Atmospheric Forcing. This follows the work done by Nilsen et al. (2004).

As a first approximation the structure of the Denmark Strait, North-Western passages and Atlantic – Norwegian Sea correlations simply resemble the spatial pattern known as the NAO or AO. But the NAO pattern itself is merely a reflection or integration of the Atlantic storm track variability. Therefore, a direct comparison with the synoptic low pressure strengths, trajectories and life times in the north-east Atlantic sector provides further insight into the causalities behind the links with the circulation indices. This has been accomplished recently by Sorteberg et al. (2004). They address the impact of the cyclonic variability on the inflow into the Nordic Seas.

Inflow of Atlantic Water into the Norwegian Sea. The physical chain of links that allows the atmospheric circulation to control the Atlantic Water inflow into the Norwegian Sea comprises several components.

The instantaneous response to the wind forcing, i.e. the Ekman transport is generally confined to the Ekman depth which extends no deeper than 50 m at middle latitudes (Pond and Pickard 1978).

Associated with a positive curl of an atmospheric low is a divergence in the Ekman transports and a compensating positive Ekman pumping. This gives positive vorticity to the waters below. For a large scale flow, a poleward displacement of the water column with associated negative advection of planetary vorticity is the only way to maintain a balance. But this Sverdrup transport, which mathematically is written as $\beta M = curl_z(\tau_n)$, is only valid for the steady state and does not take into account any negative vorticity fluxes from the eastern boundary. It's role for the inflow is further discussed in Furevik and Nilsen (2004).

Another mechanism has been identified by Orvik and Skagseth (2003). They found a statistically strong link between the wind curl over the central North Atlantic and the current strength of the Norwegian Atlantic Slope Current 15 months later through the Svinøy section. Orvik and Skagseth speculate that the Ekman Pumping associated with the positive wind curl excites a baroclinic Rossby wave that eventually breaks at the Irish shelf slope and then feeds momentum and heat into the slope current. If this contributes significantly to the exchange variability it would provide a good explanation for moderate values of the zero lag pressure correlation. However, the zero lag correlation of the climate simulation exceeds 0.5 for a time series of 300 years, which is considerably robust. Therefore, if at all the mechanism Orvik and Skagseth proposed is included in the model, it's contribution to the flux variability is rather small. This may be a problem of resolution.

Similarities and Deviations from the AO Pattern. A variety of studies exist that address the relation of the AO (or NAO) to virtually any climate or weather variable (Polyakov and Prushutinsky 1999; Dickson et al. 2000; Thompson and Wallace 2000; Black 2001; Visbeck et al. 2003; Zhang et al. 2003).

Even though the general resemblance with the AO is evident, more important is the

local structures of the correlations. In every case the correlation contours are bent such that they are aligned perpendicular to the sections. An example is the west of Greenland where the contours follow all the way through the Labrador Sea, Davis Strait, Baffin Bay, Canadian Archipelago and finally into the Arctic Ocean. Furthermore, the correlation minimum is displaced towards the left and the maximum towards the right side relative to the ocean flow direction, whereas only very small correlations, but the strongest gradients, are found over the sections. The Denmark Strait is somewhat exceptional with moderate correlation values. though this might just indicate that it's through-flow is remotely controlled fulfilling the constraint of the conservation of volume. Since correlation and regression are akin, i.e. the only difference is the weighting with the fraction of the local standard deviations, one can essentially replace the correlation values with pressure anomalies. Thus the large transports are obtained for strong, local cross-strait geostrophic winds where Ekman transports pile up water at one shore and thereby cause deep geostrophic flows. The net Fram Strait transport exhibits a relatively weak link to the local with $r \approx 0.25$ only and virtually none to the NAO index. Since the in and outgoing mean transports are an order of magnitude larger than the residual net transport, this behavior might be traced back to the competing variability of the West Spitzbergen Current and the East Greenland Current which basically are unrelated and at least partly thermohaline driven. The Norwegian Sea and Barents Sea inflows and their implications for the heat transports are discussed in more detail in sections 5.5 and 5.6.

Correlations between different Straits. At the beginning of this chapter it was shown that the simulated budgets are closed. We will now see how the compensation of the volume flux variability takes place. In table 4.1 correlations off all mass exchanges of the Arctic Seas are presented. Here, we limit our analyses to the atmospheric active season since the winter exhibits the strongest and most organized variability.

Pathways of the Pacific Water. In most of the cases values of 0.8 or higher reflect trivial relations. For instance, the inflow of Pacific Water through the Chukchi Sea is either directed to the east Siberian Sea or directly to the Central Arctic. A weak modulation of the relation by the Bering Strait inflow variability must explain the deviation from a perfect correlation. The significant out-of-phase relation between the Chukchi Sea - Central Arctic and the East Siberian - Central Arctic water exchange tells us that all Pacific Water finally ends up in the Arctic Ocean Proper regardless which route it takes. However, the ability to detect these relations is a test for the method and gives us some confidence.

Competing Atlantic - Nordic Seas Exchanges. In contrast, a non-trivial and hotly debated relation is the anti-correlation between the Atlantic inflow across the Faroe-Shetland Channel and the Iceland-Faroe Ridge described in Nilsen et al. (2004). In the BCM simulation this is captured by correlation between the Atlantic - Norwegian Sea and Atlantic Iceland Sea exchanges with $r = -4$. Nilsen et al. 2004 proposes that on longer time scales a shift of the NAO center of action accounts for this. Somewhat stronger is the relation of the Norwegian Sea inflow and the Denmark Strait outflow

that is mentioned in Nilsen et al. 2004 too.

Gyre Circulations in the Nordic Seas. These links seem tightly connected to the large scale, cyclonic gyre circulation in the center of the Nordic Seas which moves about three times more volume than the exchange with the Atlantic or Arctic Ocean (compare figure 4.2. The simulated, barotropic gyre circulation manifests itself through the high correlation of the Norwegian, Greenland and Iceland Sea exchanges. More over, it owns a deep signature in the Nordic Seas surface elevation (not shown). Presumably, it's strength is determined by a balance of the vorticity flux from the atmosphere and the sea floor. Now, it's tempting to speculate that during a prevailing positive NAO state the gyre just integrates the atmospheric cyclonic vorticity i.e. spins up and thus acts like a pump for the East Greenland Current (EGC) and the Norwegian Atlantic Current (NAC) which comprise most of the Atlantic - Arctic Ocean exchange. But, the fact that the EGC and NAC mainly are well defined slope currents with limited communication to the interior ocean opposes this simple picture.

Barents Sea Through-Flow. The Barents Sea inflow through the Barents Sea Opening (BSO) exhibits a moderate link with the Norwegian Sea inflow from the North Atlantic of r=0.4 . But, there is a high anti-correlation between the Barents Sea Opening influx and the Fram Strait exchange with the Central Arctic Ocean. This indicates that the Atlantic inflow into the Barents Sea is not determined by the strength of the NAC alone, rather the local wind field decides how much Atlantic Water is "tapped" while the current passes the Barents Sea Opening . The details of this mechanism are explored in Ingvaldsen, Asplin, and Loeng (2004). In turn, the variability in the BSO transports completely governs the exchanges of the Kara Sea with the Barents Sea (r=0.9) and with the Central Arctic (r=0.7) whereas the direct exchange of the Barents Sea with the Central Arctic remains unrelated.

Canadian Archipelago Transport Variability. The simulated flow through the Canadian Archipelago does not exhibit any strong statistical relation though it has to compensate for the sum of Fram Strait, Barents Sea Opening and Bering Strait variability. Neglecting the Bering Strait, this indicates that the volume compensation of the East Greenland Current with the Norwegian Atlantic Current and the relative strength of the AW inflow into the Barents Sea to the West Spitzbergen Current exhibit far more variability than the the net volume transport through the Greenland-Norwegian pathways.

4.4 Spin-up of the Circulation in the Future Climate

Apart from difficulties with assessing the magnitude of future changes in the Arctic Ocean and particularly the Nordic Seas no general consensus is reached in which directions these might develop.

The 'Day of Tomorrow' Scenario. The popular 'ice-age' or 'day of tomorrow' sce-

nario reasons that a freshening of the Nordic Seas impedes deep convection in these regions. The reduction in overflow associated with the absent convection should relate to a reduction of the compensating, warm Atlantic inflow of the same magnitude. The Atlantic inflow transports a considerable amount of heat into the Nordic and Arctic Seas and therefore is partly responsible for the relatively mild winter climate in Northern Europe and the sea-ice free coasts. The implications of the heat transport are discussed more thoroughly in the next chapter. Some observational studies, e.g. Hansen et al. (2001) and Hansen et al. (2004) reports a 20% reduction of the Faroe Bank Channel overflow during the second half of the 20th century. Nilsen et al. (2004) reports that this reduction could be reproduced with an OGCM forced with the atmospheric history of the same period. But, he also emphasizes that it still remains unclear to which degree this might be attributable to associated AMOC changes or wind induced transport changes.

Simulated Circulation Spin-Up. In the future scenario simulations of the BCM the controversy of this topic is well captured. Preceding the discussion of the thermohaline circulation it should be mentioned that average, simulated AMOC of the BCM is mainly confined to the middle latitudes as shown in figure 4.5 (note that the seasonal cycle might differ). Therefore, the impact of it's variability on the climate in the higher latitudes might potentially be underestimated. Figure 4.5 shows a projected 10 to 20% reduction in the AMOC strength in all but one member of the CMIP ensemble experiments. In contrary, the North Atlantic - Nordic Seas volume exchanges are slightly intensified (see figure 4.5). Yet, the projections of the single members differ greatly (see table A.1) and consequently this mean intensification turns out to be statistically not significant. Further investigation needs to be done in order to understand why the projections vary.

Seasonal Differences. However, the seasonal signals are more coherent. For instance, the volume exchange over the Iceland - Scotland ridges shows distinct positive trends during Winter, but negative trends during Summer. The member E79 does not follow this tendency, but also generally differs from the other members since it is the only CMIP experiment without any tendency of the NAO to more negative index values (Laurantin 2004). We argue that the strengthening of the winter exchange is related to the just mentioned NAO tendency. Associated to the NAO is a strong signature in the Northern Hemisphere surface pressure field captured by the Arctic Oscillation presented in figure 3.2 and already discussed in section 1.3. In contrast, the negative summer trends might indeed be related to the weakened AMOC.

Thus, it can be speculated that the thermohaline and wind driven changes are competing where the latter dominates during the active season. Still, it remains questionable that the simulations are able to reproduce the relative strengths and hence the net-effect. Thereby, the largest uncertainties are expected in the presentation of the convection and overflow processes.

4.5 Chapter Summary

Climatological Mass Exchanges. It can be concluded that the magnitudes and also the relative contributions of the mass exchanges through the Arctic Seas pathways correspond reasonably well with observational estimates and other simulations. However, a bias towards Pacific water ventilation is apparent, leading to weaker than observed Barents Sea and Fram Strait inflow. The closest match is obtained for the transport through the North Western Passages.

Inter-annual Variability of Mass Exchanges. Arctic Oscillation composite studies suggest competitive behavior of Pacific and Atlantic inflow, whereby the latter is stronger during positive index phases. While the Atlantic Inflow strengthens the East Greenland Current seems to weaken slightly. Thus, for the closed picture it remains essential to take the Bering Strait and Canadian Archipelago into account. However, an artificial tele-connection of the Pacific with the Atlantic atmospheric variability may contaminate these results.

Atlantic Inflow into the Nordic Seas. Despite a predicted weakening of the Atlantic Meridional Overturning Circulation strength no general reduction of the Atlantic Water inflow is projected. In contrast, during winter, a strengthened inflow is associated with the projected deepening of the Icelandic Low. However, in summer i.e. during the absence of strong atmospheric wind forcing slight indications for a reduced inflow are present. But, it remains to be proved that the latter is in fact related to a weakened overflow. Furthermore, the simulated Atlantic Inflow is only about 25% larger during winter than during summer. If one assumes that the atmospheric circulation has a significant role only during the active season then the major fraction of the inflow must be thermohaline or explained by breaking of baroclinic waves generated during winter. Since the simulated AMOC is rather weak in the Nordic Seas, a freshwater driven estaurine like circulation seems more likely to explain the thermohaline contribution.

Barents Sea Opening Inflow. Correlation studies emphasize that the out-of-phase relationship of the West Spitzbergen Current transport and the inflow into the Barents Sea is a more robust feature than their connection with the Atlantic Inflow into the Nordic Seas. Thus, the variability of the Barents Sea inflow depends more on how much Atlantic Water is 'tapped' from the Norwegian Atlantic Current than on the NAC strength itself. This finding is consistent with a sea level pressure correlation study which shows a maximum inflow into the Barents Sea for low pressure centers located approximately over Svalbard.

Chapter 5

Heat Budget

5.1 Introduction

Why should we be concerned about the Arctic energy balance?
Changes in the arctic energy balance have the potential to directly effect the arctic sea-ice growth and decay, ocean and atmosphere temperatures, terrestrial ice-sheets, glaciers, permafrost, snow cover, and indirectly also might alter the ocean and atmospheric circulation itself. These consequences have a wide range of implications on the pan-Arctic vegetation, animal life and human activities e.g. in the sectors transport and construction, fishery, tourism ect.

Despite a considerable ongoing research effort there is no consensus in which direction the changes of the poleward ocean and atmosphere energy flux will take in the near future. A reduced AMOC and a generally weaker equator-to-pole atmospheric temperature gradient due to the polar amplification of the predicted temperature change (Holland and Bitz 2003) point towards a reduced poleward transport in atmosphere and ocean. Opposing this tendency, e.g. moisture convergence in the tropics might fuel the Hadley Circulation which in turn then would transports more sensible heat towards the extra-tropics. An increased moisture export from the sub-tropics to the middle and higher latitudes will lead to an enhanced poleward latent heat flux. An intensified sensible and latent heat transport from the middle latitudes towards the poleward region might be associated with a positive trend in the AO. This trend also could have the potential to strengthen the wind driven ventilation of the Nordic and Arctic Seas with more inflow of warm Atlantic Water.

All analyses and results are outlined in the next section. In section 5.3 the simulated present climate poleward energy transports are briefly discussed. In section 5.4 their changes are investigated. Leaving the global perspective, future projections of the heat exchanges between the North Atlantic and the Nordic Seas are presented and discussed in section 5.5. Impacts of the oceanic heat transports on the sea ice are assessed in section 5.6 and finally a short summary with concluding remarks are given in section 5.7.

5.2 Analyses and Results

Arctic versus Global Warming. Figure 5.1 illustrates projected changes in local heat content and vertical averaged temperature relative to the global warming.

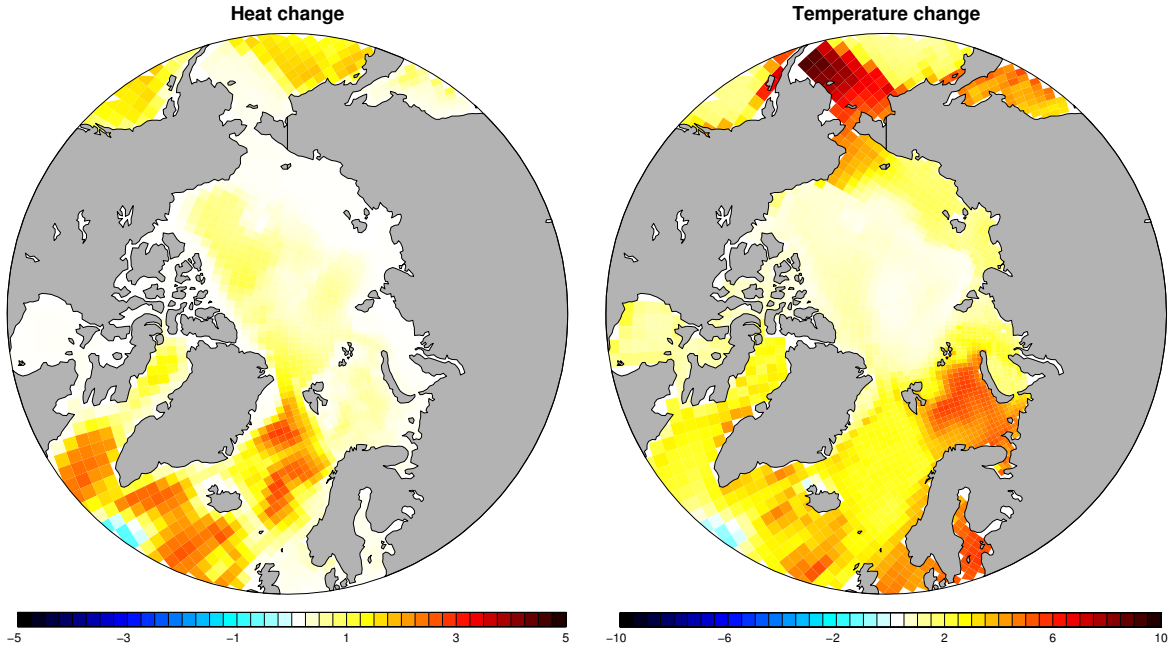

Figure 5.1: Changes for ocean heat content *(left)* and vertical avergage temperature *(right)*. All values are normalized against the global mean changes , .i.e. they present amplification factors.

Meridional Energy Transports in Atmosphere and Ocean. Meridional atmosphere and ocean heat transports are computed from the output of the BCM control experiment and greenhouse experiments, using the residual method outlined in section 2.2. Figure 5.2 shows the result for the climatological mean of the control experiment and results from observational based studies in Trenberth and Caron (2001). The overall match is fairly good with only minor discrepancies. Considering the spreading for different observational and model datasets investigated and discussed in Trenberth et al. (2001) one would expect even larger differences. Particularly, the ocean transports are close the mean of the transport results of over 15 Global Coupled Models presented in figure 5.3.

Heat Exchanges of the Arctic Seas. Applying the direct method outlined in section 2.2, advective estimates of ocean heat transports are computed for the BCM experiments. In total analogy to the mass products, the heat transports are presented in tabulated form in table A.2 and illustrated in figure 5.5. Corresponding flux patterns are shown in figure 5.7.

Eddy-Diffusive Transports. Turbulent, eddy-diffusive heat fluxes are shown for the control run in figure 5.6. The local fluxes shown in the right panel are vertical averaged over the whole water column.

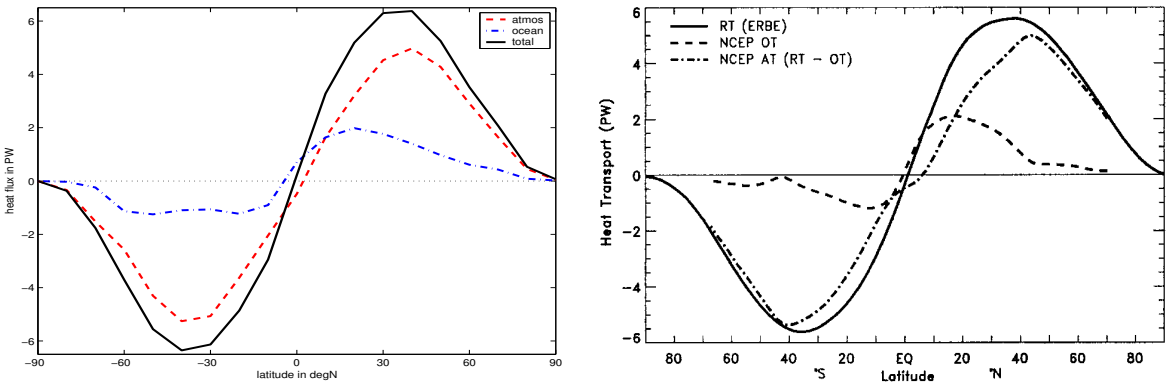

Figure 5.2: Meridional ocean and atmosphere energy transports derived from 300yr BCM control experiment *(left)* and reanalysed NCEP and observervational ERBE data (ref) *(right)*.

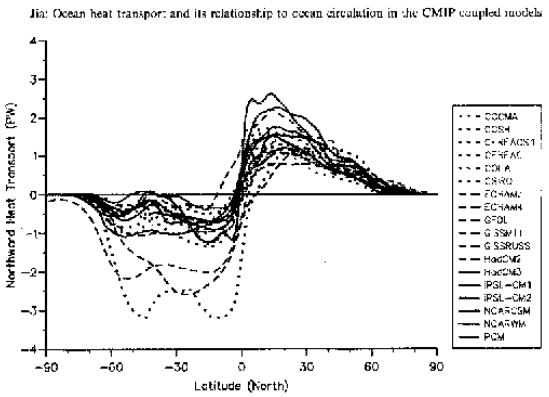

Figure 5.3: CMIP model intercomparison of meridional ocean energy transport (Jia 2003).

Climatology of Vertical Averaged Heat Transports.

Inter-annual Variability of Heat Transports in the Arctic Ocean. In analogy to the mass products, an AO composite of vertical averaged heat fluxes and projected changes of cross-sectional heat transports are present in figure 5.8.

Ocean Heat Exchanges with the North Atlantic. The temporal development of simulated Summer and Winter heat transports over the Iceland - Scotland ridge for the control and greenhouse experiments are shown in figure 5.9. Inflow temperatures of the control experiment and one CMIP member are shown in figure 5.10.

Figure 5.10 outlines a the temporal evolution of the spatial averaged temperature in the Atlantic Water inflow region for the control and one greenhouse experiment.

Sea-Ice Response to Oceanic Heat Transports. In Figure 5.13 figure correlations of maximum ice extend with the winter ocean heat transport through the Barents Sea Opening are presented for the BCM control simulation and observations. Regression of Arctic winter ice concentration on it's leading mode and Ikeda's ocean-ice-atmosphere feedback are shown in figure 5.11.

Residual and Direct Heat Budget Products for Selected Regions Table 5.1 summa-

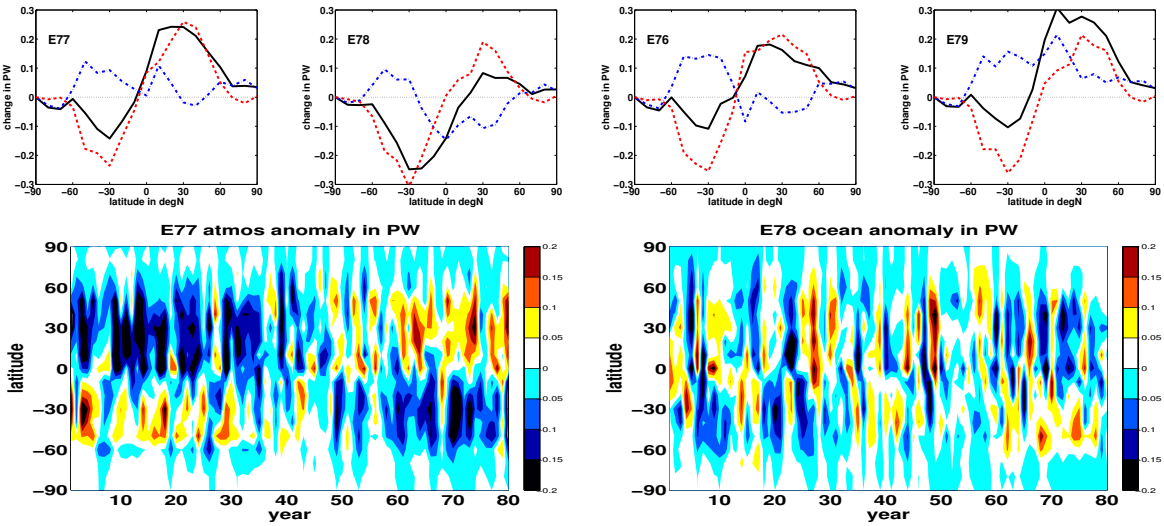

Figure 5.4: Future projections for meridional energy transports. *Top* panels show the projected changes of double CO_2 conditions after 70 years. The solid line represents the total, the dashed line the atmospheric and the dashed-dotted line the ocean changes. The *lower* panels show Hofmöller-plots with atmospheric transport anomalies of the E77 experiment and ocean anomalies of the E78 experiment. All units are in PW.

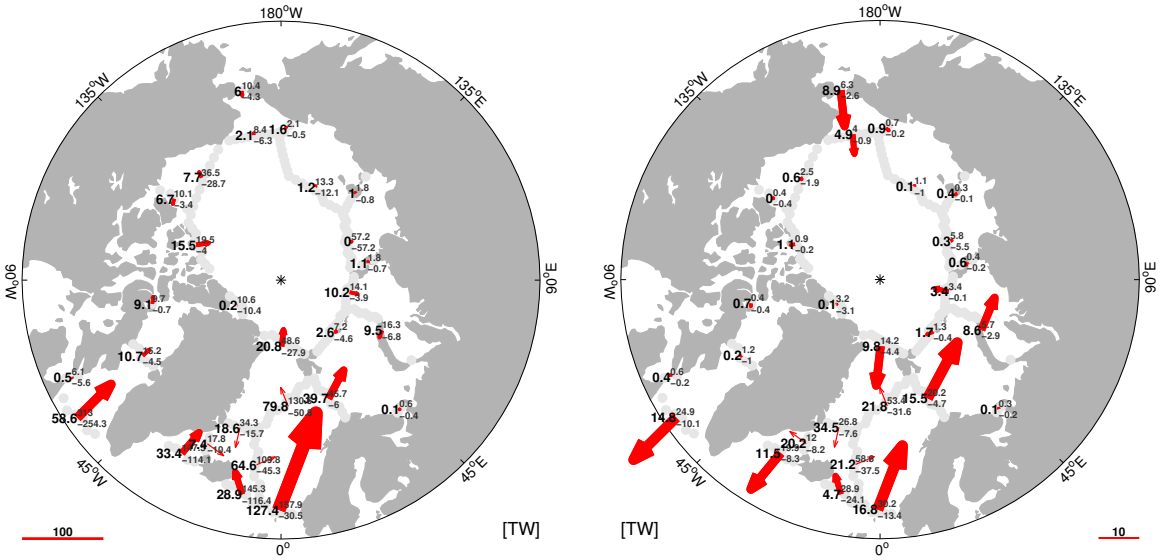

Figure 5.5: Simulated heat exchanges of the Arctic Seas. Average of 300 years control experiment *(left)* and projected echanges *(right)*.

rizes the heat budgets of selected regions in the Arctic. The Total of the Arctic Seas refers to the complete Arctic Mediterranean as shown in figure 1.2. The Arctic Ocean Proper comprises all Arctic Seas but the Labrador Sea extension and the Nordic Seas inclusive the Barents Sea. Surface exchanges as well as storage terms are shown on the left side of the tables whereas direct estimates of various components of the lateral heat transports are shown on the right side.

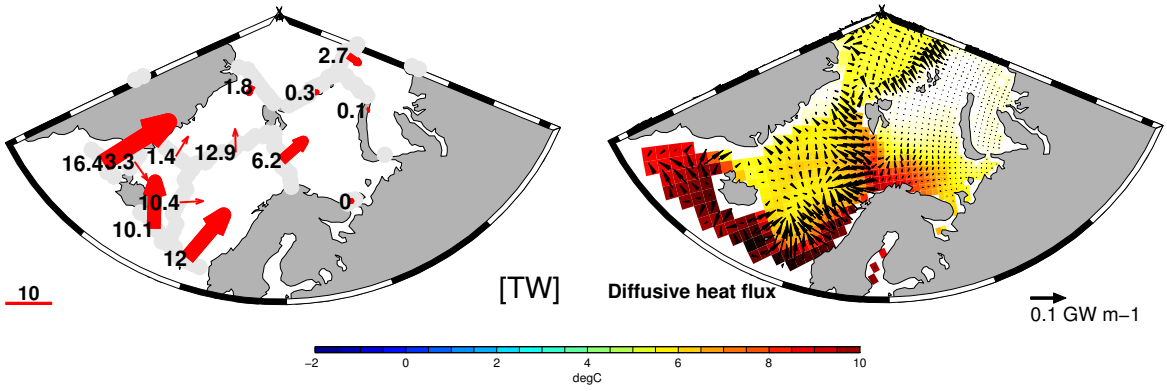

Figure 5.6: Eddy-diffusive heat fluxes of the BCM control experiment. Vertical *(right)* and cross-sectional integrated *(left)*.

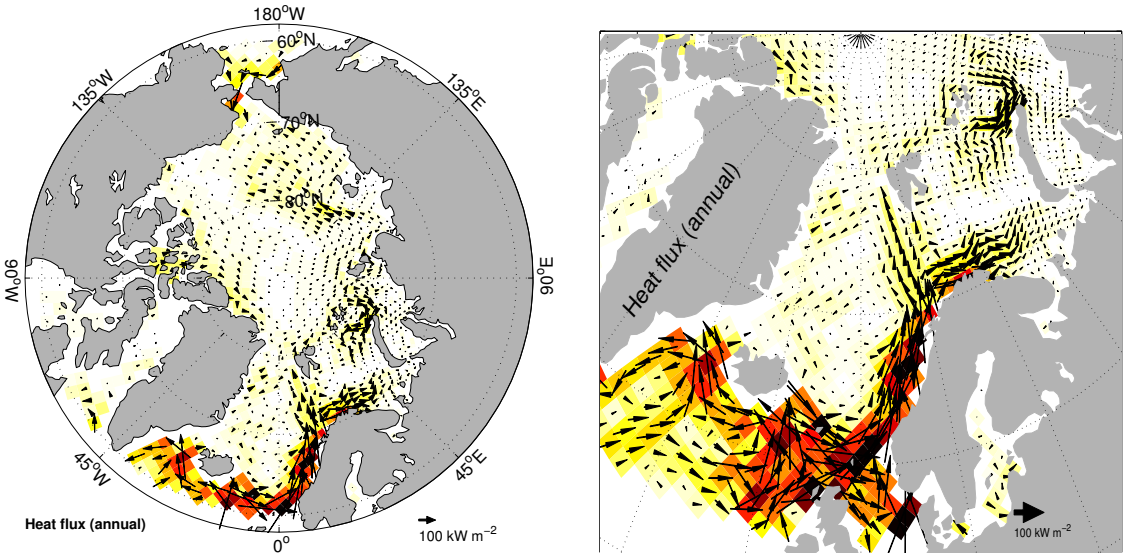

Figure 5.7: Vertical averaged heat fluxes. Shown are annual climatologies of 300 years control experiment.

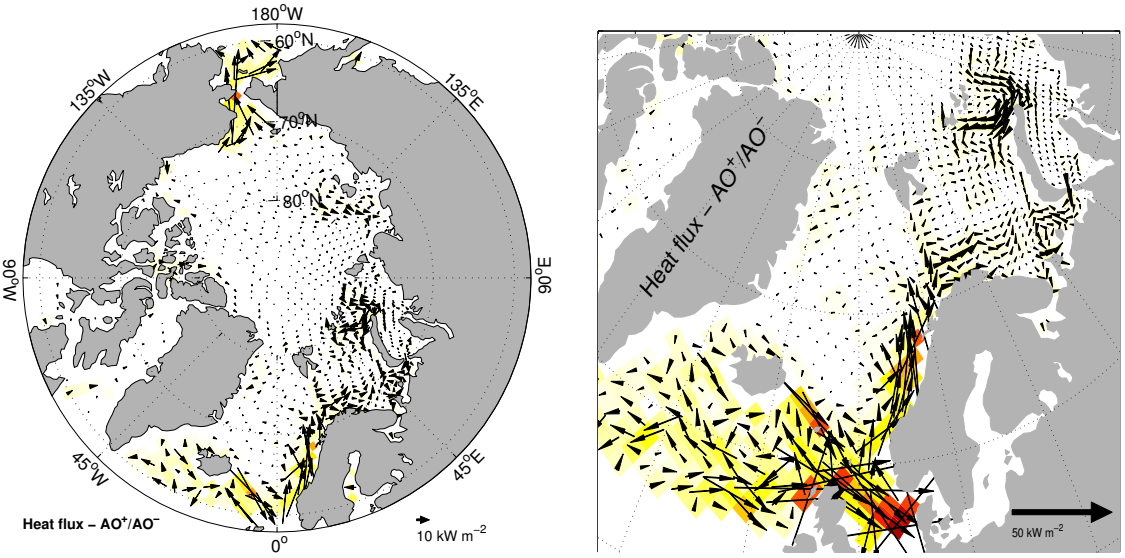

Figure 5.8: AO composite of vertical averaged heat flux. Shown are difference vectors between the AO^+ and AO^- subset mean of the BCM control experiment.

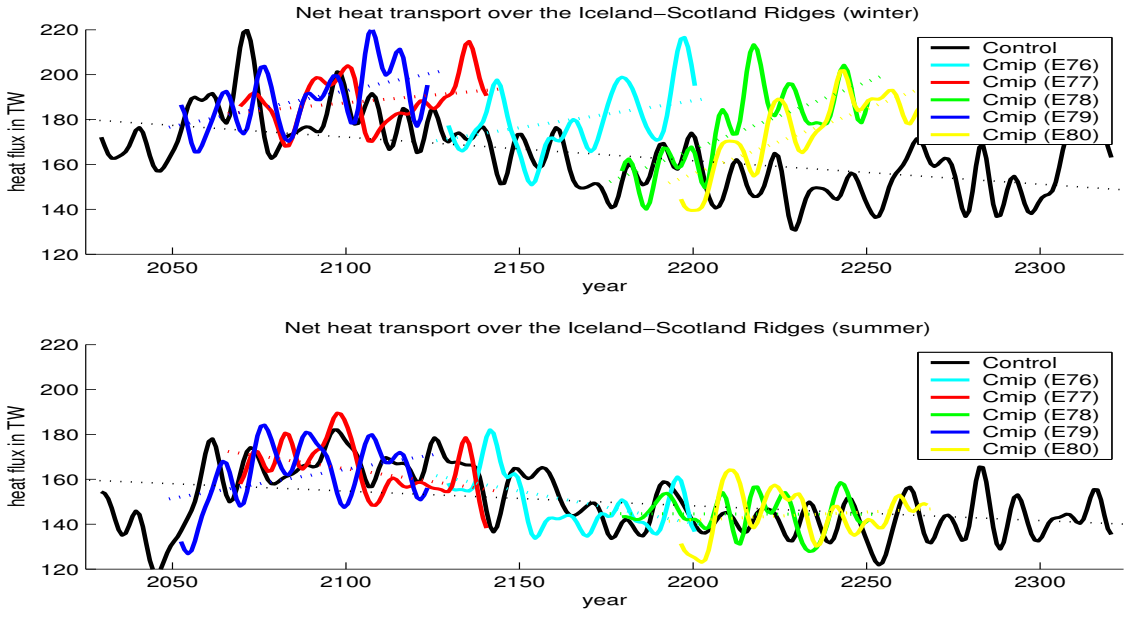

Figure 5.9: Time series of winter (djf) and summer (jja) heat transports through the Iceland-Shetland section for BCM control and greenhouse experiments.

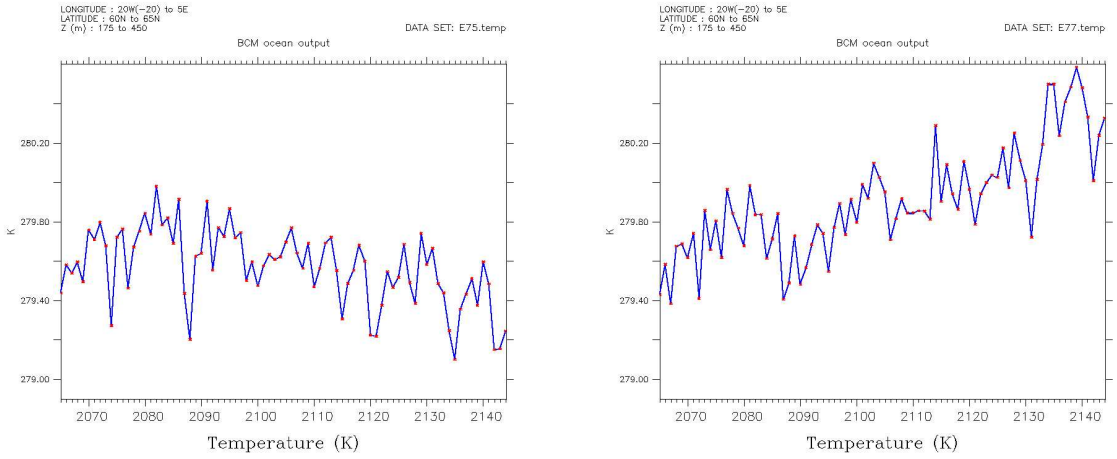

Figure 5.10: Atlantic water inflow temperature. Values are averaged from 20W-5E, 60N-65N and 400m-200m depth. Only january means are plotted.

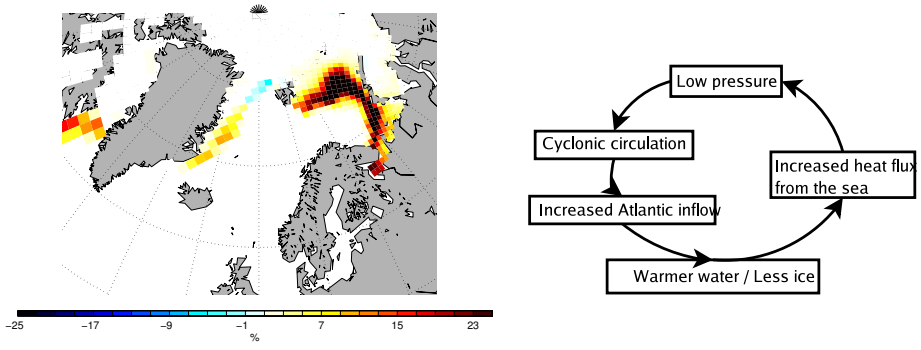

Figure 5.11: Regression of winter sea-ice concentration of the BCM control experiment on it's leading mode *(left)*. Feedback loop in the Barents Sea (after Loeng 1991) *(left)*.

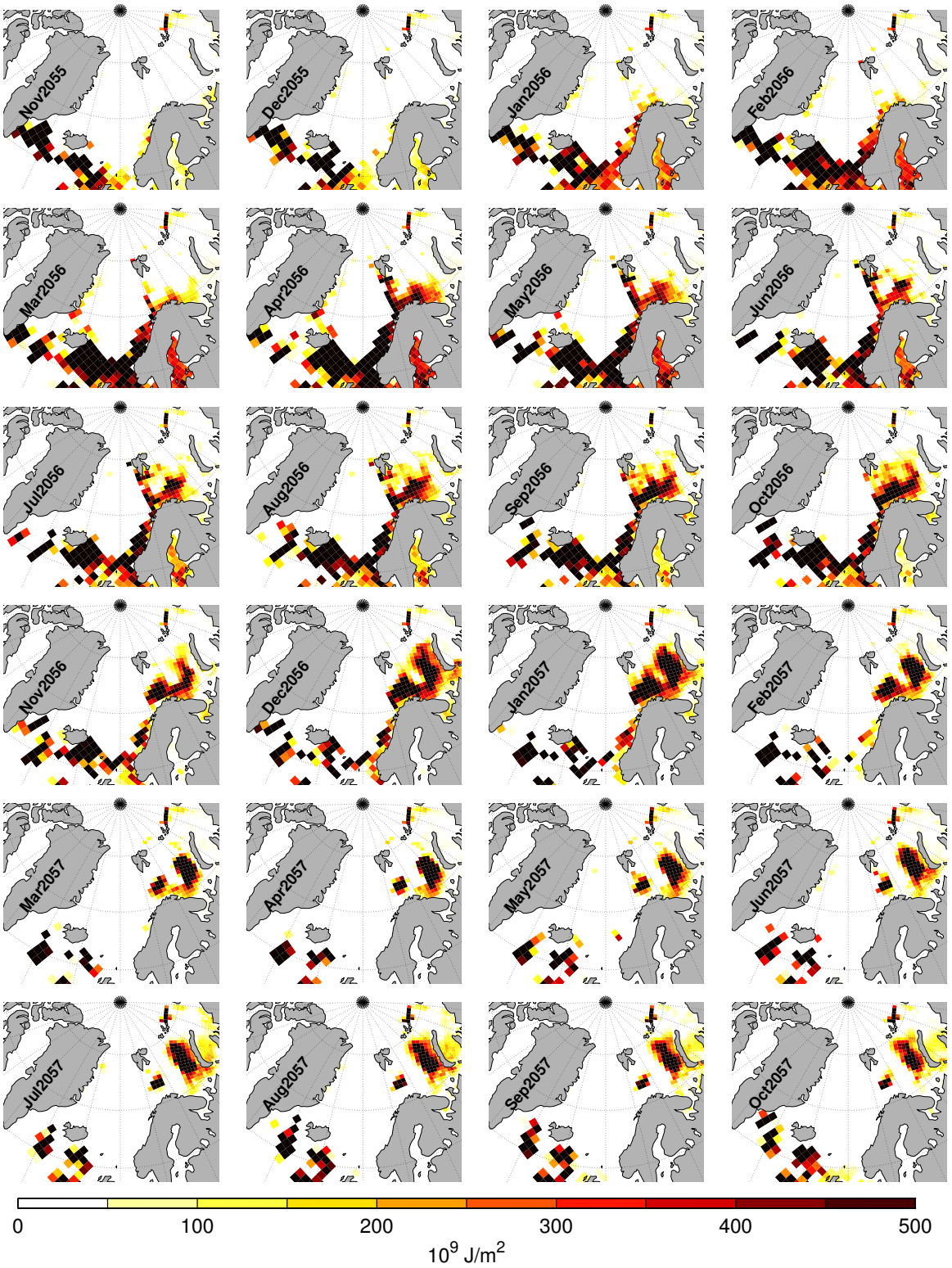

Figure 5.12: Simulated event of Atlantic Water inflow into the Barents Sea. Plotted are positive anomalies of vertical integrated heat storage.

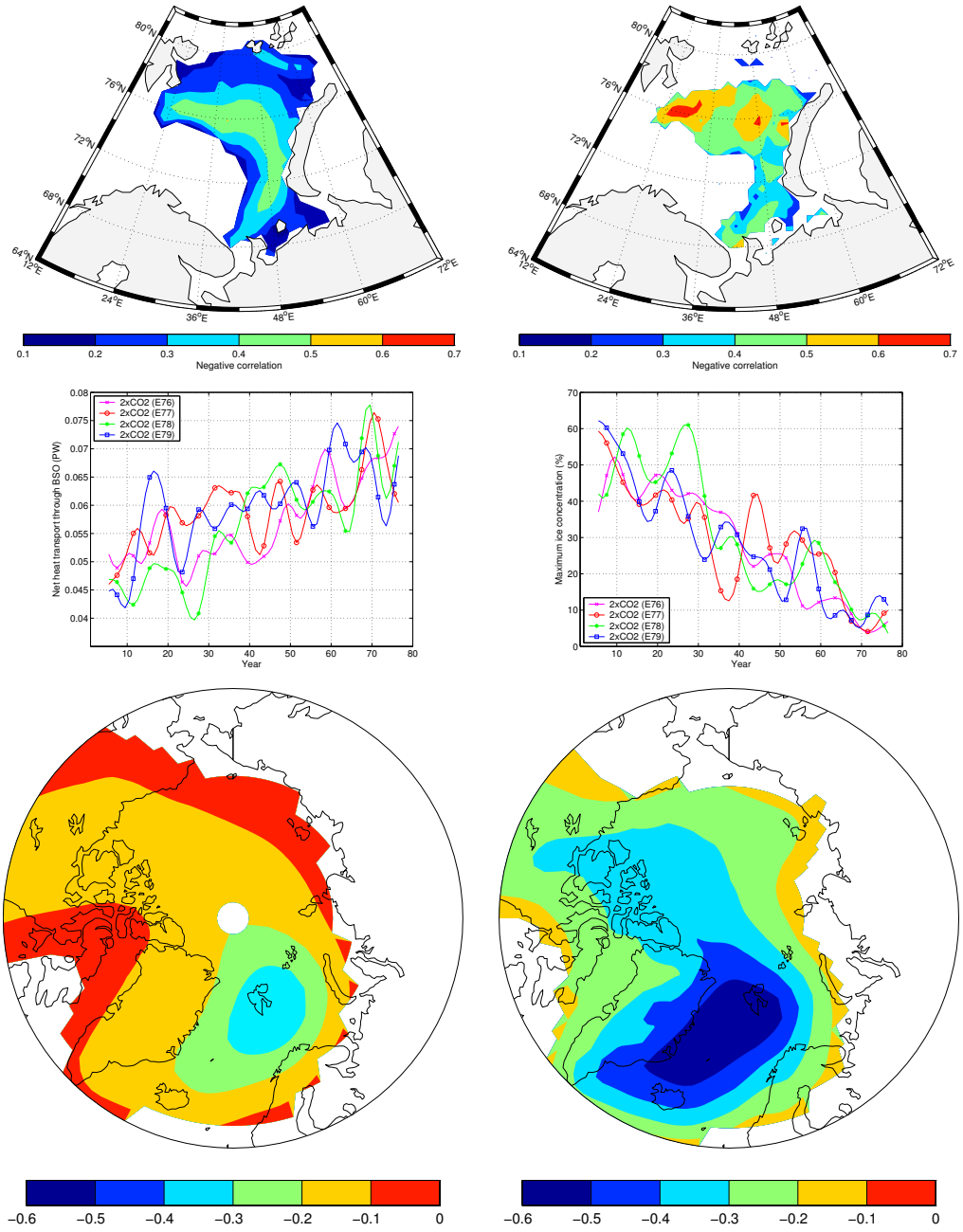

Figure 5.13: Correlations of maximum ice extend with the winter ocean heat transport through the BSO for BCM *(upper-left)* and observed AICSEX (Johannessen et al 1999) ice concentration with simulated heat transport (Nilsen et al 2003) *(upper-right)*.Smoothed time series of BSO ocean winter heat transports *(middle-left)* and maximum ice concentration of the Barents Sea *(middle-right)* in the BCM double CO_2 experiments. Correlation of winter (djfm) heat transport through the Barents Sea Opening with sea level pressure for the BCM control experiment *(left)* and MICOM hindcast with AICSEX satellite observations *(right)*. All analyses were conducted in collaboration with Olivier Laurantin and presented in detail in Laurantin 2004

.

Table 5.1: Mean residual and direct heat budget estimates for selected regions. All products are based on 300 years BCM control integration. Units are in TW for values without brackets and in W/m^2 for values in brackets.

Arctic Seas

Residual Estimate		Direct Estimate	[liquid-adv	liquid-dif	ice-adv	total]
Storage Tendency	6.8 (0.5)	Pacific Ocean	6	0	0	6
Flux Adjustment	-173 (-11.2)	Atlantic Ocean	248	35.1	0.1	283.2
Net short wave	816.6 (55.1)					
Net long wave	-598.4 (-38.9)					
Sensible heat	-219.7 (-14.2)					
Latent heat	-279.3 (-18.2)					
Net Surface	-279.7 (-18.2)					
Residual Transport	-447 (-26.9)	*Direct Transport*	254	35.1	0.1	289.2

Arctic Ocean

Residual Estimate		Direct Estimate	[liquid-adv	liquid-dif	ice-adv	total]
Storage Tendency	3.18 (1.24)	Barents S. - C. Arctic	-2.6	-0.3	0.8	-2.1
Flux Adjustment	-67 (-79.8)	Bering Strait	6	0	0	6
Net short wave	301.2 (38.7)	Fram Strait	20.8	1.8	6.8	29.4
Net long wave	-280.3 (-36)	Can. Archipelago	9.1	2.3	0	11.4
Sensible heat	-36.1 (-4.6)	Barents S. - Kara S.	-9.5	-0.1	2.1	-7.4
Latent heat	-59.2 (-7.6)					
Net Surface	-74.4 (-9.5)					
Residual Transport	-141.4 (-97.6)	*Direct Transport*	23.8	3.7	9.7	37.2

Nordic Seas

Residual Estimate		Direct Estimate	[liquid-adv	liquid-dif	ice-adv	total]
Storage Tendency	2.1 (0.9)	Barents S. Opening	-39.7	-6.2	-0.1	-46
Flux Adjustment	-27.3 (-11.5)	Denmark Strait	33.4	16.4	0	49.8
Net short wave	160.9 (70.6)	Fram Strait	20.8	10.1	-6.8	24.1
Net long wave	-99.5 (-42.1)	Island-Norway	156.3	12	0	168.3
Sensible heat	-76 (-32.3)					
Latent heat	-106 (-45.2)					
Surface Exchange	-115 (-49)					
Residual Transport	-145.8 (-59.6)	*Direct Transport*	129.8	32.3	-6.9	153.2

Barents Sea

Residual Estimate		Direct Estimate	[liquid-adv	liquid-dif	ice-adv	total]
Storage Tendency	0.2 (0.1)	Barents S. Opening	39.7	6.2	0.1	45.8
Flux Adjustment	-30.18 (13.6)	Bar. S. - C. A.	9.5	0.3	-0.8	9
Net short wave	81 (57)	Bar. S. - Kara S.	2.6	-0.1	-2.1	0.4
Net long wave	-45.6 (-31.9)					
Sensible heat	-43.4 (-30.4)					
Latent heat	-45.8 (-32.1)					
Net Surface	-53.4 (-37.4)					
Residual Transport	-83.4 (-50.9)	*Direct Transport*	51.8	6.4	-2.8	54.6

Table 5.2: Projected changes of residual and direct heat budget estimates for selected regions. All products are based on 300 years BCM control integration. Units are in TW for values without brackets and in W/m^2 for values in brackets.

Arctic Seas

Residual Estimate		Direct Estimate [liquid-adv ice-adv total]			
Storage Tendency	-	Pacific Ocean	9	0	9
Flux Adjustment	0	Atlantic Ocean	-4.8	-0.1	-4.9
Net short wave	64.9 (4.22)				
Net long wave	60.2 (9.91)				
Sensible heat	-11.4 (-0.74)				
Latent heat	-60.3 (-3.92)				
Residual Transport	53.4 (3.47)	*Direct Transport*	4.2	-0.1	4.1

Arctic Ocean

Residual Estimate		Direct Estimate [liquid-adv ice-adv total]			
Storage Tendency	-	Barents S. - C. Arctic	1.7	-0.4	1.3
Flux Adjustment	0	Bering Strait	-9	-0.1	-9.1
Net short wave	57 (7.31)	Fram Strait	-9.8	-4.1	-13.9
Net long wave	38.9 (4.99)	Can. Archipelago	0.7	0	0.7
Sensible heat	-42.3 (-5.4)	Bar. S. - Kara S.	-8.6	-4.6	-13.2
Latent heat	-48.3 (-6.2)				
Residual Transport	5.3 (0.69)	*Direct Transport*	-25	-9.1	-34.1

Nordic Seas

Residual Estimate		Direct Estimate [liquid-adv ice-adv total]			
Storage Tendency	-	Barents S. Opening	-15.1	0.1	-15
Flux Adjustment	0	Denmark Strait	-11.5	0	-11.5
Net short wave	-4.2 (-1.8)	Fram Strait	9.8	2.4	12.2
Net long wave	4.1 (1.73)	Island-Norway	16.8	0	16.8
Sensible heat	20 (8.46)				
Latent heat	0.3 (0.13)				
Residual Transport	20.2 (8.54)	*Direct Transport*	0	2.5	2.5

Barents Sea

Residual Estimate		Direct Estimate [liquid-adv ice-adv total]			
Storage Tendency	-	Barents S. Opening	15.1	-0.1	15
Flux Adjustment	0	Bar. S. - C. Arct.	-1.7	0.4	-1.3
Net short wave	7.7 (5.41)	Bar. S. - Kara S.	-8.6	4.6	-4
Net long wave	3.6 (2.42)				
Sensible heat	6.4 (4.5)				
Latent heat	-7.1 (-5.01)				
Residual Transport	10.5 (7.33)	*Direct Transport*	4.8	4.9	9.7

5.3 Energy Balance in the Present Climate

It was early recognized that zonal mean surface temperatures are not in radiative equilibrium. For a stable climate state it implies the existence of energy transports from the lower to the higher latitudes. Attempts to explain the present climate energy balance and its variability have a long history. With the launching of satellites to measure the Top Of the Atmosphere (TOA) radiation budget in combination with the qualified estimates of ocean-atmosphere heat exchanges, quantitative estimates of zonally and vertically integrated residual transports became feasible. In recent days the development of numerical models to fill spatial gaps in historical observational data and to provide future outlooks initiates the direct assessment of atmospheric and ocean transports. The direct method provides additional information over locale fluxes with their directions as well as contributions of different energy types and conversion whereas the residual method intigrates all these aspects.

Mean State Simulated ocean and atmosphere energy transports are presented and compared with observational estimates in figure 5.2. Zonally integrated fluxes are derived as a residual from TOA and surface heat divergences. Special attention is paid to flux corrections and climatic drifts. The model results match the observations within the uncertainties of the NCEP reanalysed based products and reproduce most of their features. A slight discrepancy is found poleward of $40°S$ and $40°N$ where simulated ocean transports are likely to be overestimated and atmospheric transports underestimated.

Heat Budgets. The simulated meridional ocean flux into the Arctic Mediterranean, for instance north of $62°N$ is close to 0.5 PW [a computation of table 5.1 with the exact area of the Arctic Seas gives a value of 450 W/m^2] which is well within the range of the CMIP comparison study shown by Jia (2003). The estimated advected mean heat transports from the Atlantic accounts for slightly more than half the amount and the diffusive eddy fluxes for another 10% (values are listed in table 5.1). Is the following paragraphs we attempt to address the remaining discrepancy.

Budget Uncertainties - Global. To test whether the ocean model is conserving heat we compare the total surface heat exchange of the World Oceans averaged over the control integration with the temperature drift. An average flux adjustment of +5.02 W/m^2 and a net surface exchange of -3.03 W/m^2 should be balanced by the average temperature drift which is 1.64 W/m^2. Thus, the global uncertainty is no more than 0.35 W/m^2. The nature of the global error has not been identified. In table 5.1 equivalent surface fluxes for the transports are listed. Comparing the direct with the residual transport estimates one can calculate that the discrepancy for the Arctic Mediterranean is around 20 times, for the GIN-Sea 10 times and for the Barents Sea over 30 times higher than the global error. Therefore, it can be concluded that the global heat sink, which might have it's origin in the numerical integration schemes, cannot be blamed for the mismatch in the heat budget investigated here.

Budget Uncertainties - Sea-Ice. Since the mismatch is largest in regions with high ice variability we might suspect uncertainties in the contributions of ice export/import and the thermodynamics of the ice module itself. Just recently the sea-ice model has been upgraded and improved (Mats Bentsen, personal communication). Applying the same budget analyzing tools on the data of future experiments might reveal imbalances in the heat storage of the old sea-ice code.

Budget Uncertainties - Advective Estimates. The possibility that the flux computation itself is erroneous has been tried to minimize. Since the products are virtually conserving mass one would expect a comparable accuracy for the heat and freshwater products. Moreover, earlier transport computations from the BCM group for predefined sections (Mats Bentsen, unpublished) were compared with the products presented here. They agree well and minor deviations are explained through a slight mismatch of the section locations.

Comparison of Transports through Selected Straits. The single constituencies of the budgets compare reasonably well with estimates from observations and other simulations. Through the Canadian Archipelago, Prinsenberg (2002) estimated an annual heat transport of 9.5 TW, Sadler (1976) estimated 10.8 TW and Aagaard and Greisman (1975) estimated 5.4 TW, i.e. the BCM advective transport with 9.1 TW is well within the observed range. For the Norwegian Atlantic Current Maslowski obtained some 155 TW from his pan-Arctic simulation which matches the positive Atlantic Water inflow of 158 TW of the BCM into the Norwegian Sea, as well as the net exchange of 156 TW between the Icelandic and Norwegian coasts. More over, his positive inflow of 4.7 TW through the Fram Strait is virtually equal to the 5.9 TW of the BCM whereas the net influx differs substantially as a result of a weaker East Greenland Current .

Diffusive Fluxes. Until now, we exclusively discussed the mean advective fluxes, since the observational estimate techniques are unlikely to cover eddy contributions. The diffusive heat fluxes have its greatest contribution to the heat exchange of the Arctic Seas in places where warm Atlantic Water meets the colder polar waters, i. e. in particular in the Nordic Seas and Barents Sea. Vertical and cross-section integrated climatological turbulent heat fluxes are illustrated in figure 5.6 . A striking feature is the Norwegian Atlantic Current radiating heat into the interior of the Nordic Seas. But, the question is weather the narrow, topography controlled slope current indeed communicates that much with the inner ocean. An overestimation of the heat loss might even explain the lack of deep convection in the Greenland Sea. Mixing of the advected Polar Water of the East Greenland Current with waters of Atlantic origin is captured reasonably well. However, most relevant for the integrated heat budgets are the large influx over the Denmark Strait and Island-Scotland Ridges whose sum exceeds some 30 TW , a modest flux through the BSO of approx. 6 TW and somewhat smaller fluxes from the Arctic Ocean Proper onto the shelfs, the Kara Sea in particular with 3 TW.

Variability As for the mass fluxes a comparison of the high index and low index years of the Arctic Oscillation has been conducted. The result illustrated in figure 5.8 is very clear. It shows an intensified heat transport with the Norwegian Atlantic and Norwegian Coastal Current. A large fraction continues through the Barents Sea Opening into the Barents Sea. In contrast, no signal is found in the branch entering the Arctic via the West Spitzbergen Current. Consistent with observations the Atlantic Water becomes modified in the Barents Sea by surface exchanges and interaction with sea-ice and cools below the reference temperature ($-0.1°C$ i.e. roughly corresponding to the mean temperature of the Arctic Ocean) before it enters the Kara Sea (compare with volume fluxes in figure 4.3). Thus, no positive overall increase of ocean heat transport into the Arctic is identified. On the contrary, a cooling as a consequence of an enhanced ventilation with cold Modified Atlantic Water from the Barents/Kara Sea seems so be more likely. The reduced heat inflow through the Bering Strait shown in figure 5.8 might be related to the earlier mentioned Atlantic-Pacific atmospheric tele-connection. However, it's contribute should of secondary order since the Bering Strait is very narrow and shallow. Yet, from a coupled point of view the conclusion might be different. Part of the heat that got lost to the atmosphere in the GIN-sea or Barents Sea might be returned to the ocean system, for instance by reducing the sea-ice growth.

5.4 Changes of Meridional Energy Fluxes and Arctic Heat Budgets

Changes of Meridional Atmosphere and Ocean Energy Transports Trends found in an ensemble of CMIP2 experiments suggest a robust 1% increase of poleward atmospheric heat transport under double CO2 conditions. Figure 5.4 shows that the projections of the different members are almost identically for the atmosphere. Trenberth and Stepaniak (2003) provide a mechanism capable of explaining the identified changes, which are consistent with the simultaneous strengthening of the hydrological cycle.

In connection to the global warming, increased evaporation in the subtropics, followed by a strengthened moisture import into the tropics, i.e. moisture convergence, will lead to additional latent heat release which in turn boosts the Hadley Circulation. A strong Hadley Circulation in turn exports sensible heat and very likely effects transient and stationary poleward eddy heat and moisture transports. A statistically less significant negative trend north of $70°N$ indicates a reduction of high-latitude atmospheric transport. The finding presumably originates in enhanced ocean atmosphere exchanges as a consequence of a reduced sea-ice cover leading to a weaker meridional atmospheric temperature gradient.

As shown in figure 5.4, in the ocean no coherent tendency can be found, but a reduced transport is observed during those experiments which show a weaker AMOC. A detailed analysis of that possibility is presented in the following section.

Changes of the Arctic Heat Budgets One of the hottest Arctic climate issue is the recent warming trend of the Arctic Ocean and it's implications for the Arctic ice cap. Strong evidence has been put forward of a spreading of the warm Atlantic Layer further into the Arctic Ocean (Gerdes et al. 2003; Visbeck et al. 2003; Schauer et al. 2004). Several studies address this phenomenon from different point of views. Steele and Boyd (1998) and Aagaard (1989) identify the renewal of the cold halocline layer as a key mechanism and try to explain the observed changes in terms of freshwater fluxes. In contrast, Gerdes et al. (2003) and (Schauer et al. 2004) focus on the potential of heat anomalies and trends of the warm Atlantic Water inflow through the Fram Strait. In this study, an attempt is made to find comparable features in the BCM simulations. Figure 5.1 illustrates a comparison of local, projected changes of vertical integrated and averaged ocean temperature with the corresponding global changes. In contrast to the polar amplification of Arctic surface temperature described by Holland and Bitz (2003), the heat content change of the Central Arctic Ocean is somewhat lesser than the global change. This finding is consistent with the result that the direct, absolute radiative change caused by perturbations in the atmospheric greenhouse compositions is largest in the lower latitudes. Furthermore, the sensible and latent heat loss to the atmosphere mostly compensates for the higher radiation in the ice free areas. This can be read directly from table 5.2. For instance, the Arctic Ocean absorbs additional 57 TW short and 39 TW long wave radiation which compares to an extra 42 TW sensible and 48 TW latent heat loss. In addition, a strengthened Barents branch and an accordingly week Fram Strait inflow seem to favor a cooling of the Arctic Ocean. Thus, no evidence is present that the observed the observed spreading of the Atlantic Layer is related to an enhanced greenhouse gas forcing. In contrast, the Gin Sea and North Atlantic exceed the global storage trend in heat by a factor 3 and the North Sea and Barents Sea exceed the global, vertical averaged temperature trend by more than a factor 5. Table 5.2 suggest that both, surface budget and transports with the adjacent seas contribute with about 15 W/m^2 to a substantial warming.

5.5 Future of the North Atlantic - Nordic Seas Heat Exchange

Does a slow down of the Atlantic Meridional Overturning Circulation (AMOC) reduce the ocean heat transport into the Arctic Seas?
In order to answer that question we first try to assess the observed and simulated contribution of the AMOC to the heat budget of the Nordic Seas. The following assessment will be a simplified estimate based on mean overflows and transport temperatures. The observed overflow over the Iceland Scottland ridges is estimated to 6 Sv with a temperature difference relative to the compensating warm inflow of approx. 6 K (Hansen et al. 2004). This leads to a net contribution of about 150 TW heat flux.

The simulated AMOC strength at $60°N$ (figure 4.5) corresponds roughly to the 6 Sv

observed overflow, leading to a heat flux contribution which has the same magnitude as the entire heat import (figure 5.5 and table 5.1) into the GIN sea and the complete heat loss to the atmosphere of the GIN sea. If we further assume that the relative reduction of the overflow is compareable to the relative MOC slowdown then the projected 10% to 20% MOC strength decrease (figure 4.5) corresponds to an equivalent reduction of the ocean net heat transport into the Nordic Seas. Nevertheless, the simulated transports are lacking this reduction and more surprisingly even indicate a congruent increase of the heat inflow into the Nordic Seas.

Inflow Strengthening. In all BMC greenhouse experiment members a strengthening of the Arctic Oscillation (figure 3.2) is present and strengthening of the North Atlantic Oscillation in all but one (not shown). Now, one can argue that this leads to a wind driven spin-up of the horizontal ventilation of the Nordic Seas (Furevik and Nilsen 2004) with an intensified Norwegian Atlantic Current transporting more warm Atlantic Water into the Nordic and Arctic Seas. Indeed, a correlation study on the 300 years control integration reveals a statistically significant link between the AO winter index and the net inflow over the Iceland Scottland Ridges with r=0.5. In addition a positive trend in winter, inflow is found in the greenhouse integrations (figure 4.6) as it already was the case for the AO index. Nevertheless, no significant trends are identified for the annual mean inflows (not shown) while those of the heat fluxes presented in figure 5.9 seem very persistent throughout the whole year. A comparison of the members does not indicate any significant annual trends of the volume transports through the Denmark Strait or over the Iceland Scotland Ridges.

Inflow Warming. Another possibility to compensate for the overflow reduction might be through an increase of the overflow-inflow temperature difference. Indeed, in all members this change in difference is observed and originates in a warming of the inflow waters of approximately 0.5 K with a core depth of between 200 m and 400 m (figure 5.10. For an initial temperature difference of 6 K the 0.5 K change has the potential to increase the MOC contribution by approximately 8% which still is somewhat lesser than the expected reduction due to the decreased MOC strength. A closer analysis of the inflow temperature reveals a series of warm events increasing in strength which explain a large fraction of the positive trend. Assuming that they are correlated with the inflow strength, which is plausible in the case where their nature is at least partly advective and not entirely local due to surface heat exchanges, an additional eddy heat transport will be related to them which is not included in the mean advective transports. Stronger amplitudes of fluctuations in the inflow equally contribute to the covariance $\overline{u'T'}$ and therefore have the same effect.

5.6 Sea-Ice Response to Oceanic Heat Transports

The variability of the Arctic sea-ice exhibits a strong seasonal dependency. Nevertheless, the memory of the Arctic ice cap and the ocean surface layer provides the system

a large auto-correlation with the effect that anomalies in form of extreme events might survive over several seasons. During summer time the local radiation budget together with the surface sensible heat flux are mainly responsible for sea-ice growth and melt whereas during the dark period ocean and atmospheric dynamics play a dominant role. For various reasons we will focus on the winter conditions in this work, despite that in general most concern is spent on the retreating summer ice. As already discussed in chapter 3 the sea ice cover is much better during the winter season. Another aspect is that in contrast to the summer season the variability is more organized which encourages us to investigate it more closely for dynamical links.

Arctic Sea-Ice Variability An PC/EOF analysis (figure 5.11) based on monthly mean ice concentration of 300 years BCM control experiment and 24 years satellite based Arctic Ice Cover Simulation Experiment data (Johannessen et al. 1999) reveals three variability centers which primarily are related to the winter ice. The fact that the summer variance does not show up in the first EOF indicates that it's nature is most likely local and to a high degree independent from the large scale circulation. The first variability center comprises the Labrador Sea ice that is basically governed by the atmospheric winter circulation and involved in feedbacks with the North Atlantic Oscillation (NAO) (Kvamstø, Skeie, and Stephenson 2004). The next center is located in the Greenland Sea and mostly resembles the Fram Strait ice export variability which is tightly linked to the local cross-strait atmospheric surface pressure gradient (Widell, Østerhus, and Gammelsrød 2003). The third and strongest center is defined to the Barents Sea and exactly resembles the winter ice extent of that region (for comparison see figure 3.6 in chapter 1).

Role of the Barents Sea for Arctic Climate. Beside the fact that the Barents Sea limits with Norway, an international awareness has developed that the region is of key importance for the Arctic Climate in general. Since large areas of the shelf sea are kept ice free by the inflowing warm currents, with air temperature far below the freezing point, vigorous ocean-atmosphere surface exchange of heat takes place. This contributes to a warmer Arctic surface climate. Evidence exists that ocean heat flux - sea ice - atmosphere feedbacks in that region have the potential to explain the so-called ≪early 20th century warming≫, a decade lasting event in the twenties, which affected the entire Arctic and had the same magnitude as the recently observed warming trends (Bengtsson, Semenov, and Johanessen 2004).

But equally or even more important is the modification of the inflowing Atlantic Water (AW) by cooling and delusion with sea-ice. The end-product, which eventually enters the Arctic, contributes to the renewal of the Cold Arctic Halocline. The latter in turn isolates the Arctic ice cap from the underlying warmer Atlantic Layer (AL) (Steele and Boyd 1998). In this section we will address the links between the trends and variability of the winter ice conditions and the warm currents of that particular region.

Comparison with Previous Studies. As a part of the project Monitoring the Atlantic Inflow toward the Arctic (MAIA) an observational study on the sea-ice sensitivity to

warm currents through the Barents Sea was launched (Lindquist, Rowan, and Häkansson 2003). In their study the BSO Atlantic Water inflow is represented with the help of coastal sea level data and the ice cover derived from high resolution SSM/I satellite imagery on the time scale of one day. Since their main objective was the focus on remote sensing the representation of the sea-ice conditions is excellent. But especially the ocean flux estimates exhibit a couple of uncertainties. The current structure between Bear Island is rather complex with two branches, the Norwegian Coastal Current and the Norwegian Atlantic Current (NAC) which have very different characteristics when it comes to temperature and salinity. Recirculation of the NAC in the Bear Island trough makes the picture more complicated. Even if the statistical relation between the sea level in Hammerfest and the warm inflow might be strong, which needs to be tested, the causal links proposed in the MAIA report is oversimplified and can at most account for the shelf current. Amongst others, the investigated time daily time scale is to short, since geostrophic adjustment roughly requires one pendulum day or inertial period, i.e. longer than one day at that latitude to be obtained (Pond and Pickard 1978). Secondly, aliasing in the daily means of the tides can be expected in the case no tidal correction has been applied. Statistical links based on uncorrected data might just indicate that both, the BSO influx and the Barents Sea ice conditions are effected by tides. Lastly, heat advection acts on longer than daily time scales, e.g. several months, which means it does not have any chance to have any effect.

BCM vs. Hindcast/Satellite. Our study is complemental with the objective to test the identified links for inter-annual to multi-decadal time scales on which we believe that ocean dynamics play a bigger role. Thereby, we make use of reconstructed and simulated ocean fluxes combined with observed and sea-ice. Figure 3.6 shows a close match of the observed climatological sea-ice winter maximum with those observed in the Barents Sea, with only marginal discrepancies south of Svalbard. In figure 5.13 the result of a correlation study of simulated Barents Sea Opening (BSO) winter heat influx (Nilsen et al. 2004) and satellite derived maximum ice extent (Johannessen et al. 1999) is shown. This is discussed in more detail in Laurantin (2004). Figure 5.13 demonstrates the capability of the BCM in reproducing the relation which resembles the observed pattern quite precisely. Since the control time series spans 300 years, i.e. five times longer than the NCEP-NCAR dataset, the simulated correlations exhibit a higher level of significance which exceeds 99%.

Causalities - Role of Ocean Transports. Now, that the statistical relation is established, it remains to understand the causal links. There is no doubt that a stronger than normal current into the Kara Sea and prevailing westerly winds favour ice export rather than import from the Barents Sea. But, we argue that the variation in heat transport through the Barents Sea Opening (BSO) alone has the potential to explain the reduced winter ice extent in the Barents Sea. Figure 5.12 illustrates how a simulated ocean heat anomaly is advected from the North Atlantic, along the Norwegian coast into the Barents Sea where it remains for almost one year. At the same time the winter ice concentration substantially reduced (not shown). A more quantitative

and scientific assessment is proposed as follows. The Barents Sea region defined in figure 1.2 covers an area of $1395 \times 10^3\ km^2$, which is only 0.3% less than the the latest geographical estimate of Jakobsson (2002).

For the computation of the sea-ice area the area of the grid cells containing ice is weighted with the local ice concentration. The average winter maximum of the simulated sea-ice occupies $705 \times 10^3\ km^2$ or $\approx 50\%$ of the total area. The winter-to-winter standard deviation is $114 \times 10^3\ km^2$, i.e. approx. 9% of the total area.

In contrast, the winter (djfm) averaged heat transport relative to $-0.1°C$ is 46.7 TW with a standard deviation of 8.1 TW or 17.3 %. Consequently, the winter accumulated amount of heat is equivalent to 262 km^3 sea-ice, using the model volumetric latent heat constant $c_l = 3.02 \times 10^8\ J/m^3$. Since the simulated Barents Sea sea-ice thickness varies between 0.5 and 1.5 m, i.e. it is approx. 1 m on average, the heat transport denotes twice the heat amount necessary to melt the ice. Taking under consideration that a large fraction of the anomalous heat is lost to the atmosphere, this result comes not totally unexpected.

Causalities - Role of Atmospheric Circulation. After having assessed the impact of the inflow fluctuations on the ice conditions it still remains to clarify what governs the inflow in the first place. It is reasonable to assume that atmospheric variability dominates on inter-annual and shorter time scales, so that changes the thermohaline circulation, which is poorly understood, does not need to be considered. A straight forward way to approach the problem is to correlate the inflow with the atmospheric pressure field in every point.

The correlation pattern of the winter Barents Sea Opening (BSO) net heat influx with the sea level pressure shown in figure 5.13 has a center over the north-western Barents Sea with it's maximum gradient along the Svalbard-Norway section. This is exactly the configuration one would expect to get the strongest inflow with the geostrophic wind in cross-strait direction. Beside the direct Ekman transport which might contribute to the surface inflow, piling up of water against the Norwegian coast eventually leads to a geostrophic response, intensifying the inflowing currents at all depths (Ingvaldsen et al. 2004). Beside the large incoming mid-latitude low pressure systems which are very well correlated with the NAO index since they constitute the storm tracks, local genesis of so-called polar lows exists. Yet, how their activity is related to the sea-ice concentration is debated. Figure 5.14 shows observed polar low ocurrences which might favour the influx through the BSO.

Ocean - Sea Ice - Atmosphere Feedbacks. Investigating the longevity of low pressure anomalies Ikeda (1990) identified an important feedback between the BSO-inflow and the atmospheric circulation over the Barents Sea. During winter time strong westerlies cause an increased inflow of warm AW into the Barents Sea which in turn reduce the ice extent. The area of open water is highly correlated with the atmospheric temperature in lower levels which in turn effect atmospheric stability and surface pressure. This conditions then favor the presence of anomalous lows with corresponding geostrophic winds over the BSO. More precisely, we argue that a larger ice-free area prolongs the

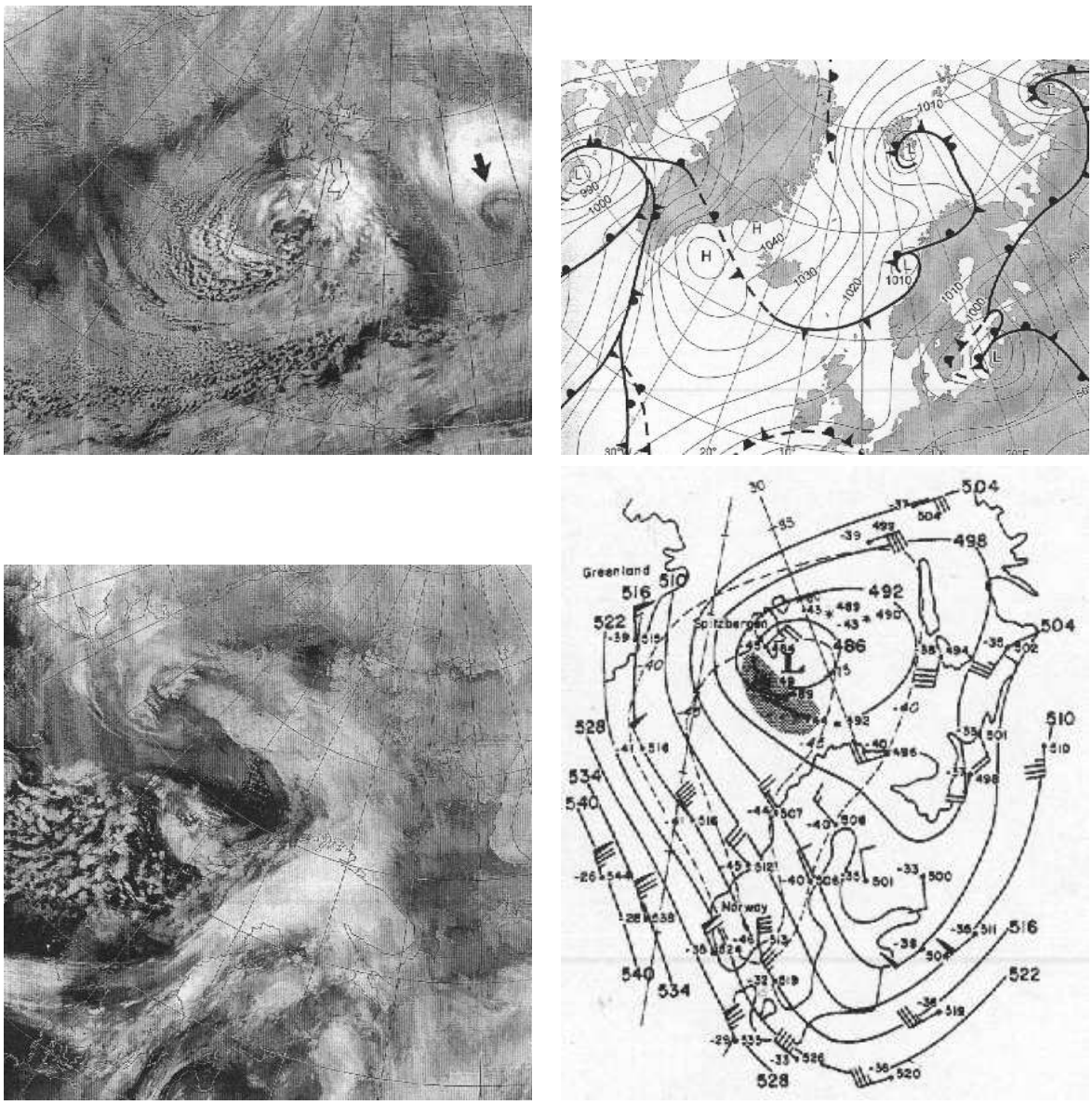

Figure 5.14: Polar Low occurences in the Barents Sea Opening region. (Rasmussen 2003)

life time of lows passing over the Barents sea. Furthermore, we argue that a wider ice edge might increases the probability of polar low generation. Based on the work of Ikeda (1990) the complete feedback loop is illustrated in Ådlandsvik and Loeng (1991) and is reproduced in figure 5.11.

However, results from the same ocean model as employed in the coupled BCM driven with observational based, reanalyzed NCEP wind fields show a correlation pattern which is closer to the typical NAO structure with it's center displaced towards the Norwegian Seas (Laurantin 2004). Since the coincidence that the NCEP data comprises the second half of the 20th century the persistence of the positive index phase might have biased the analysis, in the sense that a strong positive NAO governs over all local variability. An alternative, more interesting explanation for the mismatch is that the coupled ocean-ice-atmosphere mode, which is based on the very feedback described in Ikeda (1990),Ådlandsvik and Loeng (1991) and Bengtsson et al. (2004), cannot be captured by the ocean only model forced with an observed atmosphere.

Future Perspective Regarding the inter-annual variability no doubt is left about the presence of a strong link between warm influx and sea-ice conditions. But does the relation hold for present and future trends?
Of the observed 3% per decade Arctic ice area reduction the largest decrease, about 10.5% per decade is identified in the Barents and Kara Seas (Zhang et al. 2003). As figure 5.13 shows, a remarkable resemblance is present of the temporal development of heat inflow with that of ice area in all BCM future projections. Therefore, from statistical and causal/thermodynamical arguments it can be concluded that positive present and future trends in BSO heat influx will at least contribute to reduction of the Barents Sea sea-ice which might lead to a year-round ice free Barents Sea at the end of this century. Comparing the 1990s with the 1980s and 1970s, Schauer et al. (2002) already reported a substantial warming of the inflow of about 2 K.

5.7 Chapter Summary

Future of the North Atlantic - GIN Sea Heat Exchange. Despite a reduction of Atlantic Meridional Overturning Circulation strength the results from 5 greenhouse simulations project an inreased ocean heat transport into the Nordic Seas. Possible contributers are an intensified winter inflow in accordance with a deepening Icelandic Low, a increasing inflow temperature and enhanced eddy heat fluxes. However, shortcomings in the simulation of open ocean convection in the GIN-seas and the related Denmark Strait and Iceland-Scotland overflows might explain the moderate contribution of a weakening of the AMOC.

Implications for the Arctic Sea-Ice Large scale sea-ice changes over the entire Arctic are likely to be primarily caused directly by dynamical and thermodynamical atmospheric forcing. Some regional changes seem to be controled by oceanic fluxes, particularly the winter ice conditions of the Barents and parts of the Kara Seas.

Comparison of Residual and Direct Estimated Heat Budgets A comparison of direct with residual budgets suggest that the contributions of eddy diffusive fluxes have roughly the same order of magnitude as the advective transports by the currents. Consequently, to obtain consistent heat and freshwater balances with the direct method, an assesment or reconstruction of the eddy fluxes remains indispensable.

Chapter 6

Freshwater Budget

6.1 Introduction

Throughout the last century research very much focused on the assessment of the Arctic energy budget (Adams et al. 2000; Overland et al. 1996; Nakamura and Oort 1988). Only recently there has been a similar focus on the freshwater budget (Vörösmarty et al. 2001). A common awareness of the importance and various implications of the hydrological cycle has emerged. In the atmosphere, snowfall, cloud formation and atmospheric moisture content determine a large fraction of the Arctic radiation budget and are literally involved in all feedback processes in the Arctic. In the Arctic Ocean, the freshwater cap, forming the top of the cold halocline, insulates the sea ice from the warm Atlantic Layer and thus favors the sea ice growth. Ice and freshwater export through the Fram Strait and the passages of the Canadian Archipelago have the potential to inhibit convection and thereby modulate the thermohaline circulation as it happened in the Labrador Sea during the Great Salinity Anomaly (Haak et al. 2003). Apart from the overturning and wind driven circulation, the ventilation of the Arctic Seas resembles an Estuary circulation with a freshwater excess and export at the top and a import of salty water at intermediate levels.

In this chapter the Arctic freshwater cycle is explored. Thereby, the analyses follow the complete loop, starting with the atmospheric moisture export from the lower latitudes, continuing then with the precipitation excess in the middle and higher latitudes, river runoff into the Arctic Seas, redistribution the freshwater by ocean circulation and closing the loop with the southward export. Combing all components, simulated budgets of selected regions are stated for the present and future climate.

6.2 Analyses and Results

Atmospheric Moisture Transports – Present and Future. Figure 6.1 shows monthly averages of global mean precipitation for the present and future climate simulations, which can be understood as a measure for the strength of the global freshwater cycle. In

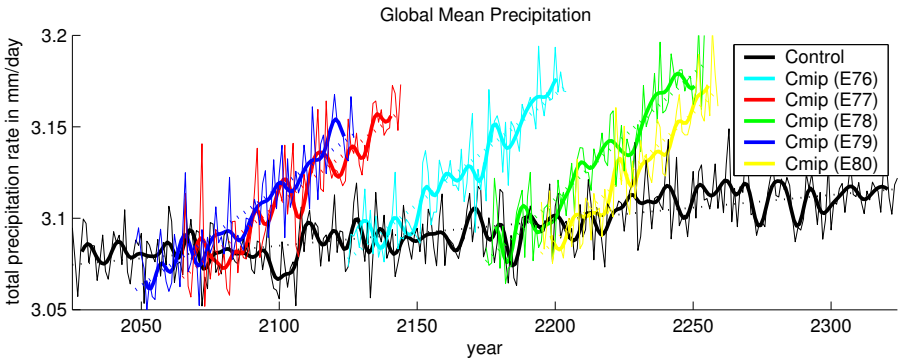

Figure 6.1: Annual mean of global averaged total precipitation rate for the BCM control and cmip experiments.

order to obtain an vertical integrated two dimensional picture one has to consider horizontal transports. In this study the direct estimation of local atmospheric fluxes is not feasible. Trenberth et al. (2001) pointed out various difficulties concerning the direct assessment of atmospheric transports, amongst others the post-processing precision losses during the interpolation to pressure levels. Therefore, we limit the analysis on the residual meridional moisture transports in the Atmosphere. The storage tendency of water in the atmosphere is negligible on longer time scales and hence not considered here. Monthly means of total precipitation P minus all surface evaporative fluxes E, including sublimation and transpiration, are integrated as in section 2.2 described. As with the computations of residual heat fluxes in the previous chapter, systematic uncertainties are introduced by the fact that the simulated global budgets are not closed. Globally, an artificial water source of 0.34 Sv is detected, that corresponds to almost 2% of the global mean precipitation. Whether this is due to the uncertainties in the model integration or post-processing is not identified. The results are summarized in figure 6.2. Shown are mean and future projections of local and zonal averaged P-E as well as the corresponding meridional moisture transports. The changes in P-E are accumulated over the typical CO_2 doubling period of 70 years to be comparable with projected changes in ocean freshwater yield. The feature most relevant for this study is the substantial transport increase of more than 10% from the subtropics to the middle and higher latitudes. This finding is discussed and explored further in section 6.3.

Ocean Signature of Changes in Freshwater Cycle. Figure 6.3 shows projected changes in freshwater content for the World Oceans and figure 6.4 the changes for in freshwater content and vertical averaged salinity for the Arctic Ocean. Changes in freshwater content are computed relative to a reference salinity of 45 psu for the world oceans and 34.9 psu for the Arctic Ocean. Note that the conversion of absolute salt contents to freshwater is highly dependent on the choice of the reference salinity whereas the conversion of salt content differences is fairly insensitive. This follows directly from equation 2.3.

The strongest salinity reduction occurs in the Siberian Shelf Seas (and in the Baltic

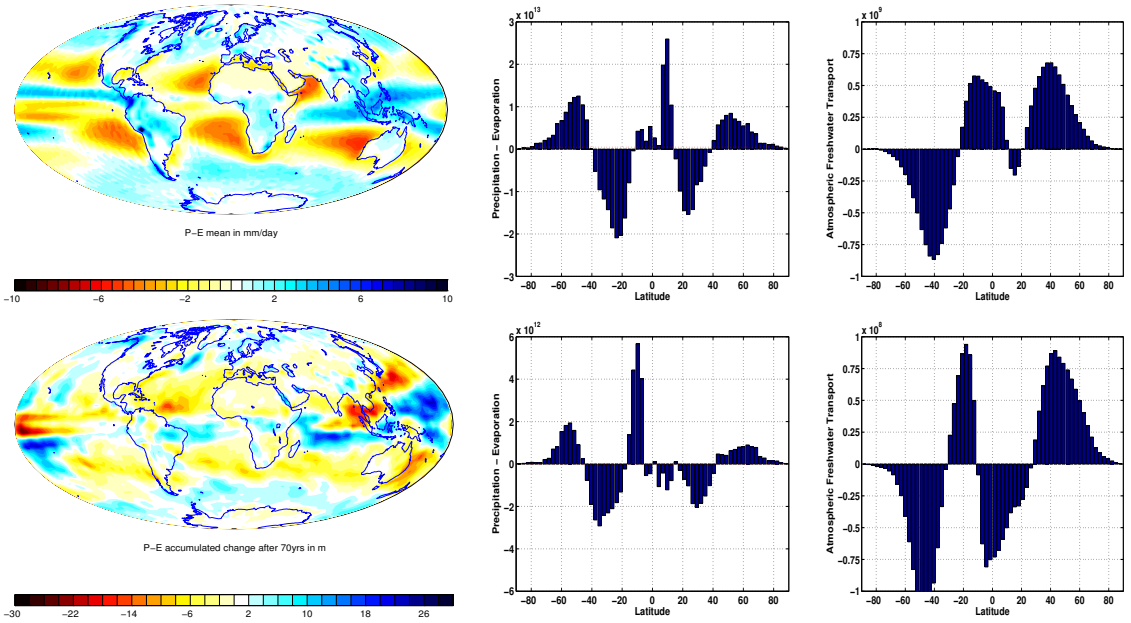

Figure 6.2: Control mean of P-E *(top-left)*, zonal integrated P-E *(top-middle)*, zonal integrated poleward atmospheric moisture flux *(top-right)*, and corresponding projected changes of the E77 experiment *(bottom)*. Units of the transports are kg/s and of zonal integrated P-E are kg/s per bin (bins have a meridional extension of 2°).

Sea for completeness sake) whereas the vertical integrated change is largest in the Ocean interior. In contrast, the pathways of the Atlantic Waters leave a deep saline trail behind which is further discussed in section 6.4. On the other side, the East Greenland Current is freshening as well as the Canadian Archipelago, Baffin and Hudson Bay. The signature in the Chukchi Sea resembles those in the Barents Sea and in general those in the North Pacific shown in figure 6.3. In order to explain mean and changes of the freshwater content distribution Arctic P-E, river runoff and freshwater transports in the ocean are analyzed in the following part of this chapter.

Runoff into the Arctic Seas. An annual climatology of simulated and observed runoff into the Arctic Seas is presented in figure 6.5. The observed estimates only account for the contribution of major rivers whereas the simulated runoff comprises the total discharge into the Arctic Seas, The simulated seasonal cycle is investigated with observations in figure 6.6. Inter-annual variability in relation to the AO is investigated in figure 6.7. Projected changes in accummulated Arctic P-E and total runoff are shown in figure 6.8.

Freshwater Exchanges of the Arctic Seas. Climatological means and projected changes of cross-sectional integrated freshwater transports are shown in figure 6.9 for water and in figure 6.10 for ice. Strongest imprints exhibit the inflow through the Bering Strait, the outflows through the Canadian Archipelago and the shelf contribution from the Kara Sea but also a stronger export through the Canadian Archipelago. However, the reduction of ice export from the Central Arctic shown in figure 6.10 has the largest contribution to the net freshwater gain of the Arctic Ocean.

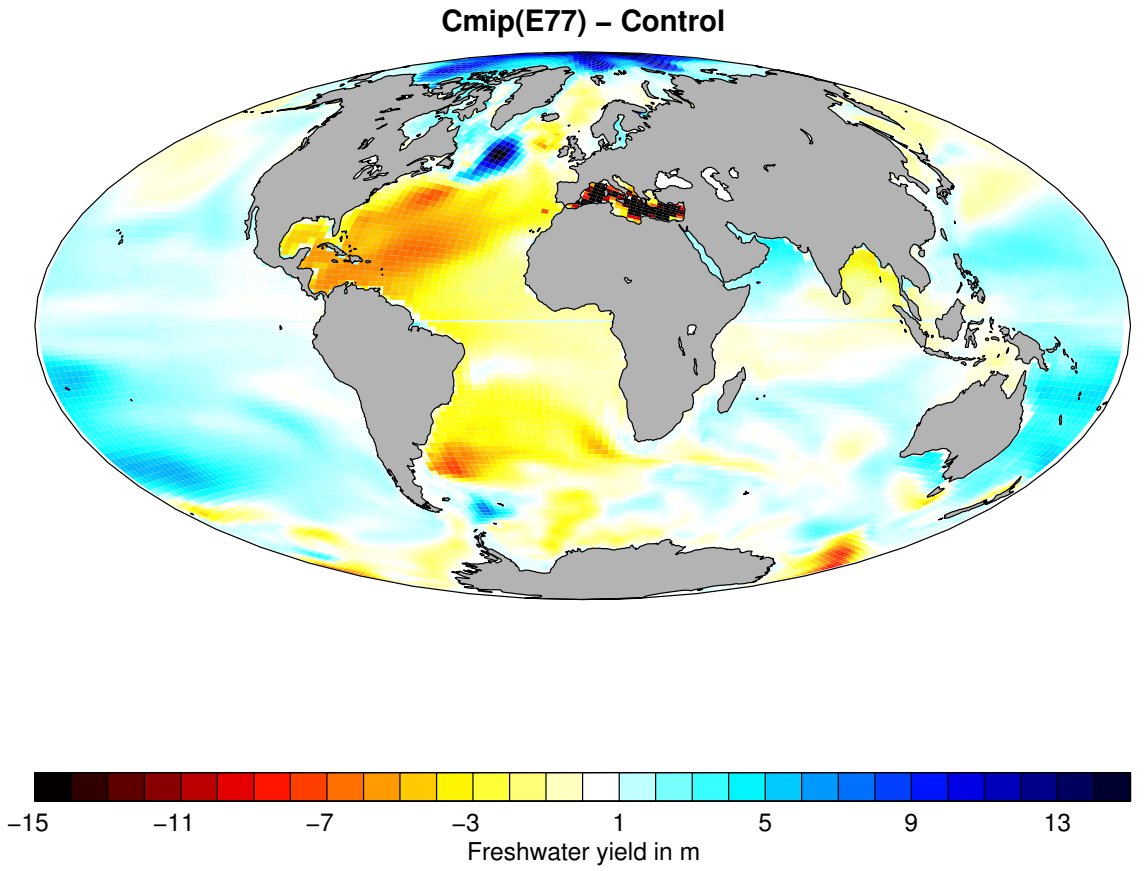

Figure 6.3: Projected changes in ocean freshwater yield of one BCM cmip member.

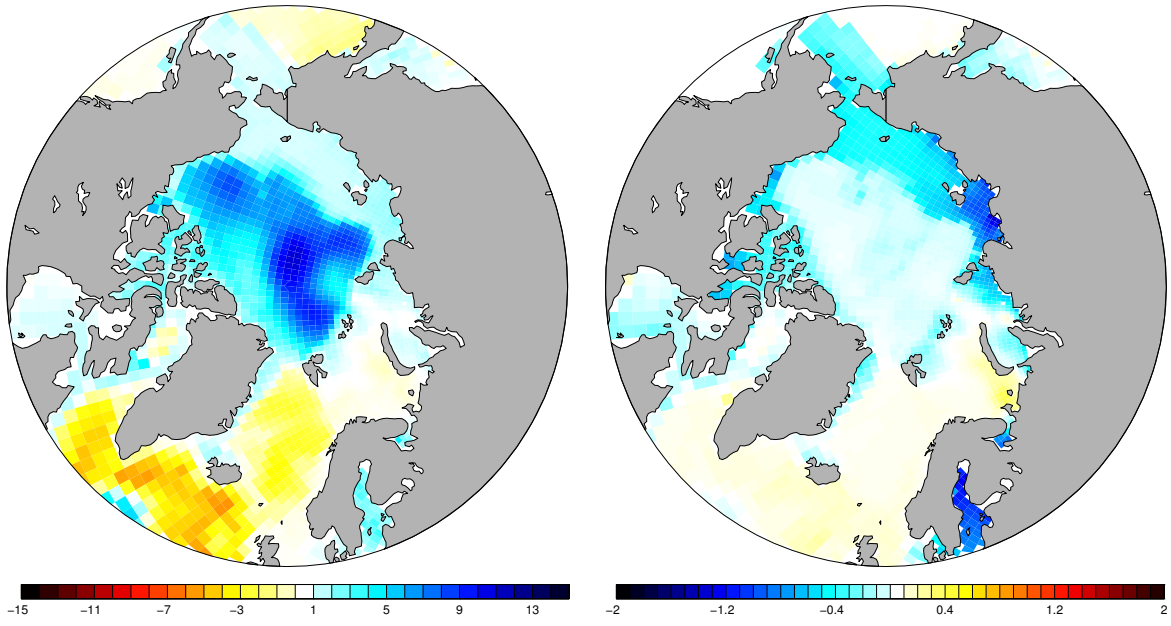

Figure 6.4: Projected changes for ocean freshwater yield *(left)* and vertical averaged salinity *(right)*.

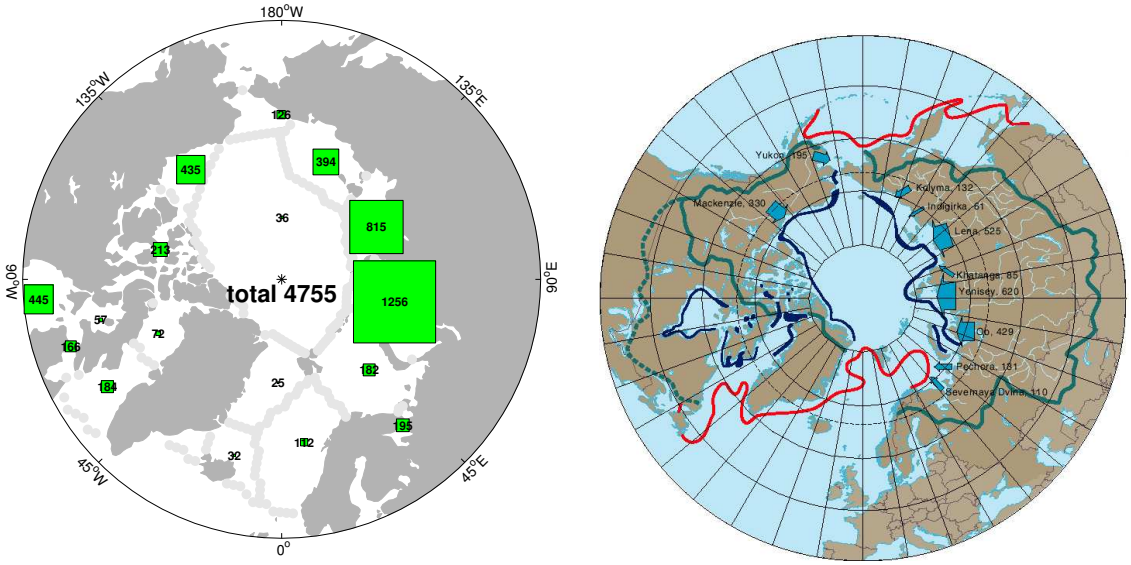

Figure 6.5: Mean total runoff into the Arctic Seas *(left)* for the BCM control experiment and observational derived river runoff (Macdonald 2002) *(right)*.

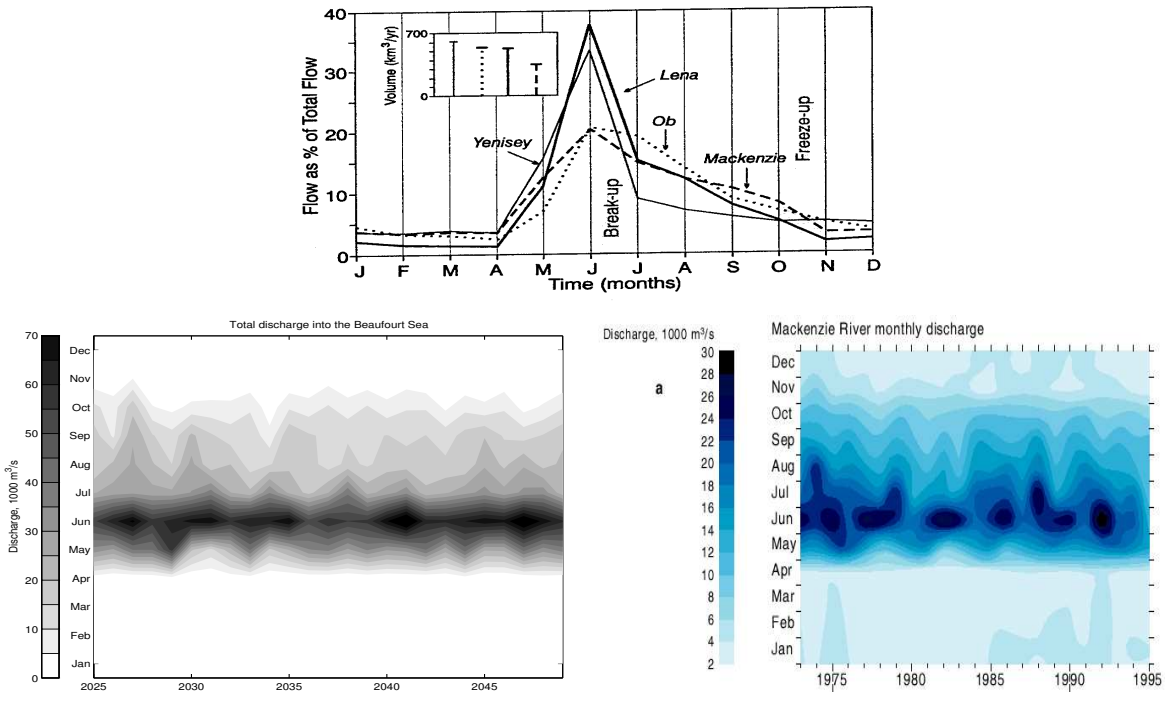

Figure 6.6: Comparison of the simulated total runoff into the Beaufort Sea *(lower-left)* with the observed Mackenzie river runoff (Macdonald 2002) *(lower-right)*. Observed seasonal cyle (Macdonald 1995) *(upper panel)*.

Flow Charts of Freshwater in the Arctic Ocean. An annual climatology of vertical averaged freshwater fluxes is provided in figure 6.11. The choice of vertical averaged instead of vertical integrated fluxes highlights the shallow sloop currents and shelf seas. A quantitatively more consistent picture is presented in figure 6.9. A striking feature

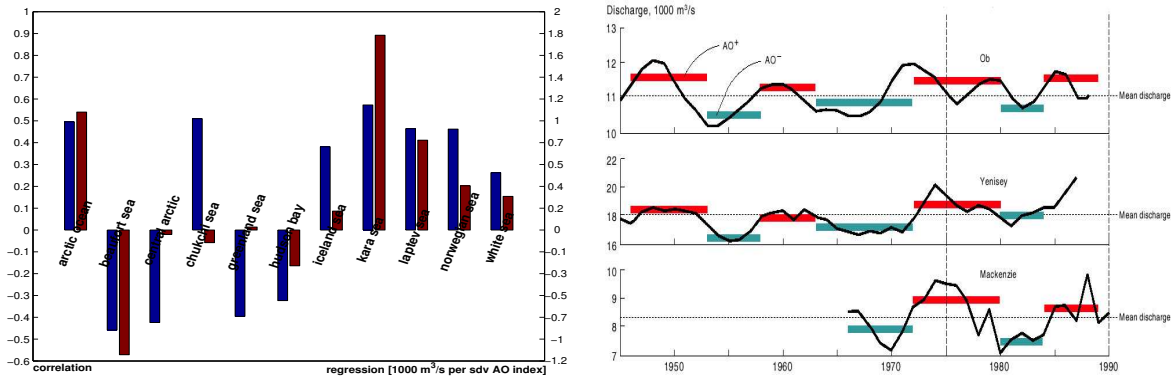

Figure 6.7: Correlation and regressions of simulated annual runoff into the Arctic Seas with the AO index of 300yr BCM control experiment *(left)* and observed time series of Arctic river discharges with marked AO phases *(right)*.

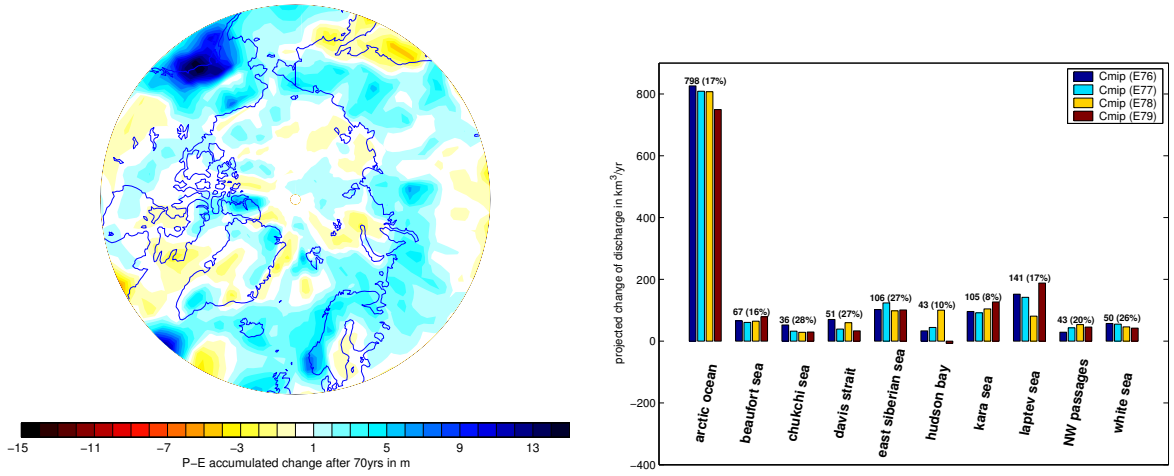

Figure 6.8: Projected changes for precipitation-evaporation *(left)* and river discharge *(right)*.

is the strong inflow from the Pacific that continues along the Siberian shelf while the discharges of the Asian rivers add on to it, and eventually meet the Atlantic water in the Kara Sea region. The export of the Arctic water through with the East Greenland current and the through the Canadian Archipelago is another distinct feature. The flow of the Atlantic Water into the Nordic Seas and eventually the Arctic Ocean Proper can be followed along the North Atlantic Current and further North the West Spitzbergen Current. Despite the relative coarse model solution the freshwater transport from the North and Baltic Sea with the Norwegian Coastal Current is well resolved. The Modified Atlantic Water in the Barents Sea does not show up in the freshwater fluxes since it's salinity virtually matches the reference value. Inter-annual variability of the freshwater flows are investigated in figure 6.12 where a composite plot for liquid and solid freshwater (sea-ice) fluxes is presented. For positive index phases the circulation of the liquid freshwater is intensified. At the same time, a strengthened transpolar drift enhances the ice export into the Barents Sea whereas the export through the

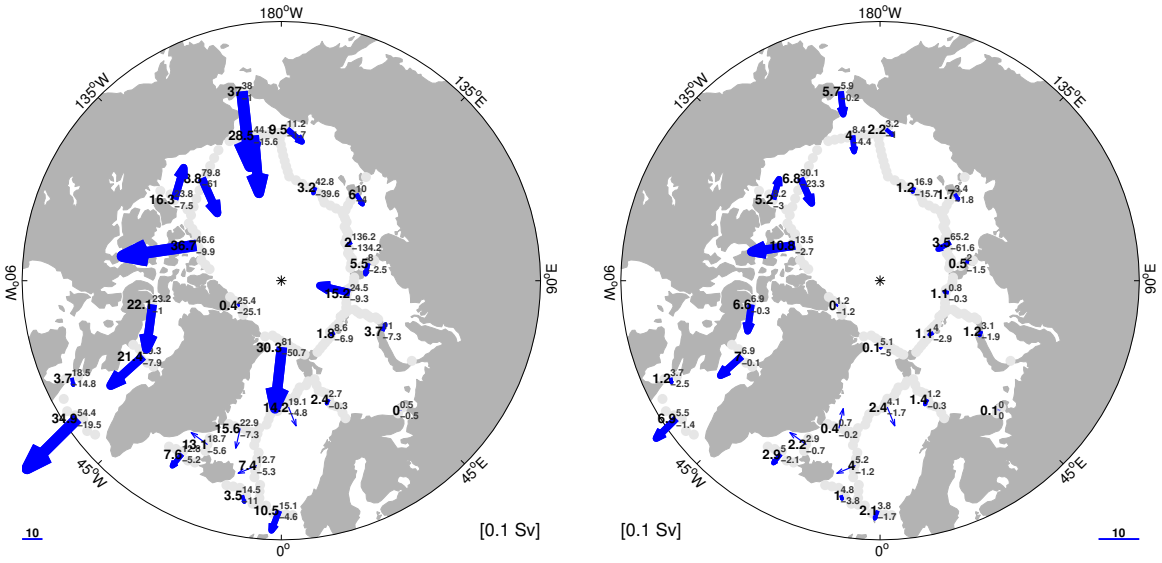

Figure 6.9: Simulated liquid freshwater exchanges of the Arctic Seas. Average of 300 years control experiment *(left)* and projected changes *(right)*.

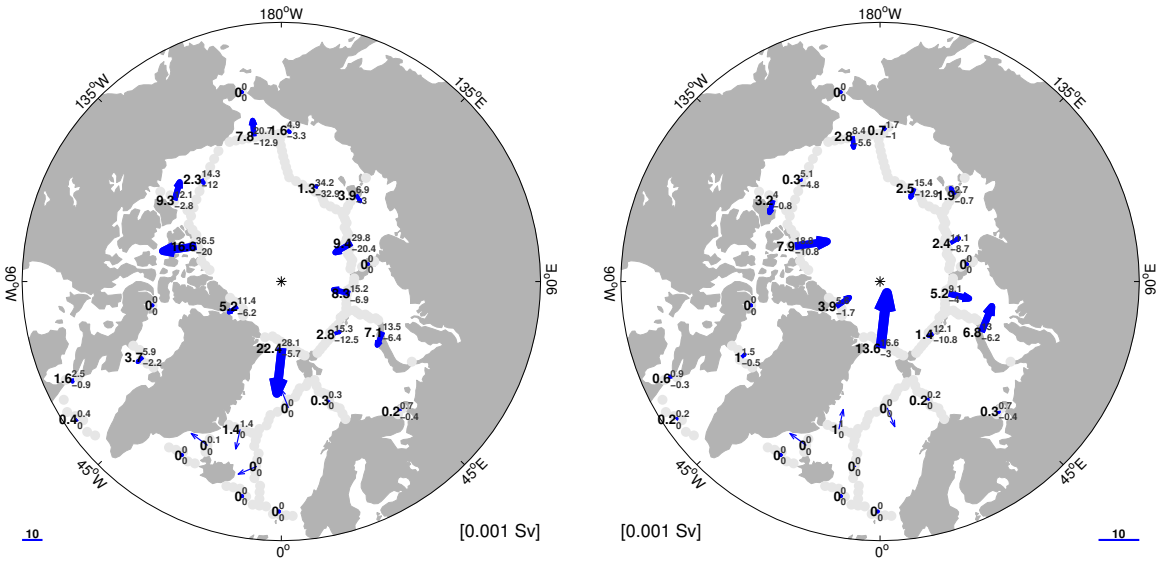

Figure 6.10: Simulated ice volume exchanges of the Arctic Seas. Average of 300 years control experiment *(left)* and projected changes *(right)*.

Fram Strait is slightly reduced leaving large amount of sea-ice re-circulating.

Freshwater Budgets for Selected Regions. Along the lines of the previous chapter, an attempt an attempt has been conducted to state simulated freshwater balances for selected regions. These are presented in table 6.1 and table 6.2. Note that the directions of the residual fluxes are defined out of the region whereas the direct estimates are defined opposite. Ideally, the residual transport estimates should match the direct estimates. But this is clearly not the case since they differ by more than a factor two.

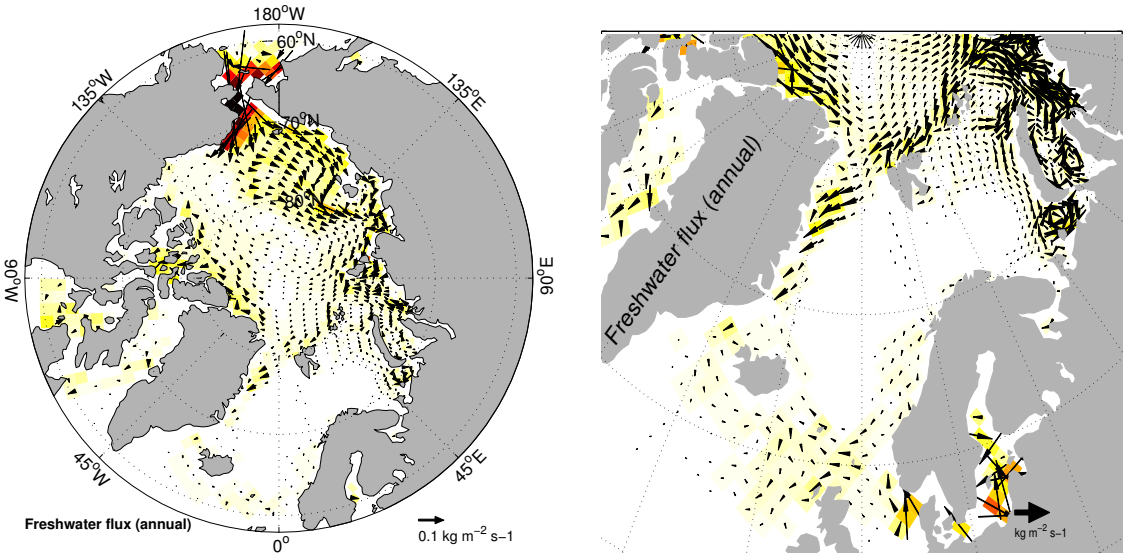

Figure 6.11: Vertical averaged liquid freshwater fluxes. Shown are annual climatologies of 300 years control experiment.

For the entire Arctic Mediterranean and the Arctic Proper the residual estimates highly exceed the direct estimates whereas in the Nordic Seas and the Barents Sea the opposite is the is the case. We have no means to assess the missing contribution from the temperature and layer thickness diffusion. Nevertheless, uncertainties of the residual budgets can be assessed by analyzing the global budget. The area averaged components for the World Oceans are $precipitation = 2.42\ mm/day$, $runoff = 0.3\ mm/day$, $storage\ tendency = 0.02\ mm/day$, and $flux\ adjustment = 0.13\ mm/day$. Hence, the global residual or error is 0.15 mm/day which is roughly one order of magnitude smaller than the regional budgets. Thus, the global error has the potential to explain 20% discrepancy if the relative error of the region is approx. 50%.

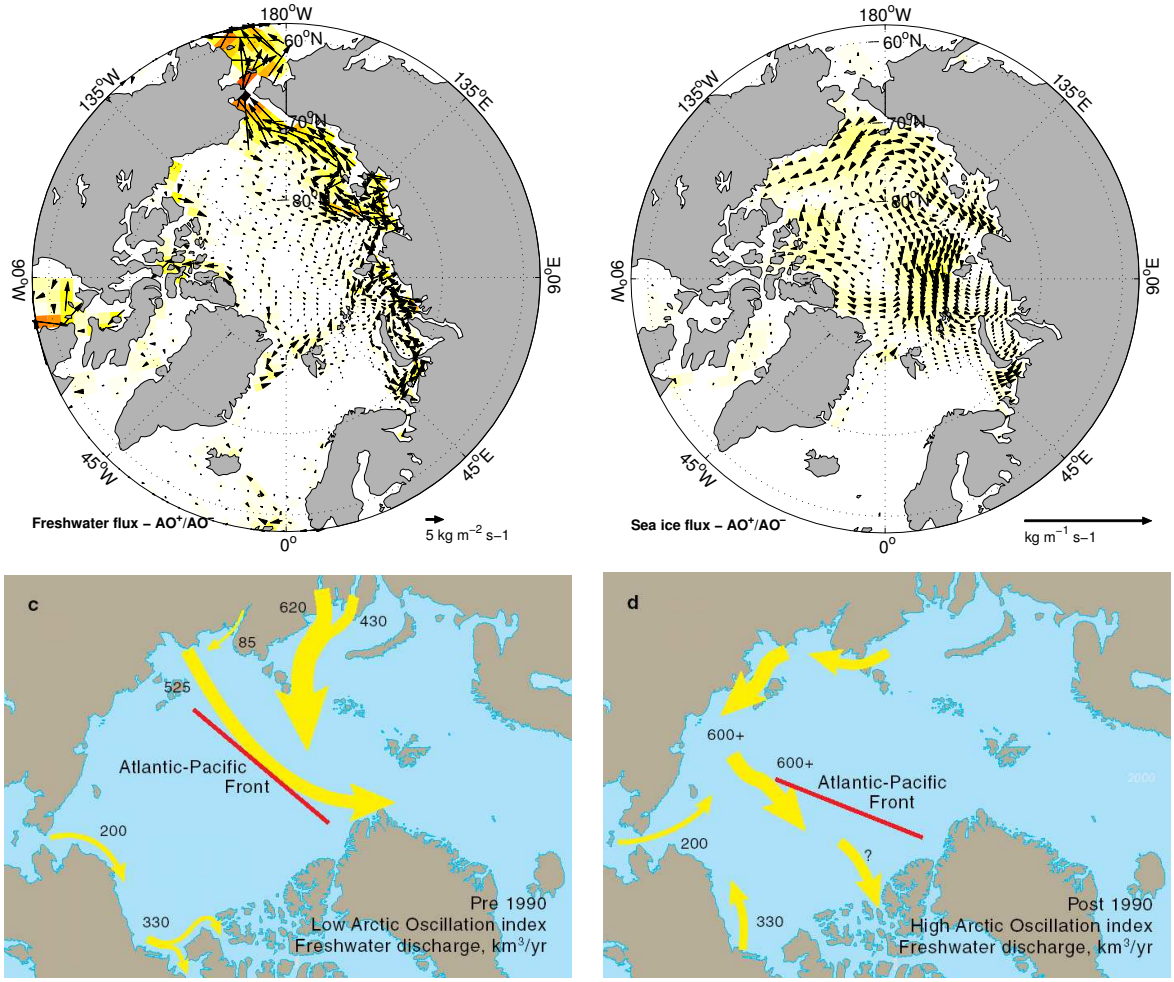

Figure 6.12: AO composite of ice and vertical averaged freshwater flux. The top panels show difference vectors between the AO^+ and AO^- subset mean of the BCM control experiment for liquid freshwater *left* and sea-ice *right*. The lower panels show observational based estimates of the freshwater pathways for the negative and positive *AO* phases (Macdonald 2002).

Table 6.1: Mean residual and direct freshwater budget estimates for selected regions. All products are based on 300 years BCM control integration. Units are in kt/s for values without brackets and in mm/day for values in brackets.

Total of the Arctic Seas

Residual Estimate		Direct Estimate [liquid-adv ice-adv total]			
Storage Tendency	6.2 (-0.04)	Pacific Ocean	106.1	0	106.1
Flux Adjustment	21.5 (0.12)	Atlantic-GIN S.	-51.8	0	-51.8
Precipitation	164.2 (0.92)	Atlantic-Labr. S.	-100.1	0.4	-99.7
Evaporation	-108.3 (0.61)				
Total Runoff	150 (0.84)				
Residual Transport	233.5 (1.31)	*Direct Transport*	-57.7	0.4	-57.3

Arctic Ocean Proper

Residual Estimate		Direct Estimate [liquid-adv ice-adv total]			
Storage Tendency	3.5 (-0.23)	Barents S.-C. Arct.	5	-2.8	2.2
Flux Adjustment	-4 (-5.03)	Bering Strait	106.1	0	106.1
Precipitation	63.7 (6.08)	Fram Strait S.	-86.8	-22.4	-109.2
Evaporation	24.5 (2.21)	Can. Arch.	-63.4	0	-63.4
Total Runoff	109.7 (12.6)	Barent S. - Kara S.	11.8	-7.1	4.7
Residual Transport	141.55 (20.67)	*Direct Transport*	-37.3	-32.3	-59.6

Nordic Seas

Residual Estimate		Direct Estimate [liquid-adv ice-adv total]			
Storage Tendency	1.8 (-0.06)	BSO	6.9	0.3	7.2
Flux Adjustment	9.5 (0.35)	Denmark Strait	-21.8	0	-21.8
Precipitation	44.1 (1.61)	Fram Strait	86.8	22.4	109.2
Evaporation	-42.4 (-1.55)	Island-Norway	-40.1	0	40.1
Total Runoff	4.34 (0.16)				
Residual Transport	17.34 (0.63)	*Direct Transport*	31.8	22.7	54.5

Barents Sea

Residual Estimate		Direct Estimate [liquid-adv ice-adv total]			
Storage Tendency	0.11 (-0.01)	BSO	-6.9	-0.3	-6.6
Flux Adjustment	15.4 (0.93)	C. Arct.-Barents S.	-5	2.8	2.2
Precipitation	22.44 (1.36)	Barents S.-Kara S.	-10.7	7.1	-17.1
Evaporation	-17.84 (-1.08)				
Total Runoff	5.75 (0.35)				
Residual Transport	25.86 (1.57)	*Direct Transport*	22.6	9.6	-31.5

Table 6.2: Projected changes of residual and direct freshwater budget estimates for selected regions. All products are based on 300 years BCM control integration. Units are in kt/s for values without brackets and in mm/day for values in brackets.

Arctic Seas

Residual Estimate		Direct Estimate [liquid-adv ice-adv total]			
Storage Tendency	-	Bering Strait	16.3	0.2	16.5
Flux Adjustment	0	Atlantic-GIN S.	-16.8	0.2	-16.6
Precipitation	34.3 (0.19)	Atlantic-Labr. S.	-20	0	-20
Evaporation	-23.8 (-0.13)				
Total Runoff	25.3 (				
Residual Transport	10.2 ((0.05)	*Direct Transport*	-20.5	0.4	-20.1

Arctic Ocean

Residual Estimate		Direct Estimate [liquid-adv ice-adv total]			
Storage Tendency	-	Barents S. - C. Arct.	1.4	1.4	2.8
Flux Adjustment	0	Bering Strait	16.3	0	16.3
Precipitation	21.9 (0.24)	Fram Strait S.	-0.3	13.6	13.3
Evaporation	-28.7 (-0.21)	Can. Arch.	-18.9	0	-18.9
Total Runoff	7	Barents S. - Kara S.	-3.4	15	11.6
Residual Transport	0.2	*Direct Transport*	-5.9	30	24.1

Nordic Seas

Residual Estimate		Direct Estimate [liquid-adv ice-adv total]			
Storage Tendency	0	Barents S. Opening	4.1	-0.2	3.9
Flux Adjustment	-	Denmark Strait	-6.4	0	-6.4
Precipitation	4.2 (0.15)	Fram Strait	0.3	-13.6	-13.3
Evaporation	-0.2 (-0.01)	Island-Norway	-8.7	-13.8	22.5
Total Runoff	1.8				
Residual Transport	5.8	*Direct Transport*	-10.7	-27.6	-38.3

Barents Sea

Residual Estimate		Direct Estimate [liquid-adv ice-adv total]			
Storage Tendency	0	Barents S. Opening	-4.1	0.2	-3.9
Flux Adjustment	-	C. Arct.-Barents S.	-1.4	-1.4	-2.8
Precipitation	4.1 (0.25)	Barents S.-Kara S.	3.4	-15	-11.6
Evaporation	-3.2 (-0.19)				
Total Runoff	0.7				
Residual Transport	2.6 (0.06)	*Direct Transport*	-2.1	-16.2	-18.3

6.3 Freshwater Budget in the Present Climate

Mean State. The Arctic region is characterized by a precipitation excess (figure 6.2 *top-left*) which implies a high relative humidity. Due to the low air temperatures, however, the water vapor saturation pressure is very low, i.e. the atmospheres capacity to carry moisture is extremely small. Thus at some locations, e.g. in Longyearbyen on Spitzbergen, the absolute dryness is comparable to the dryness of the Sahara. Therefore, about 2/3 of the Arctic Oceans freshwater supply (Howard and Cresswell 2000) originates from discharges of the large Siberian and Canadian rivers with catchment areas extending far into the mid-latitudes (figure 6.5).

A comparison of simulated with observed annual climatology of river discharge into the Arctic Seas is shown in figure 6.5 reveals that simulated Arctic runoff is highly realistic. Note that the simulated discharges include the total runoff into the shelf seas whereas the observed values represent discharges from single rivers only. For this reason, somewhat lower values are expected.

Variability *Seasonal Cycle of River Discharge.* The representation of the seasonal cycle of the river discharge seems more challenging than those of the climatological mean. For instance, the simulated discharge into the Beaufort Sea is centered in a very narrow band during the melting season with peak values that exceed twice those observed which contain more inertia and extend far into the autumn season. This discrepancy exists partly due to the simplicity of the runoff scheme that applies an e-folding discharge function for the complete catchment area regardless of the distance to the coast. Another explanation might be found in the crude presentation of lakes. Carmarck (2000) pointed out that rivers with major headwater lakes will have different seasonal runoff patterns than those without. Especially the Mackenzie river draws a considerable amount of water from Athabaska, Great Slave and Great Bear lakes to maintain moderate flows during winter time. This finding is illustrated in figure 6.6.

Atmospheric Circulation vs. Arctic Runoff. In contrast to the seasonal cycle, the inter-annual variability of the simulated river discharges appears more realistic and physical. In the simulated fields a strong link to the AO is present with increased discharges on the Siberian side and weakened on the Canadian side during the positive index phase and vice versa during the negative index phase. The most obvious explanation for this is an increased atmospheric poleward moisture transport and an enhanced precipitation associated with the AO. However, new results indicate that there also may be a relation between the winter Arctic Oscillation and the preceding Siberian summer/autumn snow cover (Gong and D. 2003), such that high AO also associates to more autumn snowfall.

In contrast, Polyakov and Prushutinsky (1999) reported that Siberian river discharges are higher in Anti Cyclonic Circulation Regime years and lower in Cyclonic Circulation Regime years, where the regimes roughly correspond to the negative and positive phase of the AO. The negative correlations on the Canadian side are statis-

tically significant in the Model. However, the observational data shown in figure 5.3 indicates rather a positive phase relation between the Mackenzie discharge and the AO index (Macdonald et al. 2002). The causes for this discrepancy is not known. To investigate this problem one would have to reconstruct longer observational time series than presented here.

As for the mass and heat fluxes, AO composites are used to identify the role of the atmospheric forcing ont the freshwater budget.

The change in freshwater outflow through the Bering Strait basically reflects a decreased Bering Strait inflow of low salinity waters from the Bering Sea. A significant increase of summer freshwater discharge from the Siberian Rivers during the AO phase (figure 6.7) contributes to intensified exports from the Kara, Leptev and Siberian Sea, shown in figure 6.12.

However, this analysis has it's limits and a comparison of the simulated freshwater fluxes with from Macdonald et al. (2002) in figure changes 6.12 is hardly possible. In order to identify the trajectories of the river water and the exact injection points to the Central Arctic Ocean it would be more adequate to perform tracer simulations.

It should be noted that during the positive AO phase all transports are pointed away from the Marginal Ice Zone , supporting the hypotheses that during recent years the persistence of the AO in the positive phase primarily caused the retreat of the Polar Front (Steele and Boyd 1998).

In contrast, the signature in the ice-drift is very complex and difficult to interpret. The ice-drift on the Pacific side of the Arctic Ocean, i.e. the Canadian Basin, Beaufort, Chukchi, East Siberian and Leptev Sea, tends to a more cyclonic direction during the AO positive phase. At the same time weak indications are present that the ice in the Baffin Bay/Davis Strait extends further south and that the eastward migration of the Barents Sea sea-ice is reduced. These are well known features and they can directly be reasoned from changes in the atmospheric surface pressure field shown in figure 3.3. Even though the results exhibit a considerable intensification of the transpolar drift, a significant link between the AO and Fram Strait ice export is absent in the model.

6.4 Freshening of the Arctic Seas Induced by an Intensified Hydrological Cycle

The intensification of the global hydrological cycle is one of the strongest signal in future climate simulations and probably the amongst the most reliable climate predictions. Employing the global mean precipitation as a integrated indicator, figure 6.1 summarizes the very distinct response of the hydrological cycle to an increased greenhouse gas emission. The trend of the control experiment, which is one magnitude of order weaker than those of the perturbation experiments, is attributable to the positive temperature drift in the World Oceans. The projected global spin-up of the freshwater cycle is as much as 3% with regional deviations far exceeding this value.

Mean and changes in zonally integrated precipitation minus evaporation (P-E) as well as the corresponding atmospheric moisture transports, are shown in figure 6.2. The terms precipitation and evaporation are not used in a strict sense as they comprise snowfall, transpiration and sublimation. That is everything that contributes to a decrease or an increase in the total water content of the atmospheric column in either liquid, solid, or gas form. Since the spatial patterns appear very robust, only the projections of one member are shown. In general, dry regions become dryer and wet regions become wetter. A strengthening of the evaporation over the sub-tropical oceans is balanced by an increased precipitation in the tropics and middle to high latitudes. Correspondingly the atmospheric meridional moisture transport indicates enhanced poleward transports exports from the sub-tropics in equator and poleward direction.

A less expected, though robust feature, is a congruent southward shift of the ITCZ in all CMIP members. Longitudinal variations shown in figure 6.2 are mostly confined to the El Niño-Southern Oscillation (ENSO) influence region and therefore likely to reflect changes in the Walker Circulation.

The World Oceans response to the freshwater surface forcing is illustrated in figure 6.3. A comparison of the change in freshwater yield with the spatial pattern of the change in P-E reveals that meridional gradients are smeared out, presumably as a consequence of the wind driven surface circulation whereas the cross ocean gradient between the Atlantic and Pacific Ocean clearly stands out. The latter feature might indicate an intensified cross-continental moisture export from the tropical Atlantic towards the Pacific. This would be consistent with a stronger Hadley Circulation, i.e. stronger trade winds at lower levels. The predicted freshening in the western part of the North Atlantic is presumably related to a south-east shift of the North Atlantic Drift (Helge Drange, personal communication) and to an increased freshwater flux with the East Greenland Current and through the Canadian Archipelago into the Labrador Sea (figure 6.10).

Departing from the global picture, we again focus on the polar regions discussing the changes in the Arctic freshwater cycle that are summarized in figure 6.4 and 6.8. In contrast to the very complex response in the sub-tropics and tropics, a homogeneous, zonally symmetric freshening dominates in the middle and high latitudes. The only exception is Alaska, where the projected changes are three times as high as anywhere else in the Arctic and likely related to ENSO changes (A. Sorteberg, personal communication). Nevertheless, they effect the Yukon discharge into the Bering Sea and in this way might amplify the freshwater import through the Bering Strait shown in figure 6.10. Changes in P-E over the central Arctic are considerable small whereas the changes over Asia and Canada contribute to an increased river discharge into the Arctic Seas of approximately 20%.

The extra freshwater input leaves a clear signature in the Arctic Ocean. However, the offshore transportations from the shallow shelves to the deeper interior is not fully understood (Aagaard 1987) and likely to be misrepresented in many model simulations

as coarse resolution ocean models do not resolve the dynamics involved.

The freshwater exchanges of the Arctic Seas comprise liquid exchange on the one hand and sea-ice import/export on the other hand. Positives changes of liquid freshwater advection into the Arctic Ocean Proper originate from the Beaufort Sea, Chukchi Sea and all Siberian shelf seas whereas an export of similar magnitude through the Northwester Passages into the Labrador Sea is present. From the response in projected freshwater yield, which exceeds the ice amount by one order of magnitude, it becomes clear that additional eddy-diffusive fluxes must be active and dominate the total transports. The ice export through the Fram Strait and also from the Kara Sea to the Barents Sea are significantly reduced. This in turn might explain a large fraction of the projected salinization and warming in the Nordic Seas.

6.5 Chapter Summary

Realistic Simulation of Freshwater Fluxes in the Arctic Seas. The Bergen Climate Model has a realistic presentation of the freshwater fluxes into the Arctic Seas. Most features of the circulation of freshwater in the Arctic Ocean have been successfully simulated. These comprise of the import through the Bering Strait, the export through Fram Strait and Canadian Archipelago, the river transports of the river discharges from the Arctic shelf to the ocean interior, and the freshwater transport with the Norwegian Coastal Current. The latter is considered as a very good achievement. For instance it demonstrates the potential of the BCM to communicate precipitation or heat anomalies in eastern Europe through the Baltic Sea, along the Norwegian coast, as far as into Barents Sea.

Simulated River Discharge into the Arctic Seas. The annual climatologies of Arctic river discharges match well with observations whereas the seasonal cycle is somewhat too concentrated on the melting season. Moreover, the inter-annual variability of the simulated total runoff is strongly modulated by the Arctic Oscillation where increased discharges on the Siberian and weakened discharges on the Canadian Side are identified. Preceding studies of Polyakov and Prushutinsky (1999) as well as from the Macdonald et al. (2002) project controvert these findings.

Freshwater Budgets. Residual estimates of freshwater exchanges of the Arctic Seas are close to what is observed whereas the direct, advective estimates generally are too small. The latter emphasizes that the simulated eddy-diffusive fluxes of salt is of the same order of magnitude as those advected and hence cannot be neglected. But unfortunately, the diffusion of layer thickness makes accurate reconstruction of simulated ocean freshwater fluxes unachievable.

Spin-up of the Hydrological Cycle. The BCM climate projections suggest a spin-up of the hydrological cycle equivalent to a trend of 3% per year in mean total precipitation, which is an order of magnitude greater than the natural variability. The intensification of the freshwater cycle is a very robust feature with it's source in the lower latitudes.

Therefore, it seems unlikely that tendencies to more positive circulation indices, e.g. of the NAO or AO, are the only explainations of the increases in atmospheric freshwater transports towards the middle and higher latitudes.

Freshening of the Arctic Seas. In relation to the intensification of the hydrological cycle an increased precipitation excess in the middle to higher latitudes is predicted. In turn this causes a 20% augmented discharge of the Pan-Arctic rivers into the Arctic Seas which is likely the main contributor to a projected freshening of the Arctic Seas. In comparison the role of freshwater release from melting multi-year ice is rather small. However, the simulated diminishing sea ice export through the Fram Strait is equivalent to a reduced freshwater export and therefore may play a significant role for the freshening in the Central Arctic. The projection that the Nordic Seas become more saline manifests presumably as a consequence of the combination of an increased Atlantic Water inflow and a decreased sea-ice import from the Fram Strait. However, these projections are not reflected in observed present trends of a strengthened Fram Strait ice export and a freshening North Atlantic.

Chapter 7

Conclusions and Future Perspectives

In this chapter we summarize the key findings of the previous chapters and propose recommendations for future studies.

Mass Budgets

1. **Climatological Mass Exchanges.** It can be concluded that the magnitudes and also the relative contributions of the mass exchanges through the Arctic Seas pathways correspond reasonably well with observational estimates and other simulations. However, a bias towards Pacific water ventilation is apparent, leading to weaker than observed Barents Sea and Fram Strait inflow. The closest match is obtained for the transport through the North Western Passages.

2. **Inter-annual Variability of Mass Exchanges.** Arctic Oscillation composite studies suggest competitive behavior of Pacific and Atlantic inflow, whereby the latter is stronger during positive index phases. While the Atlantic Inflow strengthens the East Greenland Current seems to weaken slightly. Thus, for the closed picture it remains essential to take the Bering Strait and Canadian Archipelago into account. However, an artificial tele-connection of the Pacific with the Atlantic atmospheric variability may contaminate these results.

3. **Atlantic Inflow into the Nordic Seas - Seasonal Cycle and Future Prediction.** Despite a predicted weakening of the Atlantic Meridional Overturning Circulation strength no general reduction of the Atlantic Water inflow is projected. In contrast, during winter, a strengthened inflow is associated with the projected deepening of the Icelandic Low. However, in summer i.e. during the absence of strong atmospheric wind forcing slight indications for a reduced inflow are present. But, it remains to be proved that the latter is in fact related to a weakened overflow. Furthermore, the simulated Atlantic Inflow is only about

25% larger during winter than during summer. If one assumes that the atmospheric circulation has a significant role only during the active season then the major fraction of the inflow must be thermohaline or explained by breaking of baroclinic waves generated during winter. Since the simulated AMOC is rather weak in the Nordic Seas, a freshwater driven estaurine like circulation seems more likely to explain the thermohaline contribution.

4. **Barents Sea Opening Inflow.** Correlation studies emphasize that the out-of-phase relationship of the West Spitzbergen Current transport and the inflow into the Barents Sea is a more robust feature than their connection with the Atlantic Inflow into the Nordic Seas. Thus, the variability of the Barents Sea inflow depends more on how much Atlantic Water is 'tapped' from the Norwegian Atlantic Current than on the NAC strength itself. This finding is consistent with a sea level pressure correlation study which shows a maximum inflow into the Barents Sea for low pressure centers located approximately over Svalbard.

Heat Budgets

1. **Future of the North Atlantic - GIN sea Heat Exchange.** Despite a reduction of Atlantic Meridional Overturning Circulation strength the results from 5 greenhouse simulations project an increased ocean heat transport into the Nordic Seas. Possible contributers are an intensified winter inflow in accordance with a deepening Icelandic Low, a increasing inflow temperature and enhanced eddy heat fluxes. However, shortcomings in the simulation of open ocean convection in the GIN-seas and the related Denmark Strait and Iceland-Scotland overflows might explain the moderate contribution of a weakening of the AMOC.

2. **Implications for the Arctic Sea-Ice** Large scale sea-ice changes over the entire Arctic are likely to be primarily caused directly by dynamical and thermodynamical atmospheric forcing. Some regional changes seem to be controlled by oceanic fluxes, particularly the winter ice conditions of the Barents and parts of the Kara Seas.

3. **Comparison of Residual and Direct Estimated Heat Budgets** A comparison of direct with residual budgets suggest that the contributions of eddy diffusive fluxes have roughly the same order of magnitude as the advective transports by the currents. Consequently, to obtain consistent heat and freshwater balances with the direct method, an assessment or reconstruction of the eddy fluxes remains indispensable.

Freshwater Budgets

1. **Realistic Simulation of Freshwater Fluxes in the Arctic Seas.** The Bergen Climate Model has a realistic presentation of the freshwater fluxes into the Arctic

Seas. Most features of the circulation of freshwater in the Arctic Ocean have been successfully simulated. These comprise the import through the Bering Strait, the export through Fram Strait and Canadian Archipelago, the river transports of the river discharges from the Arctic shelf to the ocean interior, and the freshwater transport with the Norwegian Coastal Current. The latter is considered as a very good achievement. For instance it demonstrates the potential of the BCM to communicate precipitation or heat anomalies in eastern Europe through the Baltic Sea, along the Norwegian coast, as far as into Barents Sea.

2. **Simulated River Discharge into the Arctic Seas.** The annual climatologies of Arctic river discharges match well with observations whereas the seasonal cycle is somewhat too concentrated on the melting season. Moreover, the inter-annual variability of the simulated total runoff is strongly modulated by the Arctic Oscillation where increased discharges on the Siberian and weakened discharges on the Canadian Side are identified. Preceding studies of Polyakov and Prushutinsky (1999) as well as from the Macdonald et al. (2002) project controvert these findings.

3. **Freshwater Budgets.** Residual estimates of freshwater exchanges of the Arctic Seas are close to what is observed whereas the direct, advective estimates generally are too small. The latter emphasizes that the simulated eddy-diffusive fluxes of salt is of the same order of magnitude as those advected and hence cannot be neglected. But unfortunately, the diffusion of layer thickness makes accurate reconstruction of simulated ocean freshwater fluxes unachievable.

4. **Spin-up of the Hydrological Cycle.** The BCM climate projections suggest a spin-up of the hydrological cycle equivalent to a trend of 3% per year in mean total precipitation, which is an order of magnitude greater than the natural variability. The intensification of the freshwater cycle is a very robust feature with it's source in the lower latitudes. Therefore, it seems unlikely that tendencies to more positive circulation indices, e.g. of the NAO or AO, are the only explanations of the increases in atmospheric freshwater transports towards the middle and higher latitudes.

5. **Freshening of the Arctic Seas.** In relation to the intensification of the hydrological cycle an increased precipitation excess in the middle to higher latitudes is predicted. In turn this causes a 20% augmented discharge of the Pan-Arctic rivers into the Arctic Seas which is likely the main contributer to a projected freshening of the Arctic Seas. In comparison the role of freshwater release from melting multi-year ice is rather small. However, the simulated diminishing sea ice export through the Fram Strait is equivalent to a reduced freshwater export and therefore may play a significant role for the freshening in the Central Arctic. The projection that the Nordic Seas become more saline manifests presumably as

a consequence of the combination of an increased AW inflow and a decreased sea-ice import from the Fram Strait. However, these projections are not reflected in observed present trends of a strengthened Fram Strait ice export and a freshening North Atlantic.

Future Perspectives The discussion on the evolution of simulated budgets remains questionable as long as they are not closed. To be able to provide stronger and more convincing results it is important to address the causes of why the simulation does not as a first approximations conserve energy and freshwater and how this might be improved. That includes the identification of potential sources and sinks in the model formulation, as well as the quite extensive post-processing which comprises various data transformations and interpolations. Since the evaluation of local budgets is very hard to archive and exhibits rather large uncertainties (Trenberth et al. 2001), we suggest to primarily focus on the on the minimization of global imbalances.

Appendix A

Tabulated Budget Products

In this chapter the advective estimates for the mass, heat and freshwater exchanges of the Arctic Seas are presented in tabulated form. The Barents Sea mass budget is used as example to explain how to read these tables.

The averaged net mass fluxes (or more precisely, equivalent volume fluxes) from the Barents Sea to the Central Arctic Ocean, Kara Sea, Norwegian Sea and White Sea are 0.4, 1.5, -1.9 and 0 Sv respectively, whereas the net outgoing flux is 0 Sv. The net exchanges are further divided into positive and negative flagged transports. The inflow from the Norwegian Sea into the Barents Sea is 2.9 Sv whereas the outflow into the Norwegian Sea is 1 Sv on average. The forth column contains the standard deviation from the annual averages of the net exchanges.

Column 5 to 7 denote the projected changes of the transports. For example, the net inflow from the Norwegian Sea into the Barents Sea is predicted to increase with 0.21 Sv as a result of a 0.5 Sv reduction of the flagged outflow from the Barents Sea to the Norwegian Sea and an 0.16 Sv increase of the flagged inflow from the Norwegian Sea into the Barents Sea. The last column denotes the spreading of the five member ensemble for the net prediction in form of a signal-to-noise ratio. The the mean prediction is divided by standard deviation of the ensemble. For the Barents Sea congruent predictions are only present for the Barents Sea Opening exchange with a signal to noise ration of 0.46. Whether this water continues to the Kara Sea or directly to the Central Arctic Ocean depends on the single ensemble member.

Table A.1: Mass transport. Units are converted to sv ($10^6 m/s$) where $\rho_0 = 1.028$ was applied.

Sections		Control				$2\times CO_2$ - Control			
from	to	net	pos	neg	sdv	net	pos	neg	s/n
Arctic seas	North atlantic	1.4	34.9	33.5	0.1	−0.04	−1.21	−1.18	< 1
	North pacific	−1.4	0	1.5	0.09	0.03	0	−0.03	< 1
	Total	0	34.9	34.9	0.02	0	−1.21	−1.2	< 1
Baffin bay	Davis strait	1.6	2.5	0.9	0.19	0	0	0	< 1
	NW passages	−1.6	0	1.7	0.19	0	0.05	0.05	< 1
	Total	0	2.5	2.5	0	0	0.04	0.04	< 1
Barents sea	Central arctic	0.4	1.1	0.7	0.16	0.07	0.18	0.11	< 1
	Kara sea	1.5	2.4	0.9	0.29	0.13	0.55	0.41	< 1
	Norwegian sea	−1.9	1	2.9	0.25	−0.21	−0.05	0.16	2.2
	White sea	0	0	0	0	0	0	0	< 1
	Total	0	4.5	4.5	0	0	0.68	0.68	< 1
Beaufort sea	Central arctic	1.3	9.6	8.4	0.24	0.04	0.26	0.22	< 1
	NW passages	−1.3	0.4	1.7	0.24	−0.04	0.04	0.08	< 1
	Total	0	10.1	10.1	0	0	0.3	0.3	< 1
Central arctic	Barents sea	−0.4	0.7	1.1	0.16	−0.07	0.11	0.18	< 1
	Beaufort sea	−1.3	8.4	9.6	0.24	−0.04	0.22	0.26	< 1
	Chukchi sea	−1.1	0.5	1.6	0.1	0.06	0.06	0.01	2.6
	East siberian sea	−0.1	2	2.2	0.06	−0.01	0.31	0.32	< 1
	Greenland sea	1.7	9	7.2	0.28	0.18	−1.72	−1.9	< 1
	Kara sea	−1.7	0.6	2.3	0.26	−0.07	−0.01	0.06	< 1
	Laptev sea	0	13	13	0.05	−0.07	1.37	1.45	4.5
	Lincoln sea	0	1.8	1.8	0	0	−0.46	−0.46	< 1
	NW passages	2.9	3.5	0.6	0.27	0.04	0.06	0.03	< 1
	Total	0	39.5	39.5	0.01	0	−0.06	−0.06	< 1
Chukchi sea	Central arctic	1.1	1.6	0.5	0.1	−0.06	0.01	0.06	2.6
	East siberian sea	0.3	0.4	0.1	0.08	0.02	0.04	0.02	< 1
	North pacific	−1.4	0	1.5	0.09	0.03	0	−0.03	< 1
	Total	0	2.1	2.1	0	0	0.06	0.06	< 1
Davis strait	Baffin bay	−1.6	0.9	2.5	0.19	0	0	0	< 1
	Hudson strait	0	1.1	1.1	0	0	−0.01	−0.01	< 1
	North atlantic	1.6	19.7	18.1	0.19	−0.01	−1.43	−1.43	< 1
	Total	0	21.7	21.7	0.01	0	−1.45	−1.44	1.3
Denmark strait	Iceland sea	−3.4	1	4.4	0.42	−0.25	−0.27	−0.02	< 1
	North atlantic	3.4	8.4	5	0.42	0.25	0.02	−0.23	< 1
	Total	0	9.4	9.4	0.01	0	−0.25	−0.25	< 1
East siberian sea	Central arctic	0.1	2.2	2	0.06	0.01	0.32	0.31	< 1
	Chukchi sea	−0.3	0.1	0.4	0.08	−0.02	0.02	0.04	< 1
	Laptev sea	0.2	0.3	0.1	0.06	0.01	0.04	0.03	< 1
	Total	0	2.5	2.5	0	0	0.38	0.38	< 1
Foxe basin	Hudson bay	−0.2	0.1	0.3	0.05	−0.04	−0.02	0.02	2.9
	Hudson strait	0.2	0.3	0.1	0.05	0.04	0.04	0	2.9
	Total	0	0.4	0.4	0	0	0.02	0.02	1.3
Gin sea	Barents sea	1.9	2.9	1	0.25	0.21	0.16	−0.05	2.2
	Central arctic	−1.7	7.2	9	0.28	−0.18	−1.9	−1.72	< 1
	North atlantic	0.6	10.8	10.2	0.3	0.04	0.09	0.05	< 1
	Total	0	39.2	39.2	0.01	0	−2.95	−2.94	< 1

Table A.1: Mass transport. Units are converted to sv ($10^6 m/s$) where $\rho_0 = 1.028$ was applied.

Section		Control				$2\times CO_2$ - Control			
from	to	net	pos	neg	sdv	net	pos	neg	s/n
Greenland sea	Central arctic	−1.7	7.2	9	0.28	−0.18	−1.9	−1.72	< 1
	Iceland sea	9.3	10.1	0.8	0.71	−1.34	−1.56	−0.21	3.4
	Norwegian sea	−7.6	9.4	17	0.69	1.52	−1.48	−3	7.3
	Total	0	26.8	26.8	0	0	−4.94	−4.94	< 1
Hudson bay	Foxe basin	0.2	0.3	0.1	0.05	0.04	0.02	−0.02	2.9
	Hudson strait	−0.2	0.2	0.4	0.05	−0.04	−0.02	0.02	3
	Total	0	0.5	0.5	0	0	0	0	1.2
Hudson strait	Davis strait	0	1.1	1.1	0	0	−0.01	−0.01	< 1
	Foxe basin	−0.2	0.1	0.3	0.05	−0.04	0	0.04	2.9
	Hudson bay	0.2	0.4	0.2	0.05	0.04	0.02	−0.02	3
	Total	0	1.6	1.6	0	0	0.01	0.01	1.5
Iceland sea	Denmark strait	3.4	4.4	1	0.42	0.25	−0.02	−0.27	< 1
	Greenland sea	−9.3	0.8	10.1	0.71	1.34	−0.21	−1.56	3.4
	North atlantic	−0.8	4.3	5.1	0.25	−0.07	0.13	0.2	< 1
	Norwegian sea	6.7	13.8	7.1	0.75	−1.53	−1	0.53	7.4
	Total	0	23.4	23.4	0.01	0	−1.09	−1.1	< 1
Kara sea	Barents sea	−1.5	0.9	2.4	0.29	−0.13	0.41	0.55	< 1
	Central arctic	1.7	2.3	0.6	0.26	0.07	0.06	−0.01	< 1
	Laptev sea	−0.2	0.1	0.3	0.06	0.06	0.04	−0.02	2
	Total	0	3.3	3.3	0	0	0.52	0.52	< 1
Laptev sea	Central arctic	0	13	13	0.05	0.07	1.45	1.37	4.5
	East siberian sea	−0.2	0.1	0.3	0.06	−0.01	0.03	0.04	< 1
	Kara sea	0.2	0.3	0.1	0.06	−0.06	−0.02	0.04	2
	Total	0	13.4	13.4	0	0	1.45	1.45	< 1
North atlantic	Davis strait	−1.6	18.1	19.7	0.19	0.01	−1.43	−1.43	< 1
	Denmark strait	−3.4	5	8.4	0.42	−0.25	−0.23	0.02	< 1
	Iceland sea	0.8	5.1	4.3	0.25	0.07	0.2	0.13	< 1
	Norwegian sea	2.8	5.2	2.4	0.37	0.21	0.29	0.07	1
	Total	−1.4	33.5	34.9	0.1	0.04	−1.18	−1.21	< 1
North pacific	Chukchi sea	1.4	1.5	0	0.09	−0.03	−0.03	0	< 1
	Total	1.4	1.5	0	0.09	−0.03	−0.03	0	< 1
NW passages	Baffin bay	1.6	1.7	0	0.19	0	0.05	0.05	< 1
	Beaufort sea	1.3	1.7	0.4	0.24	0.04	0.08	0.04	< 1
	Central arctic	−2.9	0.6	3.5	0.27	−0.04	0.03	0.06	< 1
	Total	0	4	4	0	0	0.15	0.15	< 1
Norwegian sea	Barents sea	1.9	2.9	1	0.25	0.21	0.16	−0.05	2.2
	Greenland sea	7.6	17	9.4	0.69	−1.52	−3	−1.48	7.3
	Iceland sea	−6.7	7.1	13.8	0.75	1.53	0.53	−1	7.4
	North atlantic	−2.8	2.4	5.2	0.37	−0.21	0.07	0.29	1
	Total	0	29.4	29.4	0.01	0	−2.24	−2.24	< 1

Table A.2: Heat transport (liquid). Reference temperature $T_{ref} = -0.1°C$ and TW.

Sections		Control				$2\times CO_2$ - Control			
from	to	net	pos	neg	sdv	net	pos	neg	s/n
Arctic seas	North atlantic	−178.9	549.5	729.5	22.09	4.77	82.29	77.51	< 1
	North pacific	−6	4.9	9.8	1.96	−8.95	−2.62	6.33	5.8
	Total	−185	554.4	739.3	21.99	−4.18	79.67	83.85	< 1
Baffin bay	Davis strait	−10.7	3.9	15.8	1.16	0.2	1.16	0.96	< 1
	NW passages	9.1	9.7	0.7	1	−0.72	−0.35	0.37	1.6
	Total	−1.6	14.2	15.8	0.67	−0.51	0.81	1.33	1.3
Barents sea	Central arctic	−2.6	4.4	7.4	1.15	1.69	0.39	−1.3	2
	Kara sea	−9.5	6.3	16.9	1.8	8.6	2.9	−5.7	5.5
	Norwegian sea	−39.7	6.8	45	5.14	−15.51	4.74	20.25	8.3
	White sea	−0.1	0.4	0.6	0.04	−0.09	0.21	0.3	4.2
	Total	−51.9	17.9	69.8	6.29	−5.3	8.24	13.54	2.6
Beaufort sea	Central arctic	−7.7	28.2	37	1.37	0.64	2.49	1.86	1.1
	NW passages	6.7	10.1	3.4	1.41	−0.02	0.42	0.44	< 1
	Total	−1	38.8	39.8	0.92	0.62	2.92	2.3	1.4
Central arctic	Barents sea	2.6	7.2	4.6	1.15	−1.69	−1.3	0.39	2
	Beaufort sea	7.7	36.5	28.7	1.37	−0.64	1.86	2.49	1.1
	Chukchi sea	2.1	8.4	6.3	1.31	−4.86	−0.9	3.95	4.8
	East siberian sea	1.2	13.3	12.1	0.43	0.14	1.13	0.99	< 1
	Greenland sea	−20.8	27.2	49.3	3.1	9.76	−4.44	−14.2	4
	Kara sea	10.2	14.1	3.9	1.75	−3.36	−3.45	−0.09	3.4
	Laptev sea	0	57.2	57.2	0.64	0.34	5.84	5.5	1.6
	Lincoln sea	0.2	10.6	10.4	0.06	−0.08	−3.16	−3.08	1.8
	NW passages	−15.5	2.9	20.6	1.43	1.07	0.18	−0.9	1.4
	Total	−12.3	179.2	191.4	3.13	0.68	−4.25	−4.94	< 1
Chukchi sea	Central arctic	−2.1	5.9	8.8	1.31	4.86	3.95	−0.9	4.8
	East siberian sea	−1.6	0.4	2.3	0.57	0.92	0.67	−0.25	2.6
	North pacific	−6	4.9	9.8	1.96	−8.95	−2.62	6.33	5.8
	Total	−9.7	11.2	20.9	1.67	−3.17	2.01	5.19	3.7
Davis strait	Baffin bay	10.7	15.2	4.5	1.16	−0.2	0.96	1.16	< 1
	Hudson strait	−0.5	5.6	6.1	0.6	0.38	0.57	0.18	< 1
	North atlantic	−58.6	253.7	313.6	16.13	14.78	24.89	10.1	< 1
	Total	−48.4	275.1	323.5	16.02	14.96	26.42	11.45	< 1
Denmark strait	Iceland sea	7.4	17.8	10.4	3.27	−20.17	−8.18	11.98	7.6
	North atlantic	−33.4	112.8	148.8	7.34	11.54	19.86	8.31	8.2
	Total	−26	103.7	129.7	8.76	−8.63	11.68	20.29	3.2
East siberian sea	Central arctic	−1.2	12.1	13.4	0.43	−0.14	0.99	1.13	< 1
	Chukchi sea	1.6	2.1	0.5	0.57	−0.92	−0.25	0.67	2.6
	Laptev sea	−1	0.7	1.9	0.4	0.44	0.32	−0.11	1.7
	Total	−0.6	15	15.6	0.45	−0.62	1.06	1.69	2.8
Foxe basin	Hudson bay	0.7	1.4	0.7	0.34	−0.26	−0.13	0.13	1.4
	Hudson strait	−0.2	1.1	1.4	0.4	0.65	0.58	−0.08	2.7
	Total	0.5	2.5	2	0.24	0.39	0.44	0.05	4.6
Gin sea	Barents sea	39.7	45.7	6	5.14	15.51	20.25	4.74	8.3
	Central arctic	20.8	48.6	27.9	3.1	−9.76	−14.2	−4.44	4
	North atlantic	−91.4	179.1	270.9	12.98	−5.27	33.28	38.54	< 1
	Total	−69.5	371	440.5	13.44	−6.38	95.44	101.81	1.4

Table A.2: Heat transport (liquid). Reference temperature $T_{ref} = -0.1°C$ and units TW.

Section		Control				$2\times CO_2$ - Control			
from	to	net	pos	neg	sdv	net	pos	neg	s/n
Greenland sea	Central arctic	20.8	48.6	27.9	3.1	−9.76	−14.2	−4.44	4
	Iceland sea	18.6	34.3	15.7	9.79	34.46	26.81	−7.65	5.2
	Norwegian sea	−79.8	53.8	127.7	13.26	−21.84	31.55	53.39	3.5
	Total	−40.4	133.7	174.2	8.81	2.86	44.16	41.3	1.4
Hudson bay	Foxe basin	−0.7	0.6	1.4	0.34	0.26	0.13	−0.13	1.4
	Hudson strait	1.3	2.4	1.1	0.38	−0.07	−0.09	−0.02	< 1
	Total	0.6	3.1	2.4	0.27	0.18	0.04	−0.16	2.7
Hudson strait	Davis strait	0.5	6.1	5.6	0.6	−0.38	0.18	0.57	< 1
	Foxe basin	0.2	1.3	1.1	0.4	−0.65	−0.08	0.58	2.7
	Hudson bay	−1.3	1	2.5	0.38	0.07	−0.02	−0.09	< 1
	Total	−0.7	8.5	9.2	0.64	−0.96	0.08	1.06	1.5
Iceland sea	Denmark strait	−7.4	9	19.1	3.27	20.17	11.98	−8.18	7.6
	Greenland sea	−18.6	19.3	30.7	9.79	−34.46	−7.65	26.81	5.2
	North atlantic	−28.9	116.7	145	7.71	−4.75	24.12	28.87	2.3
	Norwegian sea	64.6	109.8	45.3	10.31	21.15	58.64	37.48	4
	Total	9.6	252.2	242.6	5.9	2.1	87.09	84.98	< 1
Kara sea	Barents sea	9.5	16.3	6.8	1.8	−8.6	−5.7	2.9	5.5
	Central arctic	−10.2	3.2	14.7	1.75	3.36	−0.09	−3.45	3.4
	Laptev sea	1.1	1.8	0.7	0.41	−0.65	−0.43	0.21	3
	Total	0.4	22	21.6	0.72	−5.89	−6.23	−0.33	9.4
Laptev sea	Central arctic	0	57.2	57.2	0.64	−0.34	5.5	5.84	1.6
	East siberian sea	1	1.8	0.8	0.4	−0.44	−0.11	0.32	1.7
	Kara sea	−1.1	0.6	1.9	0.41	0.65	0.21	−0.43	3
	Total	−0.1	59.7	59.8	0.56	−0.12	5.61	5.73	< 1
North atlantic	Davis strait	58.6	313	254.3	16.13	−14.78	10.1	24.89	< 1
	Denmark strait	33.4	147.5	114.1	7.34	−11.54	8.31	19.86	8.2
	Iceland sea	28.9	145.3	116.4	7.71	4.75	28.87	24.12	2.3
	Norwegian sea	127.4	157.9	30.5	12.06	16.81	30.23	13.42	2.2
	Total	248.4	502.1	253.7	27.41	−4.77	77.51	82.29	< 1
North pacific	Chukchi sea	6	10.4	4.3	1.96	8.95	6.33	−2.62	5.8
	Total	6	10.4	4.3	1.96	8.95	6.33	−2.62	5.8
NW passages	Baffin bay	−9.1	0	10.4	1	0.72	0.37	−0.35	1.6
	Beaufort sea	−6.7	2.9	10.5	1.41	0.02	0.44	0.42	< 1
	Central arctic	15.5	19.5	4	1.43	−1.07	−0.9	0.18	1.4
	Total	−0.3	23.5	23.8	0.43	−0.34	−0.1	0.25	1.4
Norwegian sea	Barents sea	39.7	45.7	6	5.14	15.51	20.25	4.74	8.3
	Greenland sea	79.8	130.6	50.8	13.26	21.84	53.39	31.55	3.5
	Iceland sea	−64.6	47.9	107.3	10.31	−21.15	37.48	58.64	4
	North atlantic	−127.4	31.6	156.8	12.06	−16.81	13.42	30.23	2.2
	Total	−72.5	252.1	324.6	11.55	−0.61	124.54	125.16	< 1

Table A.3: Heat transport (ice). Units are in TW.

Sections		Control				$2\times CO_2$ - Control			
from	to	net	pos	neg	sdv	net	pos	neg	s/n
Arctic seas	North atlantic	−0.1	0	0.1	0.15	0.06	0	−0.07	< 1
	North pacific	0	0	0	0	0	0	0	< 1
	Total	−0.1	0	0.1	0.15	0.06	0	−0.07	< 1
Baffin bay	Davis strait	−1.1	0.7	1.8	0.4	0.3	−0.14	−0.45	1.2
	NW passages	0	0	0	0	0	0	0	< 1
	Total	−1.1	0.7	1.8	0.4	0.3	−0.14	−0.45	1.2
Barents sea	Central arctic	0.8	4.6	3.8	1.13	−0.41	−3.66	−3.25	< 1
	Kara sea	2.1	4.1	1.9	1.01	−2.04	−3.92	−1.88	6.4
	Norwegian sea	−0.1	0	0.1	0.1	0.06	0	−0.06	2.2
	White sea	0.1	0.2	0.1	0.08	−0.08	−0.2	−0.12	2.6
	Total	3	8.9	5.9	1.6	−2.47	−7.78	−5.31	4.9
Beaufort sea	Central arctic	−0.7	3.6	4.3	1.03	−0.1	−1.53	−1.44	< 1
	NW passages	2.8	3.7	0.8	0.82	−0.97	−1.2	−0.24	2.2
	Total	2.1	7.3	5.1	0.87	−1.06	−2.74	−1.67	3.7
Central arctic	Barents sea	−0.8	3.8	4.6	1.13	0.41	−3.25	−3.66	< 1
	Beaufort sea	0.7	4.3	3.6	1.03	0.1	−1.44	−1.53	< 1
	Chukchi sea	−2.4	3.9	6.3	1.5	0.85	−1.68	−2.53	2.7
	East siberian sea	−0.4	9.9	10.3	2.33	0.76	−3.9	−4.66	1.3
	Greenland sea	−6.8	1.7	8.5	1.74	4.11	−0.91	−5.03	8
	Kara sea	2.5	4.6	2.1	0.79	−1.56	−2.76	−1.2	8.9
	Laptev sea	2.8	9	6.2	1.41	−0.72	−3.35	−2.62	1.4
	Lincoln sea	−1.6	1.9	3.4	0.59	1.18	−0.52	−1.7	8.8
	NW passages	−5	6	11	1.53	2.4	−3.27	−5.67	3.3
	Total	−10.9	45.1	56	2.98	7.52	−21.08	−28.6	11.5
Chukchi sea	Central arctic	2.4	6.3	3.9	1.5	−0.85	−2.53	−1.68	2.7
	East siberian sea	−0.5	1	1.5	0.52	0.22	−0.31	−0.53	< 1
	North pacific	0	0	0	0	0	0	0	< 1
	Total	1.9	7.3	5.4	1.34	−0.63	−2.84	−2.21	3.4
Davis strait	Baffin bay	1.1	1.8	0.7	0.4	−0.3	−0.45	−0.14	1.2
	Hudson strait	0.5	0.7	0.3	0.25	−0.17	−0.26	−0.09	3.1
	North atlantic	−0.1	0	0.1	0.15	0.06	0	−0.07	< 1
	Total	1.5	2.5	1.1	0.53	−0.42	−0.71	−0.3	< 1
Denmark strait	Iceland sea	0	0	0	0.04	0	0	0	< 1
	North atlantic	0	0	0	0	0	0	0	1.1
	Total	0	0	0	0.04	0	0	0	< 1
East siberian sea	Central arctic	0.4	10.3	9.9	2.33	−0.76	−4.66	−3.9	1.3
	Chukchi sea	0.5	1.5	1	0.52	−0.22	−0.53	−0.31	< 1
	Laptev sea	−1.2	0.9	2.1	0.62	0.59	−0.22	−0.81	1.9
	Total	−0.3	12.7	13	2.17	−0.39	−5.4	−5.02	< 1
Foxe basin	Hudson bay	−0.3	0.2	0.4	0.1	0.02	−0.02	−0.04	1.1
	Hudson strait	−0.4	0.2	0.6	0.15	0	−0.02	−0.02	< 1
	Total	−0.7	0.4	1.1	0.25	0.02	−0.04	−0.07	< 1
Gin sea	Barents sea	0.1	0.1	0	0.1	−0.06	−0.06	0	2.2
	Central arctic	6.8	8.5	1.7	1.74	−4.11	−5.03	−0.91	8
	North atlantic	0	0	0	0	0	0	0	1.1
	Total	6.4	8.6	2.1	1.71	−3.88	−5.09	−1.22	7.6

Table A.3: Heat transport (ice). Units are in TW.

Section		Control				$2\times CO_2$ - Control			
from	to	net	pos	neg	sdv	net	pos	neg	s/n
Greenland sea	Central arctic	6.8	8.5	1.7	1.74	−4.11	−5.03	−0.91	8
	Iceland sea	−0.4	0	0.4	0.25	0.29	−0.01	−0.3	4.7
	Norwegian sea	0	0	0	0	0	0	0	< 1
	Total	6.3	8.5	2.1	1.67	−3.82	−5.03	−1.22	7.6
Hudson bay	Foxe basin	0.3	0.4	0.2	0.1	−0.02	−0.04	−0.02	1.1
	Hudson strait	0.3	0.7	0.4	0.15	−0.03	−0.09	−0.05	1.2
	Total	0.5	1.1	0.6	0.25	−0.06	−0.13	−0.07	1.1
Hudson strait	Davis strait	−0.5	0.3	0.7	0.25	0.17	−0.09	−0.26	3.1
	Foxe basin	0.4	0.6	0.2	0.15	0	−0.02	−0.02	< 1
	Hudson bay	−0.3	0.4	0.7	0.15	0.03	−0.05	−0.09	1.2
	Total	−0.3	1.3	1.7	0.25	0.21	−0.16	−0.37	4.3
Iceland sea	Denmark strait	0	0	0	0.04	0	0	0	< 1
	Greenland sea	0.4	0.4	0	0.25	−0.29	−0.3	−0.01	4.7
	North atlantic	0	0	0	0	0	0	0	1
	Norwegian sea	0	0	0	0	0	0	0	< 1
	Total	0.4	0.4	0	0.22	−0.3	−0.3	−0.01	4.6
Kara sea	Barents sea	−2.1	1.9	4.1	1.01	2.04	−1.88	−3.92	6.4
	Central arctic	−2.5	2.1	4.6	0.79	1.56	−1.2	−2.76	8.9
	Laptev sea	0	0	0	0	0	0	0	< 1
	Total	−4.6	4	8.7	1.26	3.6	−3.08	−6.68	13.1
Laptev sea	Central arctic	−2.8	6.2	9	1.41	0.72	−2.62	−3.35	1.4
	East siberian sea	1.2	2.1	0.9	0.62	−0.59	−0.81	−0.22	1.9
	Kara sea	0	0	0	0	0	0	0	< 1
	Total	−1.7	8.2	9.9	1.51	0.13	−3.43	−3.56	< 1
North atlantic	Davis strait	0.1	0.1	0	0.15	−0.06	−0.07	0	< 1
	Denmark strait	0	0	0	0	0	0	0	1.1
	Iceland sea	0	0	0	0	0	0	0	1
	Norwegian sea	0	0	0	0	0	0	0	1.1
	Total	0.1	0.1	0	0.15	−0.06	−0.07	0	< 1
North pacific	Chukchi sea	0	0	0	0	0	0	0	< 1
	Total	0	0	0	0	0	0	0	< 1
NW passages	Baffin bay	0	0	0	0	0	0	0	< 1
	Beaufort sea	−2.8	0.8	3.7	0.82	0.97	−0.24	−1.2	2.2
	Central arctic	5	11	6	1.53	−2.4	−5.67	−3.27	3.3
	Total	2.2	11.9	9.7	1.48	−1.43	−5.91	−4.47	2
Norwegian sea	Barents sea	0.1	0.1	0	0.1	−0.06	−0.06	0	2.2
	Greenland sea	0	0	0	0	0	0	0	< 1
	Iceland sea	0	0	0	0	0	0	0	< 1
	North atlantic	0	0	0	0	0	0	0	1.1
	Total	0.1	0.1	0	0.1	−0.06	−0.06	0	2.2

Table A.4: Freshwater transport (liquid). Reference salinity $S_{ref} = 34.8$ and units kt/s.

Sections		Control				$2\times CO_2$ - Control			
from	to	net	pos	neg	sdv	net	pos	neg	s/n
Arctic seas	North atlantic	162	277.3	115.3	17.28	36.79	−17.68	−54.48	3.6
	North pacific	−106.1	−1.2	113	9.29	−16.29	−16.8	−0.51	3.3
	Total	55.9	280.1	224.3	19.81	20.49	−34.48	−54.99	1.9
Baffin bay	Davis strait	61.4	83.9	22.6	7.86	20.18	0.34	−19.84	3.4
	NW passages	−63.4	−1.6	70.9	7.9	−18.88	−19.68	−0.81	3.4
	Total	−2	86.9	88.9	1.54	1.3	−19.35	−20.65	1.7
Barents sea	Central arctic	5	24.7	19.7	3.37	3.11	−8.4	−11.51	1.6
	Kara sea	10.7	31.5	20.8	6.19	−3.42	−8.83	−5.41	1
	Norwegian sea	6.9	7.8	0.9	2.81	4.14	0.8	−3.34	2.9
	White sea	−0.1	1.4	1.5	0.07	−0.17	−0.07	0.1	3.8
	Total	22.5	65.4	42.8	5.69	3.66	−16.5	−20.16	4.3
Beaufort sea	Central arctic	53.8	228.7	174.9	13.7	19.37	−66.87	−86.24	4.4
	NW passages	−46.6	17.9	71.6	10.42	−15.03	−23.49	−8.47	3
	Total	7.2	250.2	242.9	6.43	4.34	−90.37	−94.7	5.8
Central arctic	Barents sea	−5	18.5	25.9	3.37	−3.11	−11.51	−8.4	1.6
	Beaufort sea	−53.8	171.3	232.2	13.7	−19.37	−86.24	−66.87	4.4
	Chukchi sea	−81.5	41.8	129.4	8.58	−11.53	−24.1	−12.56	3.4
	East siberian sea	−9.3	113	123.1	4.56	−3.42	−48.5	−45.07	3.6
	Greenland sea	86.8	232.1	145.3	10.06	0.29	−14.18	−14.47	< 1
	Kara sea	−43.7	21.8	74.9	6.56	−3.16	−0.78	2.38	< 1
	Laptev sea	−5.7	384.5	390.2	4.67	−10.17	−186.69	−176.52	6.1
	Lincoln sea	−1	71.8	72.9	0.56	−0.07	3.48	3.54	< 1
	NW passages	105.1	133.5	28.3	11.95	31	−7.64	−38.65	3.4
	Total	−8.1	1201.2	1209.3	12.18	−19.54	−376.16	−356.63	5.3
Chukchi sea	Central arctic	81.5	126.4	44.8	8.58	11.53	−12.56	−24.1	3.4
	East siberian sea	27.3	32.2	4.9	7.2	6.35	−2.75	−9.1	2.1
	North pacific	−106.1	−1.2	113	9.29	−16.29	−16.8	−0.51	3.3
	Total	2.7	161.4	158.8	3.24	1.59	−32.12	−33.71	3.1
Davis strait	Baffin bay	−61.4	18	88.5	7.86	−20.18	−19.84	0.34	3.4
	Hudson strait	−10.7	42.5	53.1	2.08	−3.42	−10.6	−7.19	2.2
	North atlantic	100.1	155.8	55.7	14.05	19.8	4.04	−15.77	1.8
	Total	28.1	220.9	192.8	9.43	−3.8	−26.4	−22.63	< 1
Denmark strait	Iceland sea	−37.5	6.5	63.2	6.78	−6.41	−8.33	−1.92	1.2
	North atlantic	21.8	36.7	15	8.17	8.25	−5.99	−14.24	1.6
	Total	−15.7	52.8	68.6	5.67	1.84	−14.32	−16.16	2.3
East siberian sea	Central arctic	9.3	122.7	113.4	4.56	3.42	−45.07	−48.5	3.6
	Chukchi sea	−27.3	4	33.2	7.2	−6.35	−9.1	−2.75	2.1
	Laptev sea	17.2	28.6	11.4	5.63	4.76	−5.06	−9.82	2.3
	Total	−0.8	156.2	157	2.25	1.84	−59.23	−61.07	1.6
Foxe basin	Hudson bay	−22.6	4.7	28.5	5.74	−7.46	−6.35	1.11	2.7
	Hudson strait	25.7	33.9	8.2	6.18	7.23	−1.33	−8.56	2.6
	Total	3.1	39.2	36.1	1.33	−0.22	−7.68	−7.45	< 1
Gin sea	Barents sea	−6.9	6.3	2.4	2.81	−4.14	−3.34	0.8	2.9
	Central arctic	−86.8	140.4	237	10.06	−0.29	−14.47	−14.18	< 1
	North atlantic	51.8	79.9	28.1	9.73	14.26	−10.8	−25.06	3.6
	Total	−13.5	344.1	357.6	12.93	13.68	−42.28	−55.97	3.6

Table A.4: Freshwater transport (liquid). Reference salinity $S_{ref} = 34.8$ and units kt/s.

Section		Control				$2\times CO_2$ - Control			
from	to	net	pos	neg	sdv	net	pos	neg	s/n
Greenland sea	Central arctic	−86.8	140.4	237	10.06	−0.29	−14.47	−14.18	< 1
	Iceland sea	44.7	65.5	20.8	9.74	−1.21	−1.89	−0.68	< 1
	Norwegian sea	40.8	54.7	13.9	7.76	6.89	−4.87	−11.76	1.3
	Total	−1.4	265.4	266.8	8.4	5.39	−21.24	−26.63	2.2
Hudson bay	Foxe basin	22.6	27.9	5.2	5.74	7.46	1.11	−6.35	2.7
	Hudson strait	−8.1	24.1	33.4	6.54	−7.67	−6.97	0.7	3.6
	Total	14.5	52.5	38	1.94	−0.21	−5.87	−5.65	< 1
Hudson strait	Davis strait	10.7	53.1	42.5	2.08	3.42	−7.19	−10.6	2.2
	Foxe basin	−25.7	7.6	34.5	6.18	−7.23	−8.56	−1.33	2.6
	Hudson bay	8.1	32.8	24.7	6.54	7.67	0.7	−6.97	3.6
	Total	−7	94.1	101.1	2.25	3.85	−15.05	−18.91	2.9
Iceland sea	Denmark strait	37.5	53.6	16.1	6.78	6.41	−1.92	−8.33	1.2
	Greenland sea	−44.7	−5.1	91.4	9.74	1.21	−0.68	−1.89	< 1
	North atlantic	10.1	41.5	31.4	2.44	2.73	−10.92	−13.64	4.2
	Norwegian sea	−21.3	33.7	17.8	8.32	−11.47	−14.92	−3.45	2.1
	Total	−18.4	131	149.4	4.79	−1.12	−28.45	−27.32	1.1
Kara sea	Barents sea	−10.7	16.6	35.7	6.19	3.42	−5.41	−8.83	1
	Central arctic	43.7	70.2	26.5	6.56	3.16	2.38	−0.78	< 1
	Laptev sea	−15.9	6.4	23.5	5.09	1.36	−4.27	−5.63	< 1
	Total	17.1	98	80.9	4.46	7.94	−7.31	−15.24	2.1
Laptev sea	Central arctic	5.7	390.2	384.5	4.67	10.17	−176.52	−186.69	6.1
	East siberian sea	−17.2	10.8	29.1	5.63	−4.76	−9.82	−5.06	2.3
	Kara sea	15.9	22.9	7	5.09	−1.36	−5.63	−4.27	< 1
	Total	4.4	424.4	420.1	3.53	4.05	−191.97	−196.02	4.8
North atlantic	Davis strait	−100.1	51.2	160.4	14.05	−19.8	−15.77	4.04	1.8
	Denmark strait	−21.8	5.4	46.3	8.17	−8.25	−14.24	−5.99	1.6
	Iceland sea	−10.1	33.7	39.2	2.44	−2.73	−13.64	−10.92	4.2
	Norwegian sea	−30	21	35.3	6.23	−6.01	−10.82	−4.81	1.5
	Total	−162	111.3	281.3	17.28	−36.79	−54.48	−17.68	3.6
North pacific	Chukchi sea	106.1	109	2.9	9.29	16.29	−0.51	−16.8	3.3
	Total	106.1	109	2.9	9.29	16.29	−0.51	−16.8	3.3
NW passages	Baffin bay	63.4	66.3	3	7.9	18.88	−0.81	−19.68	3.4
	Beaufort sea	46.6	68.1	21.5	10.42	15.03	−8.47	−23.49	3
	Central arctic	−105.1	20.2	141.6	11.95	−31	−38.65	−7.64	3.4
	Total	4.8	162.8	157.9	1.9	2.91	−47.92	−50.82	6.3
Norwegian sea	Barents sea	−6.9	6.3	2.4	2.81	−4.14	−3.34	0.8	2.9
	Greenland sea	−40.8	35	33.6	7.76	−6.89	−11.76	−4.87	1.3
	Iceland sea	21.3	36.4	15.1	8.32	11.47	−3.45	−14.92	2.1
	North atlantic	30	43.2	13.2	6.23	6.01	−4.81	−10.82	1.5
	Total	3.6	94.3	90.7	8.57	6.45	−23.36	−29.82	2.8

Table A.5: Freshwater transport (ice). Units in are kt/s.

Sections		Control				$2\times CO_2$ - Control			
from	to	net	pos	neg	sdv	net	pos	neg	s/n
Arctic seas	North atlantic	0.4	0.4	0	0.51	−0.2	0.01	0.22	< 1
	North pacific	0	0	0	0	0	0	0	< 1
	Total	0.4	0.4	0	0.51	−0.2	0.01	0.22	< 1
Baffin bay	Davis strait	3.7	5.9	2.2	1.32	−1.01	0.48	1.48	1.2
	NW passages	0	0	0	0	0	0	0	< 1
	Total	3.7	5.9	2.2	1.32	−1.01	0.48	1.49	1.2
Barents sea	Central arctic	−2.8	12.5	15.3	3.76	1.35	12.11	10.76	< 1
	Kara sea	−7.1	6.4	13.5	3.35	6.76	12.99	6.24	6.4
	Norwegian sea	0.3	0.3	0	0.33	−0.19	0.01	0.2	2.2
	White sea	−0.2	0.4	0.7	0.26	0.26	0.66	0.4	2.6
	Total	−9.9	19.6	29.5	5.31	8.18	25.77	17.59	4.9
Beaufort sea	Central arctic	2.3	14.3	12	3.4	0.32	5.08	4.76	< 1
	NW passages	−9.3	2.8	12.1	2.72	3.21	3.99	0.78	2.2
	Total	−7.1	17	24.1	2.87	3.53	9.07	5.54	3.7
Central arctic	Barents sea	2.8	15.3	12.5	3.76	−1.35	10.76	12.11	< 1
	Beaufort sea	−2.3	12	14.3	3.4	−0.32	4.76	5.08	< 1
	Chukchi sea	7.8	20.7	12.9	4.98	−2.8	5.57	8.37	2.7
	East siberian sea	1.3	34.2	32.9	7.71	−2.5	12.92	15.43	1.3
	Greenland sea	22.4	28.1	5.7	5.77	−13.62	3.02	16.64	8
	Kara sea	−8.3	6.9	15.2	2.62	5.17	9.14	3.97	8.9
	Laptev sea	−9.4	20.4	29.8	4.68	2.39	11.08	8.69	1.4
	Lincoln sea	5.2	11.4	6.2	1.96	−3.91	1.72	5.63	8.8
	NW passages	16.6	36.5	20	5.07	−7.95	10.83	18.77	3.3
	Total	36.1	185.5	149.4	9.85	−24.89	69.8	94.69	11.5
Chukchi sea	Central arctic	−7.8	12.9	20.7	4.98	2.8	8.37	5.57	2.7
	East siberian sea	1.6	4.9	3.3	1.73	−0.72	1.02	1.74	< 1
	North pacific	0	0	0	0	0	0	0	< 1
	Total	−6.2	17.8	24	4.42	2.08	9.39	7.32	3.4
Davis strait	Baffin bay	−3.7	2.2	5.9	1.32	1.01	1.48	0.48	1.2
	Hudson strait	−1.6	0.9	2.5	0.84	0.57	0.86	0.29	3.1
	North atlantic	0.4	0.4	0	0.51	−0.2	0.01	0.22	< 1
	Total	−4.8	3.5	8.4	1.74	1.38	2.36	0.98	< 1
Denmark strait	Iceland sea	0	0	0.1	0.14	0	0	0	< 1
	North atlantic	0	0	0	0	0	0	0	1.1
	Total	0	0	0.1	0.14	0	0	0	< 1
East siberian sea	Central arctic	−1.3	32.9	34.2	7.71	2.5	15.43	12.92	1.3
	Chukchi sea	−1.6	3.3	4.9	1.73	0.72	1.74	1.02	< 1
	Laptev sea	3.9	6.9	3	2.05	−1.95	0.72	2.67	1.9
	Total	1	43	42.1	7.2	1.28	17.89	16.61	< 1
Foxe basin	Hudson bay	0.9	1.4	0.5	0.34	−0.08	0.07	0.15	1.1
	Hudson strait	1.4	2.1	0.8	0.51	0	0.07	0.07	< 1
	Total	2.3	3.5	1.3	0.83	−0.08	0.14	0.22	< 1
Gin sea	Barents sea	−0.3	0	0.3	0.33	0.19	0.2	0.01	2.2
	Central arctic	−22.4	5.7	28.1	5.77	13.62	16.64	3.02	8
	North atlantic	0	0	0	0	0	0	0	1.1
	Total	−21.3	7.1	28.4	5.67	12.83	16.87	4.03	7.6

Table A.5: Freshwater transport (ice). Units in are kt/s.

Section		Control				$2\times CO_2$ - Control			
from	to	net	pos	neg	sdv	net	pos	neg	s/n
Greenland sea	Central arctic	−22.4	5.7	28.1	5.77	13.62	16.64	3.02	8
	Iceland sea	1.4	1.4	0	0.82	−0.98	0.03	1.01	4.7
	Norwegian sea	0	0	0	0.01	0	0	0	< 1
	Total	−21	7.1	28.1	5.54	12.65	16.67	4.02	7.6
Hudson bay	Foxe basin	−0.9	0.5	1.4	0.34	0.08	0.15	0.07	1.1
	Hudson strait	−0.9	1.4	2.3	0.5	0.11	0.29	0.17	1.2
	Total	−1.8	1.9	3.7	0.82	0.2	0.44	0.24	1.1
Hudson strait	Davis strait	1.6	2.5	0.9	0.84	−0.57	0.29	0.86	3.1
	Foxe basin	−1.4	0.8	2.1	0.51	0	0.07	0.07	< 1
	Hudson bay	0.9	2.3	1.4	0.5	−0.11	0.17	0.29	1.2
	Total	1.1	5.5	4.4	0.83	−0.69	0.53	1.22	4.3
Iceland sea	Denmark strait	0	0.1	0	0.14	0	0	0	< 1
	Greenland sea	−1.4	0	1.4	0.82	0.98	1.01	0.03	4.7
	North atlantic	0	0	0	0	0	0	0	1
	Norwegian sea	0	0	0	0	0	0	0	< 1
	Total	−1.3	0.1	1.4	0.74	0.98	1.01	0.03	4.6
Kara sea	Barents sea	7.1	13.5	6.4	3.35	−6.76	6.24	12.99	6.4
	Central arctic	8.3	15.2	6.9	2.62	−5.17	3.97	9.14	8.9
	Laptev sea	0	0	0	0	0	0	0	< 1
	Total	15.4	28.7	13.3	4.19	−11.93	10.2	22.13	13.1
Laptev sea	Central arctic	9.4	29.8	20.4	4.68	−2.39	8.69	11.08	1.4
	East siberian sea	−3.9	3	6.9	2.05	1.95	2.67	0.72	1.9
	Kara sea	0	0	0	0	0	0	0	< 1
	Total	5.5	32.8	27.3	4.99	−0.44	11.36	11.8	< 1
North atlantic	Davis strait	−0.4	0	0.4	0.51	0.2	0.22	0.01	< 1
	Denmark strait	0	0	0	0	0	0	0	1.1
	Iceland sea	0	0	0	0	0	0	0	1
	Norwegian sea	0	0	0	0	0	0	0	1.1
	Total	−0.4	0	0.4	0.51	0.2	0.22	0.01	< 1
North pacific	Chukchi sea	0	0	0	0	0	0	0	< 1
	Total	0	0	0	0	0	0	0	< 1
NW passages	Baffin bay	0	0	0	0	0	0	0	< 1
	Beaufort sea	9.3	12.1	2.8	2.72	−3.21	0.78	3.99	2.2
	Central arctic	−16.6	20	36.5	5.07	7.95	18.77	10.83	3.3
	Total	−7.2	32.1	39.3	4.9	4.74	19.55	14.82	2
Norwegian sea	Barents sea	−0.3	0	0.3	0.33	0.19	0.2	0.01	2.2
	Greenland sea	0	0	0	0.01	0	0	0	< 1
	Iceland sea	0	0	0	0	0	0	0	< 1
	North atlantic	0	0	0	0	0	0	0	1.1
	Total	−0.3	0	0.3	0.32	0.19	0.2	0.01	2.2

Appendix B

BCM - Live Access Server

As part of the master study the BCM - Live Access Server has been developed. The BCM - Live Access Server offers on-line visualization of the output of BCM climate experiments and was firstly installed at the end of 2003 under

http://www.gfi.uib.no/∼ingo/LAS/index.html

Concept A Live Access Server (LAS) is any web-application for visualization of scientific data which receives a specific request and then on-line generates graphs or makes the data available in another form. Thus, it is much more than a browser-application that merely accesses an archive of pre-generated figures.

Requirements The most popular, and presumably the only available multiple-use LAS is developed by the TMAP group at NOAA's Pacific Marine Environmental Lab (*http://ferret.pmel.noaa.gov/Ferret/LAS/*). Since this server has a very long list of system requirements, including a system administrator with full network permissions and time to maintain the server, we decided to develop our own purpose-built LAS system for the BCM climate model output. The major difference is that the BCM-LAS can be run from any personal web-side presuming that the user has access to the data catalogs. Moreover, only a minimum of auxiliary software is needed which can be downloaded for free and installed in home any catalog. Thus the total requirements are a unix or linux operative system, a www-server with php version 3 or higher and the visualization application ferret version 5.7 or future successors.

Datasets Currently, ocean and atmospheric data from the BCM control experiment E75 and from a set of anthropogenic emission experiments are made available. For comparison purposes NCEP, COADS and LEVITUS are also included, even though these datasets can be found on their project sites.

How-To Despite a large variety of options the usage has been designed to be as simple and intuitive as possible. Thereby, the complete request is divided into four

steps in order to exclude combinations of incompatible options, e .g a contour plot from a single time series. The first step comprises the selection of the dataset and output type. In the next step, the sampling dimensions, i. e. the plot type, are chosen. The corresponding limits and strides are set in the third step. Additional plot options are selected in the final step. After the request is submitted and processed a link to the output is returned.

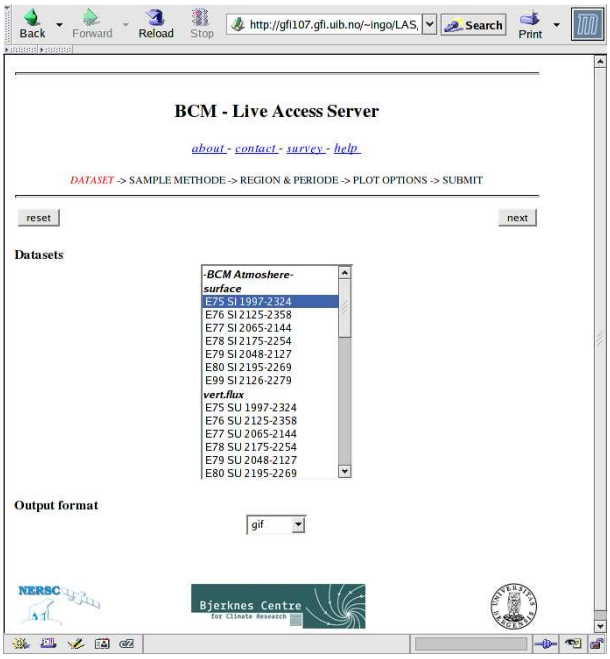

Figure B.1: Start page of the BCM - Live Access Server (*http://www.gfi.uib.no/~ingo/LAS/index.html*)

Special Features In case the dataset contains more dimensions than selected then averaging over the unselected dimensions can be partly or entirely done, e. g. vertical, zonal, or temporal averaging.

Future Plans First priority has the implementation of more statistics, e. g. seasonal and annual averages, variance and anomaly computations. This is inspired by the functionality of Climate Data Analysis Tools (CDAT) interface (*http://esg.llnl.gov/cdat/*) that is coordinated by the Program for Climate Model Diagnosis and Intercomparison (PCMDI) (*http://www-pcmdi.llnl.gov/*) Secondly, the possibility vector plots with underlying contour plots will be made available. Furthermore, we consider to employ the NetCDF Operatores (NCO) (
http://nco.sourceforge.net) for the data-dump. NCO is optimized for basic operations and handling of large datasets, while preserving the complete header information and structure of the files. In contrast, ferret automatically regrids and creates its own file attributes.

Examples

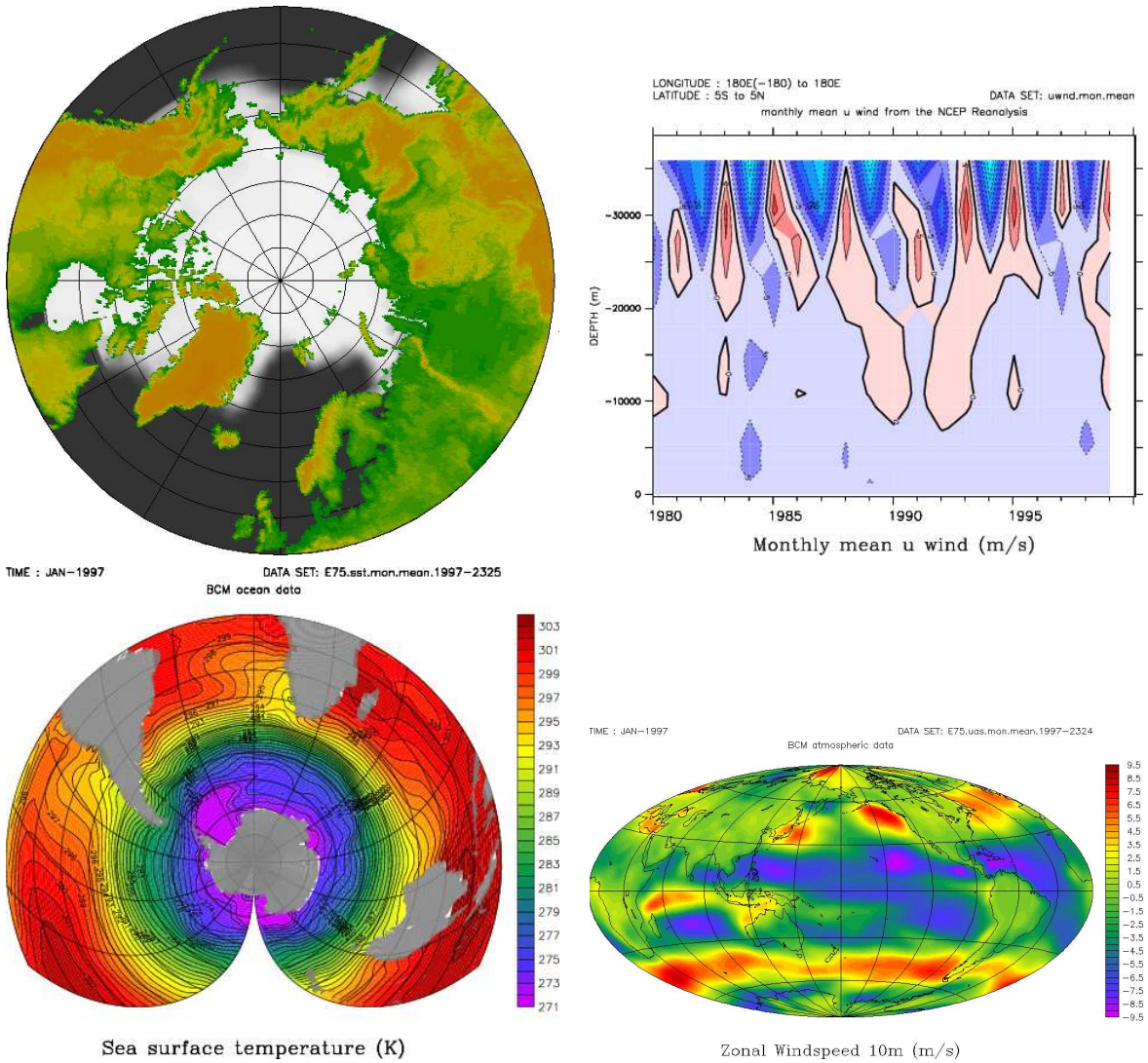

Figure B.2: Snapshoot of the BCM winter ice concentration *(upper-left)* . Observed Quasi Biennual Oscillation (QBO) of the years 1980 to 1999 *(upper-right)*. Snapshoot of the BCM sea surface temperature *(lower-left)* . Snapshoot of the BCM wind speed at 5 meters *(lower-right)* .

References

Aagaard, K. (1987). Ventilation of the Arctic cold Halocline: rates of diapycnal and isopycnal transport, oxygen, utilization and primary production inferred using chloroflouromethane distributions. *Deep-Sea Research 34*.

Aagaard, K. (1989). The Role of Sea Ice and Other Fresh Water in the Arctic Circulation. *Journal of Geophysical Research 94*, 14585–14498.

Aagaard, K., L. K. Coachman, and E. Carmack (1981). On the halocline of the Artic Ocean. *Deep-Sea Research 28a*, 529–545.

Aagaard, K. and P. Greisman (1975). Towards new volume and heat budgets for the Arctic Ocean. *Journal of Geophysical Research 80*, 3821–3827.

Adams, J. M., N. A. Bond, and J. E. Overland (2000). Regional Variability of the Arctic Heat Budget in Fall and Winter. *Journal of Climate 13*, 3500–3510.

Ådlandsvik, B. and H. Loeng (1991). A study of the climate system in the Barents Sea. *Polar Research 10*, 45–49.

Ambaum, M. H. P. and B. J. Hoskins (2002). The NAO Troposhere-Stratosphere Connection. *American Meteorolgical Society 15*, 1969–1978.

Bengtsson, L., V. A. Semenov, and O. M. Johanessen (2004). The Early Twentieth-Century Warming in the Arctic – A Possible Machanism. *Americaan Meteorological Society*, 4045–4057.

Bentsen, M. and H. Drange (2000). Parameterizing surface fluxes in ocean models using the NCEP/NCAR reanalysis data. *RegClim General Technical Report 4*, 149–158.

Bentsen, M., H. Drange, T. Furevik, and T. Zhou (2002). Variability of the Atlantic meridional overturning Circulation in an isopycnic coordinate OGCM. *draft*.

Black, R. X. (2001). Stratospheric Forcing of Surface Climate in the Arctic Oscillation. *Journal of Climate 15*, 268–271.

Bleck, R., C. Rooth, D. Hu, and L. T. Smith (1992). Salinity-driven Thermocline Transients in a Wind- and Thermohaline-forced Isopynic Coordinate Model of the North Atlantic. *Journal of Physical Oceanography 22*.

Bossuet, C., M. Déqué, and D. Cariolle (1998). Impact of a simple parameterization of convective gravity-wave drag in a stratosphere-troposphere general circulation model and its sensitivity to vertical resolution. *Ann Geophzsicae 16*, 238–249.

Carmarck, E. C. (2000). The Arctic Ocean's Freshwater Budget. *The Freshwater Budget of the Arctic Ocean. British Crown*, 91–125.

Covey, C., K. M. AchutaRao, U. Cubasch, P. Jones, S. J. Lambert, M. E. Mann, T. J. Phillips, and K. E. Taylor (2003). An Overview of Results from the Coupled Model Intercomparison Project (CMIP). *Global and Planetary Change 37*, 103–133.

Dickson, R. and R. Boscolo (2002). The Artic-Subartic Ocean Flux Study (ASOF): Rational, Scope and Methodes. *Exchanges 25*.

Dickson, R. R., T. J. Osborn, J. Hurrel, J. W.and Meincke, J. Blindheim, B. Adlandsvik, T. Vinje, G. Alekseev, and W. Maslowski (2000). The Arctic Ocean Response to the North Atlantic Oscillation. *American Meteorological Society 13*, 2671–2696.

Dommenget, D. and M. Latif (2001). A Cautionary Note on the Interpretation of EOFs. *Journal of Climate 15*, 216–225.

Douville, H., J. F. Royer, and J. F. Mahfouf (1995). A new snow parametrization for the Météo-France climate model. PART II: validation in a 3D GCM experiment. *Climate Dynamics 12*, 37–52.

Drange, H. and K. Simonsen (1996). Formulation of Air-Sea Fluxes in the ESOP2 Version of MICOM. *Technical Report 125 Nansen Environmental and Remote Sensing Center, Bergen, Norway*.

Fichefet, T. and P. Gaspar (1988). A model study of upper ocean-sea ice interaction. *Journal of Geophysical Research 18*, 181–195.

Fissel, D., J. Birch, H. Melling, and R. Lake (1988). Non-tidal flows in the Northwest Passage. *Canadian Institute of Ocean Science - Technical Report 98*.

Furevik, T., M. Bentsen, H. Drange, I. K. T. Kindem, Kvamstø, and A. Sorteberg (2003). Description and evaluation of the bergen climate model: ARPEGE coupled with MICOM. *Climate Dynamics 21*, 27–51.

Furevik, T. and J. E. Ø. Nilsen (2004). Large-Scale Atmospheric Circulation Variablity and its Impacts on the Nordic Seas Ocean Climate – a Review. *Submitted to Climate Variability in the Nordic Seas, Geophysical Monograph Series, AGU*.

Gaspar, P. (1988). Modeling the seasonal cycle of the upper ocean. *Journal of Physical Oceanography 18*, 161–180.

Gerdes, R., M. J. Karcher, F. Kauker, and U. Schauer (2003). Causes and development of repeated Artic Ocean warming events. *Geophysical Research Letters 30*.

Gong, G. and E. D. (2003). Relative impacts of Siberian and North American snow anomalies on the winter Arctic Oscillation. *Geophysical Research Letters 16*.

Haak, H., J. Junclaus, U. Mikolajewicz, and M. Latif (2003). Formation and Propagation of Great Salinity Anomalies. *Geophysical Research Letters*.

Hansen, B. and S. Østerhus (2000). North Atlantic–Nordic Seas exchanges. *Progress in Oceanography 45*, 109–208.

Hansen, B., S. Østerhus, D. Quadfasel, and W. Turrell (2004). Already the Day After Tomorrow. *Science 305*, 953–954.

Hansen, B., W. Turrell, and S. Østerhus (2001). Decreasing overflow from the Nordic Seas into the Atlantic Ocean through the Faroe Bank Channel. *Nature 411*, 927–930.

Harder, M. (1996). Dynamik, Rauhigkeit und Alter des Meereises in der Arktis. *PhD thesis Alfred-Wegener-Institut für Polar- und Meeresforschung*.

Hartmann, D. L. (2004). ATM S 552: "Objective Analysis" – Course Notes . *http://www.atmos.washington.edu/∼dennis/552_Notes_ftp.html*.

Haynes, P. H., C. J. Marks, M. E. McIntyre, T. G. Shepherd, and P. Shine (2000). On the "donward control" of extratropical diabatic circulations by eddy-induced zonal mean forces. *Journal of Atmospheric Science 126*, 1515–1532.

Hibler, W. D. (1979). A dynamic thermodynamic sea ice model. *Journal of Geophysical Research 9*, 815–846.

Holland, M. M. and C. M. Bitz (2003). Polar amplification of climate change in coupled models. *Climate Dynamics 21*, 221–232.

Hopkins, T. S. (1991). The GIN Sea - A synthesis of its physical oceanography and literatur review 1971 - 1985. *Earth Sience Review 30*, 175–319.

Howard, C. and D. Cresswell (2000). The Arctic Ocean Freshwater Budget of a Climate General Circulation. *The Freshwater Budget of the Arctic Ocean. British Crown*, 127–139.

Hurrell, J. W., M. P. Hoerling, and C. K. Folland (2000). Climate Variability over the North Atlantic. *Academic Press " Meteorology at the Millenium": Contributions from Invited Speakers*.

Ikeda, M. (1990). Feedback Mechanism among Decadal Oscillations in the Northern Hemisphere Atmospheric Circulation, Sea Ice and Ocean Circulation. *Annales of Glaciology 14*, 120–123.

Ingvaldsen, R. B., L. Asplin, and H. Loeng (2004). Velocity field of the western entrance of the Barents Sea. *Journal of Geophysical Research 109*.

Intergovernmental Panel on Climate Change - IPCC (2001). Climate Change 2001: The Scientific Basis. Contribution of Working Group I to the Third Assessment

Report of the Intergovernmental Panel on Climate Change. *Cambridge University Press*.

Iversen, T. (1996). Atmospheric transport pathways for the Arctic. *In: Wolff E. and R.C. Bales. Chemical exchange between the atmosphere and polar snow. Global Environmental Change. NATO ASI Series I 43*, 71–92.

Jakobbson, M., N. Z. Cherkis, J. Woodward, R. Macnab, and B. Coakley (2003). New grid of Arctic bathymetry aids scientists and mapmakers. *Eos, Transactions, American Geophysical Union 81*, 89,93,96.

Jakobsson, M. (2002). Hypsometry and volume of the Arctic Ocean and its constituent seas. *Geochemistry Geophysics Geosystems 3*.

Jia, Y. (2003). Ocean heat transport and its relationship to ocean circulation in the CMIP coupled models. *Climate Dynamics 20*, 153–174.

Johannessen, O. M., E. V. Shalina, and M. Miles (1999). Satellite Evidence for an Arctic Sea Ice Cover in Transformation. *Science 286*, 1937–1939.

Johnson, M. A. and I. V. Polyakov (2001). The Laptev Sea as a source for recent Arctic Ocean Salinity changes. *Geophysical Research Letters 28(10)*, 2017–2020.

Johnson, M. A., A. Y. Proshutinsky, and I. V. Polyakov (1999). Atmospheric patterns forcing two regimes of Arctic circulation: A return to anticyclonic conditions? *Geophysical Research Letters 26(11)*, 1621–1624.

Kalney, E., M. Kanamitsu, R. Kistler, W. Collins, D. Deaven, L. Gandin, M. Iredell, S. Saha, G. White, J. Wollen, Y. Zhu, A. Leetma, B. Reynolds, M. Chelliah, W. Ebisuzaki, W. Higgins, J. Janowiak, K. C. Mo, C. Ropelewski, J. Wang, R. Jenne, and D. Joseph (1996). The NCEP/NCAR 40–Year Reanalysis Project. *Bulletin of the American Meteorogical Society 77*, 437–472.

Kvamstø, N. G., P. Skeie, and D. B. Stephenson (2004). Impact of Labrador Sea-Ice extent on the North Atlantic Oscillation. *International Journal Of Climatology 24*, 603–612.

Laurantin, O. (2004). Promotion d'eleves Ingenieurs del'ENM 2001/2004: Inter–annual to multi–decadel variability of the Arctic atmosphere-sea ice-ocean climate system. *Meteo France, Ecole Nationale de la Meteorolgie*.

Laxon, S., N. Peacock, and D. Smith (2003). High interannual variability of sea ice thickness in the Arctic region. *Nature 425*.

Leith, C. E. (1973). The standard error of time-averaged estimates of climatic means. *Journal of Applied Meteorology 12*, 1066–1069.

Levitus, S. and T. P. Boyer (1994). World Ocean Atlas 1994 volume 4: temperature. NOAA Atlas NESDIS 4. *US Department of Commerce, Washington, D.C*.

Lindquist, K., E. Rowan, and B. Häkansson (2003). Sea ice sensitivity to warm currents through the Barents Sea. *Report to the European Comission*.

Lott, F. (1999). Alleviation of stationary biases in a GCM through a mountain drag parameterization scheme and a simple representation of mountain lift forces. *Monthly Weather Review 125*, 788–801.

Macdonald, R. W. and J. Bewers (1996). Contaminants in the arctic marine environment: priorities ans protection. *ICES J. mar. Sci. 53*, 537–563.

Macdonald, R. W., T. Harner, J. Fyfe, H. Loeng, and T. Weingartner (2002). AMAP Assessment 2002: The Influence of Global Change on Contaminant Pathways to, within, and from the Arctic.

Macdonald, R. W., D. W. Paton, E. C. Carmack, and A. Omstedt (1995). The freshwater budget and under-ice spreading of Mackenzie River water in the Canadian Beaufort Sea based on salinity and O18/O16 measurements in water and ice. *Journal of Geophysical Research 100*, 895–919.

Maslowski, W., D. Marble, W. Walczowski, U. Schauer, and A. J. Semtner (2004). On climatological mass, heat and salt transports through the Barents Sea and Fram Strait from pan-Arctic coupled ice-ocean model simulation. *Journal of Geophysical Research 109*.

Moritz, R. E., C. M. Bitz, and E. J. Steig (2002). Dynamics of Recent Climate Change in the Arctic. *Science 297*.

Mysak, L. A. (2001). Patterns of the Arctic circulation. *Science 239*, 1269–1270.

Nakamura, N. and A. H. Oort (1988). Atmospheric Heat Budgets of the Polar Regions. *Journal of Geophysical Research 93*, 9510–9524.

Newell, J. P. (1996). Sea-ice and atmospheric circulation anomalies in the Labrador Sea region associated with extremes of the southern oscillation. *International Journal of Climatology 16*, 63–71.

Nilsen, J. E. Ø., Y. Gao, T. Furevik, and M. Bentsen (2004). Simulated North Atlantic–Nordic Seas water mass exchanges in an isopycnic coordinate OGCM. *Geophysical Research Letters*.

Oki, T. Sud, Y. C. (1998). Design of total run off integrating pathways (TRIP): a global river channel network. *Earth interactions 2*, 1–37.

Orvik, K. A. and Ø. Skagseth (2003). The impact of the wind stress curl in the North Atlantic on the Atlantic inflow to the Norwegian Sea toward the Arctic. *Geophysical Research Letters 30*.

Overland, J. E., P. Turet, and A. H. Oort (1996). Regional Variations of Moist Static Energy Flux into the Arctic. *Journal of Climate*.

Parkinson, C. L. and W. M. Washington (1979). A large-scale numerical model of sea ice. *Journal of Geophysical Research 84*, 311–337.

Polyakov, I. V. and J. M. A. Prushutinsky, A. Y. (1999). Seasonal cycles in two regimes of Arctic climate. *Journal of Geophysical Research 25*, 761–788.

Pond, S. and G. L. Pickard (1978). *Butterworth-Heinemann*.

Prinsenberg, S. J. (2002). Volume, heat and freshwater fluxes through the canadian arctic archipelago: present understanding and future research plans.

Proshutinsky, A., M. Steele, J. Zhang, G. Holloway, N. Steiner, S. Häkkinen, D. M. Holland, R. Gerdes, C. Koebler, M. Karcher, M. Johnson, W. Maslowski, Y. Zhang, W. Hibler, and J. Wang (2001). The Arctic Ocean Model Intercomparison Project (AOMIP). *EOS 82(51)*, 637–644.

Roach, A., K. Aagaard, C. Pease, S. Salo, T. Weingartner, V. Pavlov, and M. Kulakov (1995). Direct measurements of transport and water properties through the Bering Strait. *Journal of Geophysical Research 100*, 18,443–18,457.

Rothrock, D. A., Y. Yu, and G. A. Maykut (1999). Thinning of the Arctic Sea-Ice Cover. *Geophysical Research Letters 23*, 3469–3472.

Rudels, B. (1987). On the mass balance of the Polar Ocean with special emphasis on the Fram Strait. *Skr. Nor. Polarinst. 188*, 1–53.

Sadler, H. E. (1976). Water, heat, and salt transports through Nares Strait, Ellesmere Island. J. Fish. *Res. Board Can. 33*, 2286–2295.

Schauer, U., H. Loeng, B. Rudels, V. K. Ozhigin, and W. Dieck (2002). Atlantic Water flow through the Barents and Kara Seas. *Deep-Sea Research I 49*, 2281–2298.

Schauer, U., S. Osterhus, and G. Rohardt (2004). Arctic warming through the Fram Strait: Oceanic heat transport from 3 years of measurements. *Journal of Geophysical Research 109*.

Schlosser, P., D. Bauch, R. Fairbanks, and G. Bönisch (1994). Arctic river-runoff: mean residence time on the shelves and in the halocline. *Deep-Sea Research 41*.

Semtner, J. A. (1976). A model for thermodynamic growth of sea ice in numerical investigations of climate. *Journal of Physical Oceanography 6*, 683–730.

Serreze, M. C., J. E. Walsh, F. S. Shapin III, T. Osterkamp, M. Dyurgerov, V. Romanovsky, W. C. Oechel, J. Morison, T. Zhang, and R. G. Barry (2000). Observational evidence of recent change in the northern high latitude environment. *Climate Change 46*, 159–207.

Shindell, D. T., R. L. Miller, G. Schmidt, and L. Pandolfo (1999). Simulation of recent northern winter climate trends by greenhouse-gas forcing. *Nature 399*, 452–455.

Simonsen, K. (1996a). Implications of the natural freshwater surface condition in the Nordic Seas. *Submitted to Tellus*.

Simonsen, K. (1996b). Meltwater fluxes into the high northern latitude seas and possible impact on the circulation in the Nordic Seas and Arctic Ocean. *Submitted to Paleoceanography*.

Simonsen, K. and P. M. Haugan (1996). Heat budgets of the Artic Mediterranean and sea surface heat flux parameterizations for the Nordic Seas. *Journal of Geophysical Research 101*, 6553–6576.

Sorteberg, A., N. G. Kvamstø, and Ø. Byrkjedal (2004). Wintertime Nordic Seas Cyclone Variablity and its Impact on Oceanic Volume Tansports Into the Nordic Seas. *in press*.

SSC, S. and S. IWG (2003). SEARCH: Study of Environmental Arctic Change, Implementation Strategy, Revision 1.0.

Stabeno, P. and J. E. Overland (2001). Bering Sea shift toward an earlier spring transition. *Eos, Transactions, American Geophysical Union 82(29)*, 317–321.

Steele, M. and T. Boyd (1998). Retreat of the cold halocline layer in the Artic Ocean. *Journal of Geophysical Research 103*, 10,419–10,435.

Steiner, N., G. Holloway, R. Gerdes, Häkkinen, D. Holland, M. Karcher, F. Kauker, W. Maslowski, A. Proshutinsky, M. Steele, and J. Zhang (2004). Comparing modeled streamfunction, heat and freshwater content in the Arctic Ocean. *Science Direct 6*, 265–284.

Stepaniak, D. Vertically Integrated Mass, Moisture, Heat, and Energy Budget Products Derived from the NCEP/NCAR Reanalysis. *http://www.cgd.ucar.edu/cas/catalog/newbudgets/*.

Thompson, D. W. J. and J. M. Wallace (2000). Annular Modes in the Extratropical Circulation. Part I: Month-to-Month Variability. *Journal of Climate 13*, 1000–1016.

Trenberth, K. and J. M. Caron (2001). Estimates of Meridional Atmosphere and Ocean Heat Transports. *American Meteorological Society*, 3433–3443.

Trenberth, K. E., J. M. Caron, and D. P. Stepaniak (2001). The atmospheric energy budget and implications for surface fluxes and ocean heat transports. *Climate Dynamics 17*, 259–276.

Trenberth, K. E. and D. P. Stepaniak (2003). Seamless Poleward Atmospheric Energy Transports and Implications for the Hadley Circulation. *Journal of Climate 4456*.

Trenberth, K. E., D. P. Stepaniak, and J. M. Caron (2001). Accuracy of atmospheric energy budgets. *Journal of Climate*.

Visbeck, M., E. P. Chassignet, R. G. Curry, T. L. Delworth, R. R. Dickson, and G. Krahmann (2003). The Ocean's Response to North Atlantic Oscillation Variability. *The North Atlantic Oscillation: Climatic Significance and Environmental Impact, Geophysical Monograph 134*, 113–145.

Vörösmarty, C. J., L. D. Hinzman, B. J. Peterson, D. H. Bromwich, L. C. Hamilton, J. Morison, V. E. Romanovsky, M. Strum, and R. S. Webb (2001). The

Hydrological Cycle and its Role in Arctic and Global Environmental Change: A Rational and Strategy for Synthesis Study.

Wallace, J. M. and D. W. J. Thompson (2002). Annular modes and climate prediction. *Physics Today*, 28–33.

Weingarten, T. J., D. J. Cavalieri, K. Aagaard, and Y. Sasaki (1998). Circulation, dense water formation, and outflow on the northeast Chukchi shelf. *Journal of Geophysical Research*, 7647–7661.

Widell, K., S. Østerhus, and T. Gammelsrød (2003). Sea ice velocity in the Fram Strait monitored by moored instruments. *Geophysical Research Letters 30*.

Wijffels, S. E., R. W. Schmitt, H. L. Bryden, and A. Stigebrandt (1992). Transport of Freshwater by the Oceans. *American Meteorological Society*, 155–162.

Zhang, X., M. Ikeda, and J. E. Walsh (2003). Arctic Sea Ice and Freshwater Changes Driven by the Atmospheric Leading Mode in a Coupled Sea Ice–Ocean Model. *American Meteorological Society*, 2159–2177.